Spring 4-25-2022

Comparing Polarimetric Signatures of Proximate Tornadic and Non-Tornadic Supercells in Similar Environments

Devon Healey
University of Nebraska-Lincoln, dhealey2@huskers.unl.edu

COMPARING POLARIMETRIC SIGNATURES OF PROXIMATE TORNADIC AND NON-TORNADIC SUPERCELLS IN SIMILAR ENVIRONMENTS

by

Devon J. Healey

A THESIS

Presented to the Faculty of

The Graduate College at the University of Nebraska

In Partial Fulfillment of Requirements

For the Degree of Master of Science

Major: Earth and Atmospheric Sciences

Under the Supervision of Professor Matthew S. Van Den Broeke

Lincoln, NE

May 2022

COMPARING POLARIMETRIC SIGNATURES OF PROXIMATE TORNADIC AND NON-TORNADIC SUPERCELLS IN SIMILAR ENVIRONMENTS

Devon J. Healey, M.S.

University of Nebraska, 2022

Advisor: Matthew S. Van Den Broeke

While much research has shown that characteristics of the environment surrounding supercells can potentially indicate their likelihood to become tornadic, it is not uncommon for tornadic and non-tornadic supercells to coexist in seemingly similar environments. In these situations, it is difficult operationally to separate tornadic from non-tornadic supercells using environmental observations alone. Given that tornadic and non-tornadic supercells have been found to coexist in similar environments, something must be occurring beneath the observational and/or model gridscale that is supporting tornadogenesis in some supercells while inhibiting it in others. This study examines dual-polarimetric radar signatures of proximate tornadic and non-tornadic supercells in similar environments to determine if this can be a valuable method to distinguish proximate tornadic and non-tornadic supercells. Much research has examined dual-polarimetric signatures of supercells; however, not while controlling for environment between tornadic and non-tornadic supercells. A collection of proximity supercell groups is collected, and a method to quantify environmental similarity between storms is developed. Using this method, we select tornadic – non-tornadic supercell pairs that appear to have the most similar environment within proximity supercell groups.

These pairs are run through an automated tracking algorithm which identifies and quantifies polarimetric signatures in each supercell. Differential reflectivity (Z_{DR}) arcs show no statistically significant differences between supercells; however, the maximum value within the arc may be larger in non-tornadic supercells. The difference in separation distance between the Z_{DR} arc and the specific differential phase (K_{DP}) foot between tornadic and non-tornadic supercells is statistically significant, with tornadic supercells having larger separations. The key finding from this research is that tornadic supercells have larger Z_{DR} column and hailfall areas in the 30 minutes prior to tornadogenesis. In about two-thirds of pairs, the tornadic supercell had a larger Z_{DR} column area than the non-tornadic supercell prior to tornadogenesis. The statistically significant difference in Z_{DR} column area between storms may be operationally beneficial.

Acknowledgements:

I would first like to acknowledge and thank my advisor, Professor Matthew Van Den Broeke for being willing to take me on as a graduate student, even across the border from Canada. I appreciate his patience, guidance, and willingness to teach me on things both big and small in meteorology. I have grown a lot under his tutelage. I would also like to acknowledge Matthew Wilson, for his critical support on this project, allowing me to use his Python algorithm for this project, and for teaching me as well throughout my time with him. I would like to acknowledge my committee members, Professors Mark Anderson and Adam Houston for their feedback and guidance on this project and thesis. Above all, I thank my beautiful wife for her outstanding and extraordinary support throughout my education while continually being a wonderful mother for our two beautiful children. I would not have been able to complete this thesis without her support. Finally, I acknowledge NOAA grants NA18OAR4590307 and NA19OAR4590340, through which this research was funded.

Table of Contents

Multimedia Objects

Chapter I: Introduction

Supercell thunderstorms can produce some of the most violent and devastating weather on the planet, arguably the most significant of which is the tornado. Although most supercells are non-tornadic (Trapp et al. 2005), tornadic supercells and particularly significant tornadic supercells (F/EF-2 rating or greater), are responsible for a disproportionate amount of damage, injuries, and fatalities from supercell thunderstorm events (Brooks and Doswell 2001; Ashley 2007; and citations within). Operationally, much emphasis has been placed on improving the ability to distinguish tornadic from non-tornadic supercell environments (Thompson et al. 2003, 2012; Parker 2014; Nowotarski and Jones 2018; Coniglio and Parker 2020; and many others). Research has identified 'typical' environments that tend to be associated with tornadic and non-tornadic supercells. Tornadic supercell environments generally possess higher convective available potential energy (CAPE), less convective inhibition (CIN), greater storm-relative helicity (SRH) and low-level bulk wind difference (BWD), and lower lifting condensation levels (LCLs) than non-tornadic supercell environments (Kerr and Darkow 1996; Thompson et al. 2003; Esterheld and Giuliano 2008; Thompson et al. 2012; Nowotarski and Jensen 2013; Nowotarski and Jones 2018; Coniglio and Parker 2020; and many others). However, there is still much overlap in the known environments of tornadic and non-tornadic supercells, which introduces additional challenges to operational meteorologists on days when multiple supercells coexist in a similar meso-beta scale environment (Klees et al. 2016).

When multiple supercells occur simultaneously within a similar meso-beta scale environment, operational meteorologists are presented with a unique challenge in anticipating which supercell(s) is (are) more likely to become tornadic without using typical distinguishing

environmental characteristics. It is likely that in situations such as these, environmental differences smaller than the meso-beta scale exist between tornadic and non-tornadic supercells (Klees et al. 2016). However, these differences are too small to be captured by the observational or model gridscale, and any differences potentially captured may not appear significant enough to distinguish tornadic from non-tornadic supercells. Along with small scale environmental heterogeneities likely existing in these situations, it is also likely that other storm-to-storm differences exist, such as microphysical characteristics that may play a role in tornado production (e.g., French et al. 2015; Van Den Broeke 2020). Furthermore, differences in how storms initiated and the environmental conditions that supported initiation could play a role in determining which storms will ultimately become tornadic (e.g., Houston and Niyogi 2007; Rousseau-Rizzi et al. 2017).

With the upgrade of the WSR-88D radar network to include dual-polarization (hereafter dual-pol) capabilities, microphysical characteristics of larger sample sizes of supercells can now be inferred (Seliga and Bringi 1976; Balakrishnan and Zrnić 1990; Conway and Zrnić 1993; Kumjian and Ryzhkov 2008; Van Den Broeke 2016, 2017, 2020). Research has identified repeatable dual-pol signatures in supercells that can be examined to infer microphysical processes and storm-scale dynamics within each supercell (Kumjian and Ryzhkov 2008; Romine et al. 2008; Van Den Broeke et al. 2008). These signatures include the differential reflectivity (Z_{DR}) arc (Dawson et al. 2014), Z_{DR} columns (Conway and Zrnić 1993), hail signatures in the forward flank (Kumjian and Ryzhkov 2008), separation between the Z_{DR} arc and the specific differential phase (K_{DP}) foot (Loeffler et al. 2020), and the tornadic debris signature (Ryzhkov et al. 2005; Van Den Broeke 2015). Research has attempted to identify differences between

dual-pol signatures in tornadic and non-tornadic supercells that could provide insight into microphysical processes that may be supporting (or preventing) tornadogenesis (French et al. 2015; Homeyer et al. 2020; Loeffler et al. 2020; Van Den Broeke 2020). Research has also examined how dual-pol signatures vary within a single tornadic supercell throughout its lifetime, with much emphasis on the period immediately prior to tornadogenesis (Crowe et al. 2012; Van Den Broeke 2020). Connections between dual-pol signatures and tornado lifecycles may support operational meteorologists in issuing more timely and accurate tornado warnings (Crowe et al. 2012; Van Den Broeke 2017).

For tornadic and non-tornadic supercells occurring in a similar environment, dual-pol signatures may allow for inferences about differences in storm structure between supercells. This may provide a means to distinguish tornadic from non-tornadic supercells in such scenarios. This thesis will examine and compare dual-pol radar signatures of tornadic and non-tornadic supercells occurring within similar environments to test the hypothesis that differences in signatures exist between tornadic and non-tornadic supercells coexisting in a similar environment. Ideally, findings from this work will provide operational meteorologists with additional methods to distinguish tornadic from non-tornadic supercells. Chapter 2 provides a background of supercells, supercell environments, and dual-pol radar and signatures. Chapter 3 describes case selection and how similar environments for a group of supercells was defined. Methods for examining dual-pol radar signatures of supercells are also presented in this chapter. Chapter 4 presents and discusses results, and Chapter 5 will conclude with a summary and discussion of key results.

Chapter II: Background

I: Supercells and Supercell Environments

a. Supercells

Supercell thunderstorms, defined as thunderstorms possessing a long-lived, rotating updraft, or mesocyclone (Lemon and Doswell 1979; Thompson et al. 2003), can produce the most devastating weather on the planet. Browning (1964) first coined the term "supercell" referring to "single large cells with characteristic structures" that deviate to the right of mean winds in the atmosphere. Lemon and Doswell (1979) were among the first to examine supercell structure and formation. They developed the first conceptual model of the supercell thunderstorm (Figure 2.1), depicting a strong, persistent, rotating updraft and two downdraft regions – the forward-flank downdraft (FFD), and the rear-flank downdraft (RFD).

Research has found that mesocyclogenesis generally occurs when horizontal vorticity, associated with vertical wind shear or buoyancy gradients, is tilted into the vertical by a strong updraft (Kerr and Darkow 1996; Esterheld and Giuliano 2008; Peters et al. 2020). Hodographs are a critical tool in assessing likelihood of supercell formation, as they provide an overview of vertical wind profiles and allow inference of the presence of horizontal vorticity. Vertical wind profiles that veer and increase in speed with height tend to be supportive of supercell development provided that convection initiation can occur, and a strong updraft can be maintained (Kerr and Darkow 1996 and citations within). Given that deep convection initiation occurs, a strong, persistent updraft can then tilt horizontal vorticity into the vertical and form a mid-level mesocyclone (Rotunno 1981; Davies-Jones 1984). A veering wind profile that

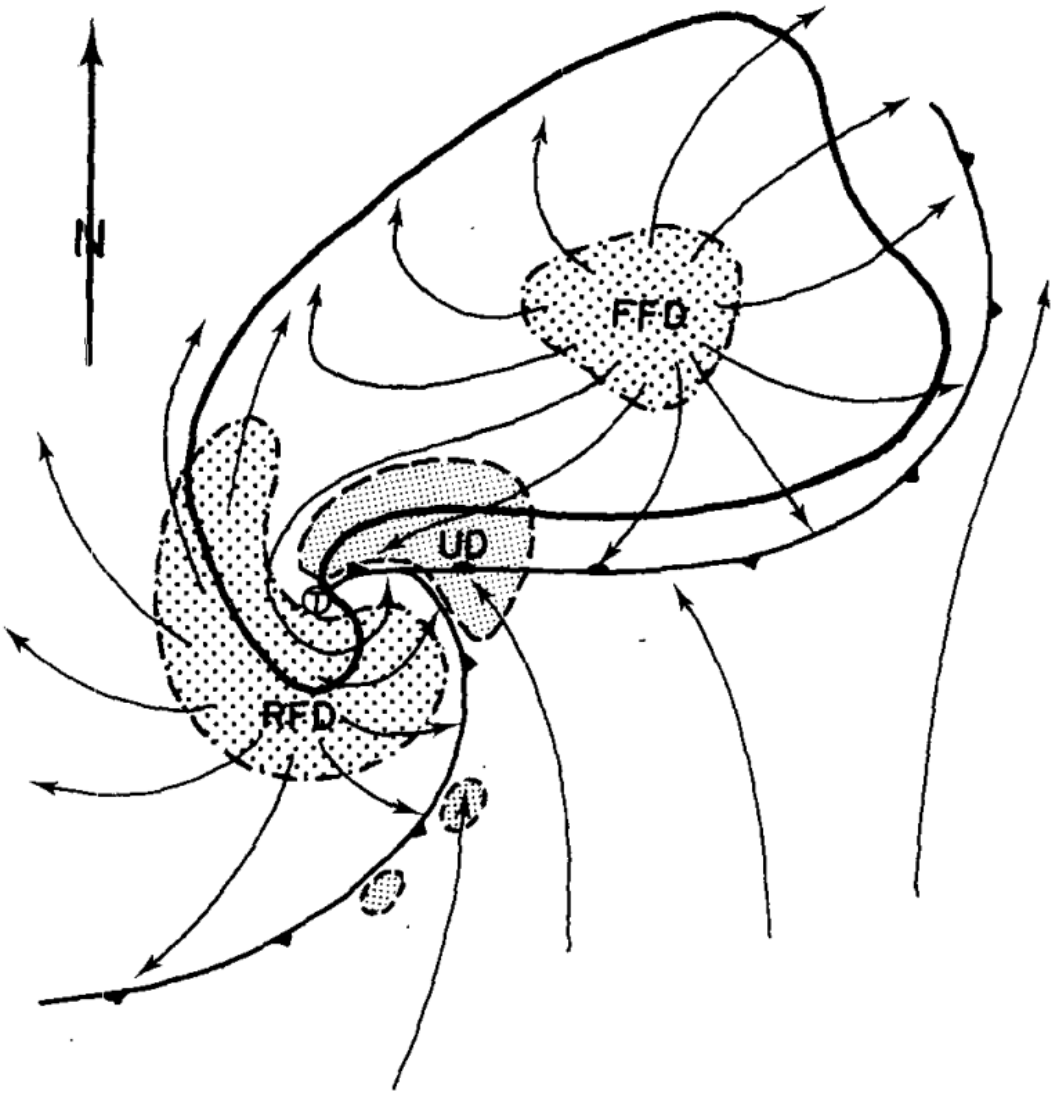

Figure 2.1: One of the first plan view schematics of the supercell thunderstorm, developed by Lemon and Doswell (1979). The solid line represents a typical radar outline of a supercell. Coarsely stippled regions indicate downdraft regions and are each labelled to represent the corresponding region (RFD = rear-flank downdraft, FFD = forward-flank downdraft). The updraft region is labeled “UD” and is finely stippled. Tornado location is labeled with a small “T”, and wind directions relative to the storm are represented by thin black arrows. [Figure 7 from Lemon and Doswell (1979)]

increases in speed with height allows for dynamic pressure perturbations to support longevity of the storm system and mesocyclone. The mesocyclone likewise further strengthens the updraft through vertical dynamic pressure perturbations and allows for the warm, buoyant updraft to remain separated from the cool downdraft regions, which additionally promotes longevity (Davies-Jones 1984).

For a supercell to become tornadic, low-level mesocyclogenesis must occur (Brandes 1978; Lemon and Doswell 1979). Low-level mesocyclogenesis can occur from additional tilting and stretching of baroclinically generated horizontal vorticity by density gradients in the environment or from the storm itself (Nowotarski et al. 2015 and citations within). Lemon and Doswell (1979) hypothesized that there may be connections between the RFD and low-level mesocyclogenesis and tornadogenesis. Research supports this hypothesis and has shown that storm downdrafts may support tornadogenesis through additional tilting of horizontal vorticity into the vertical, particularly at low-levels, and by bringing this vertical vorticity down toward the surface (Davies-Jones 1982; Davies-Jones and Brooks 1993; Nowotarski et al. 2015). The tightening and stretching of vertical vorticity to the surface creates a violent rotation center through conservation of angular momentum, thus forming the tornado. However, not all supercells become tornadic. In fact, only 26% of mesocyclones identified in a study by Trapp et al. (2005) became tornadic. Many non-tornadic supercells can still experience low-level mesocyclogenesis. Understanding why tornadogenesis does not subsequently occur despite the presence of strong low-level rotation is still an area of active research (e.g., Trapp 1999; Van Den Broeke 2021).

b. Supercell Environments

Supercells tend to require a particular distribution of thermodynamic and kinematic environmental characteristics to develop (e.g., Thompson et al. 2003, 2007). Research has focused heavily on environments associated with supercells to allow for operational meteorologists to identify these environments hours in advance and warn accordingly to protect the public (Thompson et al. 2003, 2007; Esterheld and Giuliano 2008; Thompson et al. 2012; Nowotarski and Jensen 2013; Parker 2014; Nowotarski and Jones 2018; Coniglio and Parker 2020; and many others). Environmental variables that have shown value in distinguishing supercell from non-supercell environments include CAPE, CIN, LCL heights, BWD, and SRH (e.g., Thompson et al. 2003, 2012). Environments with high CAPE, low LCL, and strong BWD are generally more conducive to supercell development. As mentioned previously, vertical wind profiles that veer and increase in speed with height tend to promote supercell development. These wind profiles generally result in greater BWD and greater SRH (Kerr and Darkow 1996; Esterheld and Giuliano 2008; Coniglio and Parker 2020). 0-6 km BWD has been relied on more for distinguishing supercell from non-supercell environments (Figure 2.2), while 0-1 km BWD and SRH (which is generally only measured from 0-1 or 0-3 km above ground level [AGL]), are better indicators of the potential for low-level mesocyclogenesis and therefore tornado potential. Parameters such as the bulk Richardson number (BRN; Weisman and Klemp 1982; Thompson et al. 2003) and the supercell composite parameter (SCP; Thompson et al. 2003) combine several environmental variables to assess the likelihood of supercell formation.

Supercell environments can be further distinguished as tornadic or non-tornadic. Much research has focused on tornadic supercell environments to improve understanding of tornado development and dynamics, and to improve forecasts and warnings (Fawbush and Miller 1954;

Beebe 1958; Thompson et al. 2003; Parker 2014; Coniglio and Parker 2020). Additionally, research has focused on differences between tornadic and non-tornadic environments to allow operational meteorologists to better predict if any particular supercell will become tornadic based on the environment surrounding the storm (Thompson et al. 2003; Parker 2014; Coniglio and Parker 2020). Thompson et al. (2003) employed the Rapid Update Cycle-2 (RUC-2) model to collect near-storm soundings of tornadic and non-tornadic supercells and found that tornadic supercells generally had larger mixed-layer CAPE (MLCAPE; Figure 2.3), lower mixed-layer LCLs (MLLCLs; Figure 2.4), and higher SRH (Figure 2.5). They also found that significant tornadic supercells (≥F/EF2) almost always (81%) had relative humidity values greater than 65% in the lowest kilometer and 0-1 km SRH greater than 75 $m^2 s^{-2}$. Parker (2014) examined observed soundings from the second Verification of the Origins of Rotation in Tornadoes Experiment (VORTEX2) that were obtained near to tornadic and non-tornadic supercells. He also found that tornadic supercell environments generally possessed greater CAPE and SRH, and lower LCLs than non-tornadic supercell environments. More recently, Coniglio and Parker (2020) examined observed soundings from all field campaigns studying supercell environments for the past three decades. Consistently, they found that tornadic supercell environments also had greater CAPE and SRH, lower LCLs, and stronger storm-relative winds at all levels. Their findings agreed with those from Thompson et al. (2003) that significant tornadic supercells have even greater low-level relative humidity and SRH compared to non-tornadic or weakly tornadic supercells (Coniglio and Parker 2020). These and many other findings have given valuable guidance to operational and research meteorologists, arguably helping save lives through improved forecasts and warnings.

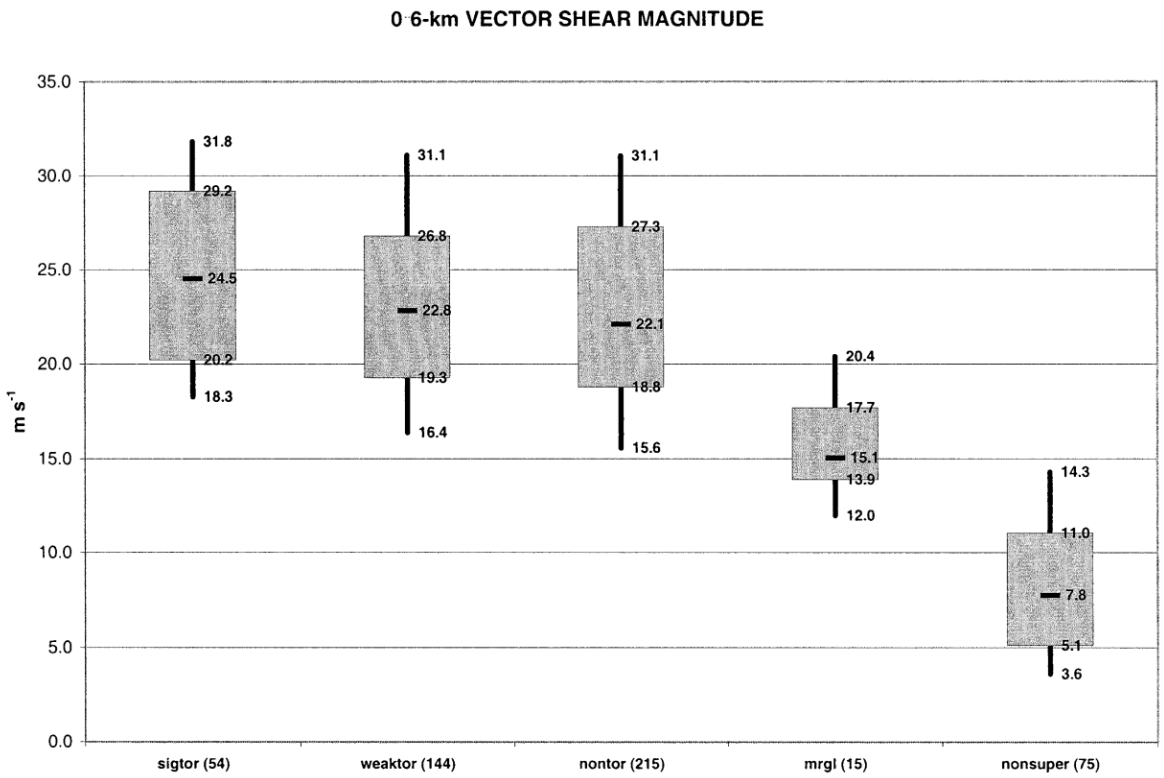

Figure 2.2: Box and whiskers plot of 0-6 km BWD (m s^{-1}) for (reading from the left): significant tornadic supercells, weakly tornadic supercells, non-tornadic supercells, marginal supercells, and non-supercells. The shaded box covers the 25th to 75th percentiles, and the whiskers extend to the 10th and 90th percentiles. The median values are marked by heavy black dashes within each box. [Figure 8 from Thompson et al. (2003)]

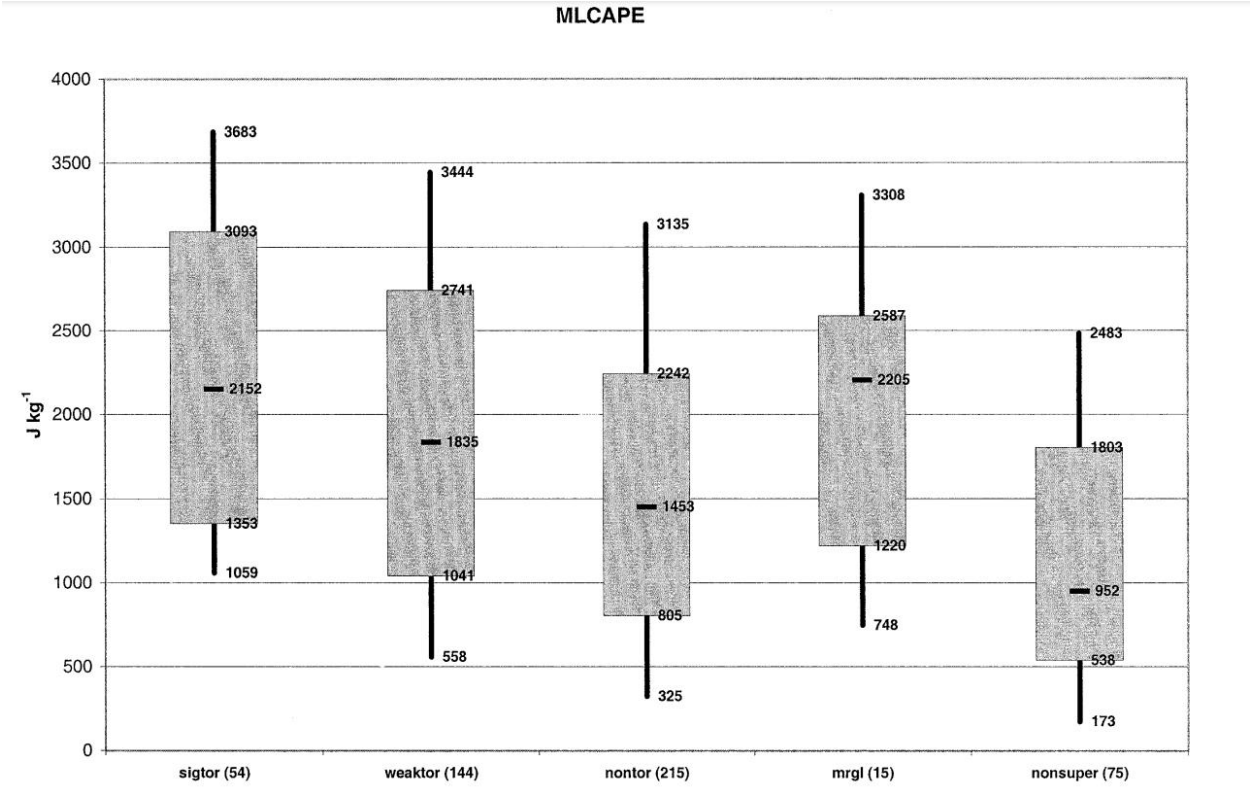

Figure 2.3: As in Figure 2.2., except for MLCAPE (J kg^{-1}). [Figure 6 from Thompson et al. (2003)]

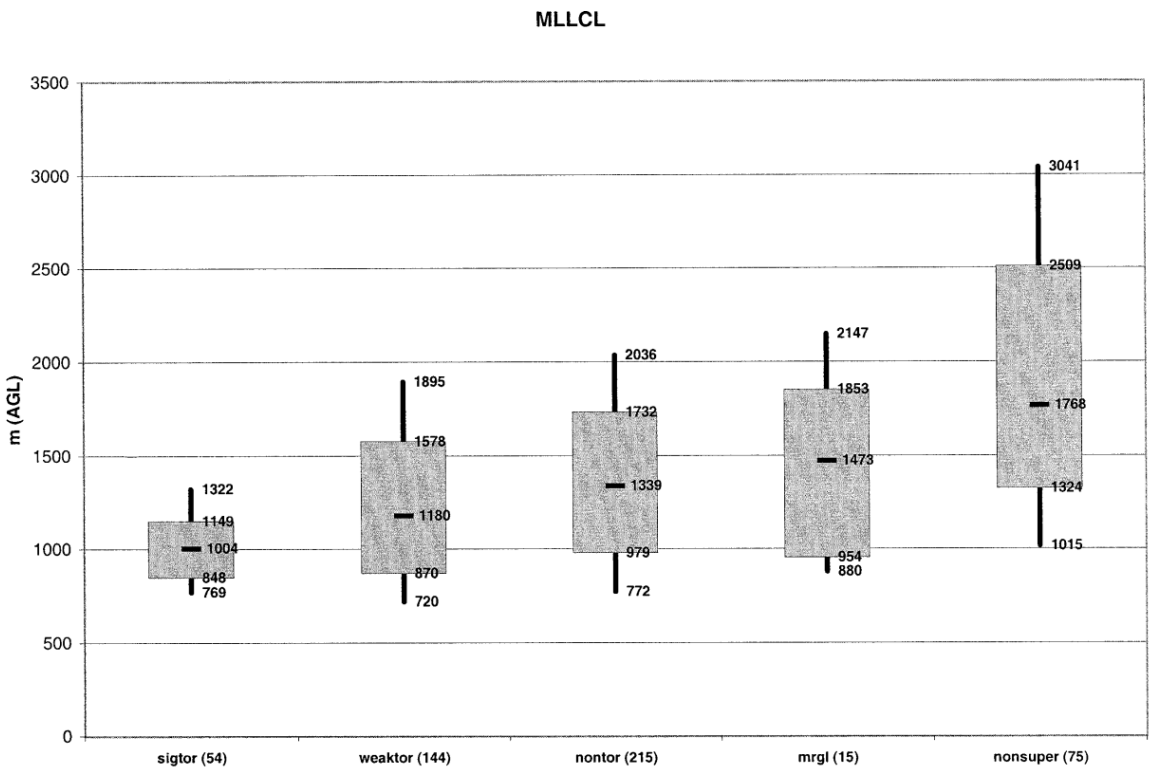

Figure 2.4: As in Figure 2.2., except for MLLCL (m above ground level). [Figure 7 from Thompson et al. (2003)]

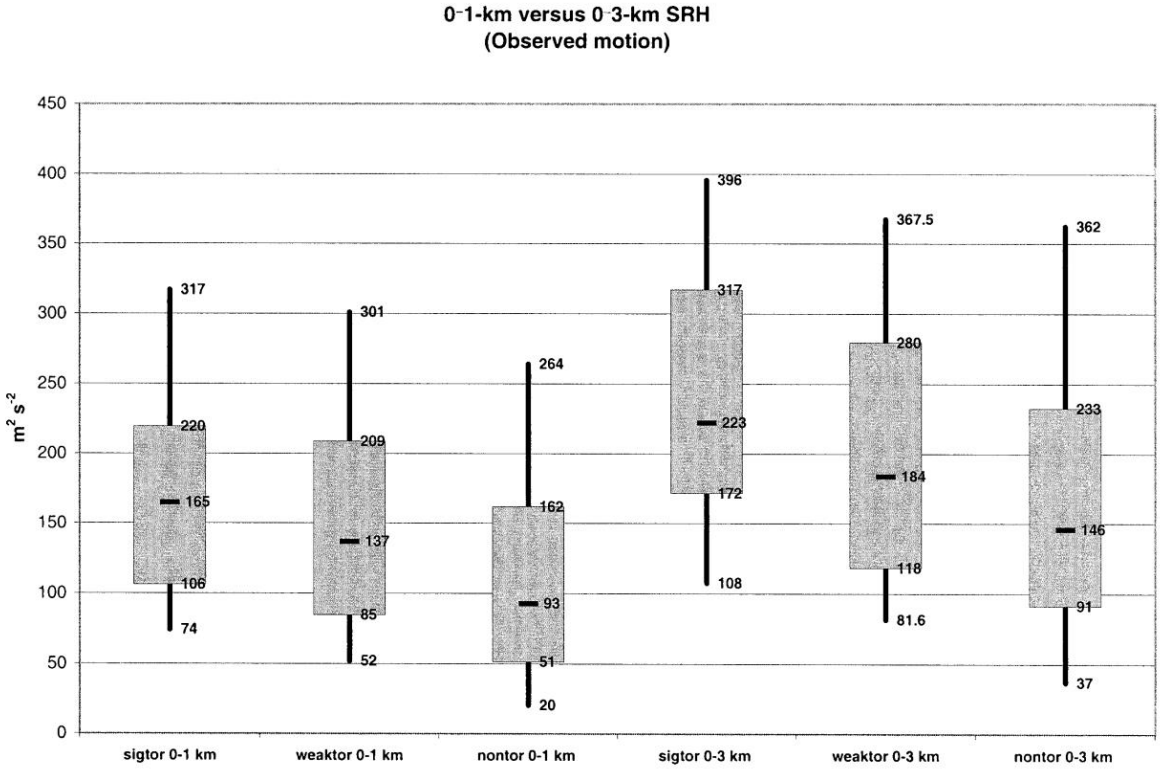

Figure 2.5: 0-1 km SRH ($m^2 s^{-2}$) and 0-3 km SRH ($m^2 s^{-2}$) for significant tornadic supercells, weakly tornadic supercells, and non-tornadic supercells. The three box and whisker plots on the left are for 0-1 km SRH, while the three on the right are for 0-3 km SRH. The details of box and whiskers distributions are the same as in Figure 2.2. [Figure 10 from Thompson et al. (2003)]

However, there is still much overlap in the known environments of tornadic and non-tornadic supercells. For example, while most significant tornadic supercells in the study by Thompson et al. (2003) had relative humidity values greater than 65% in the lowest kilometer and 0-1 km SRH greater than 75 $m^2 s^{-2}$, there were still some significant tornadic supercells that occurred below those values. Thus, environmental variables cannot always give a conclusive assessment on whether the observed or forecast environment will support tornadic supercell development or not. Further, tornadic and non-tornadic supercells have been observed to exist in similar meso-beta scale environments (Klees et al. 2016). This presents significant challenges to operational meteorologists attempting to forecast and warn for hazards using the meso-beta scale or greater observation network. While previous research has shown that meso-gamma scale or smaller environmental heterogeneities can significantly influence tornadogenesis or tornadogenesis failure (Klees et al. 2016), these differences would be unobservable using the meso-beta scale observation network to examine near-storm environments.

Klees et al. (2016) observed a tornadic and non-tornadic supercell in northeastern Colorado that developed nearly simultaneously and progressed in proximity to one another (Figure 2.6). Fifteen soundings were launched near these supercells to examine spatial and temporal variability of the near-storm environments. The environment of the tornadic supercell was consistent with a weakly tornadic environment while the environment surrounding the non-tornadic supercell was more representative of a non-tornadic environment according to the results of Thompson et al. (2012). Overall, however, there was much overlap in the environments of the two supercells (Figure 2.7; Klees et al. 2016). Research-grade radiosondes at very high spatial and temporal resolution in the study by Klees et al. (2016) identified small-

scale variations in the near-storm environments of these two supercells. However, from an operational standpoint, these supercells would appear to be occurring in a very similar environment, and it can be argued that the larger-scale, or meso-beta scale environment for these two storms was similar. The findings from Klees et al. (2016) reinforce two points about tornadic and non-tornadic supercell environments: 1) meso-gamma scale or smaller environmental heterogeneities can significantly impact tornadogenesis, and 2) tornadic and non-tornadic supercells can occur in environments that are quite similar relative to the observational network.

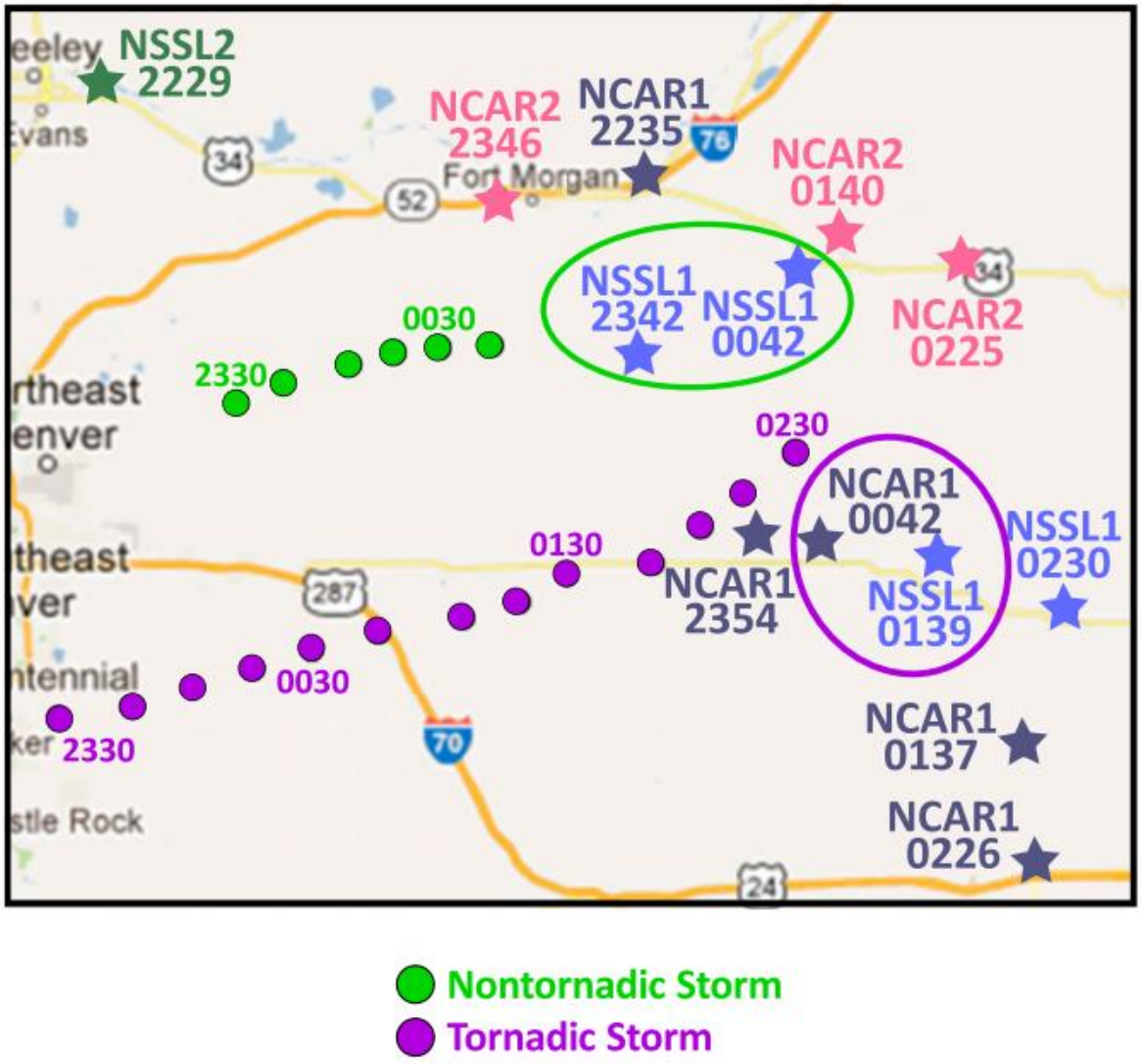

Figure 2.6: Map from Klees et al. (2016) showing locations of the tornadic and non-tornadic mid-level mesocyclone locations every 15 minutes. Stars indicate locations where the VORTEX-2 team launched radiosondes to assess the near-storm environments. The stars that are circled are used for environmental comparisons in the study by Klees et al. (2016). [Figure 6 (a) from Klees et al. (2016)]

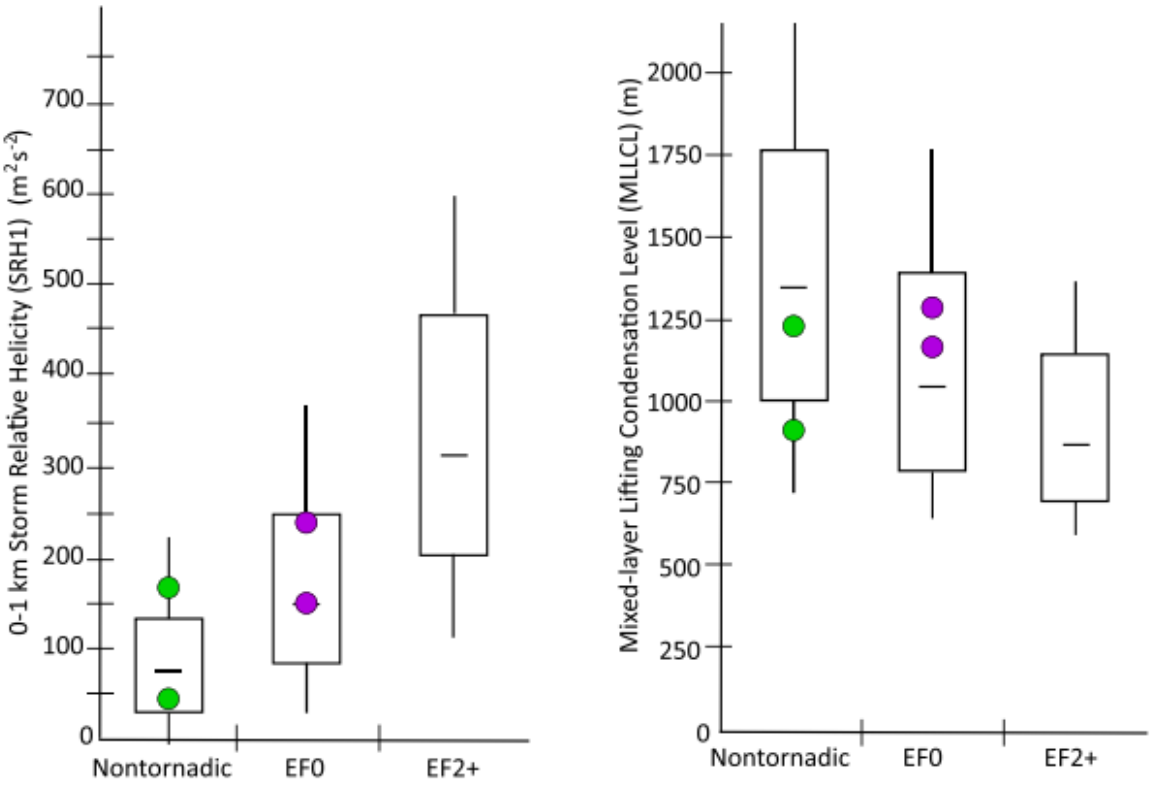

Figure 2.7: Box and whiskers plots of distributions of 0-1 km SRH (m^2 s^{-2}; left) and MLLCL (m above ground level; right) from Thompson et al. (2012) for non-tornadic supercells, weakly tornadic supercells, and significant tornadic supercells. Boxes span from the 25th percentile to the 75th. Whiskers extend to the 10th and 90th percentiles. The solid line within each box represents the median value. Green dots are values obtained from the soundings circled by the green circle in Figure 2.6, that correspond to the non-tornadic supercell environment, while purple dots are values obtained from the soundings circled by the purple circle in Figure 2.6, that correspond to the tornadic supercell environment. [Figure 6 (b) and (c) from Klees et al. (2016)]

Consider the following example to further demonstrate the potential for tornadic and non-tornadic supercells to occur in a similar meso-beta scale environment. On 30 June 2018, two supercells were progressing across south-central Nebraska within <40 km of each other (Figure 2.8). The tornadic supercell spawned a tornado at 2044 UTC and a second tornado at 2100 UTC. Maximum low-level normalized rotation (NROT; Cooper and Vorst 2016; Gibson 2017) in the non-tornadic supercell was observed by the Hastings, Nebraska radar (KUEX) at about 2112 UTC, however no tornado was reported. Maximum low-level NROT values were comparable between the tornadic (1.05 at 0.5^{o} elevation scan) and non-tornadic (1.05 at 0.5^{o} elevation scan) supercells prior to tornadogenesis. Synoptically, a low-pressure system was present over the Colorado-Kansas border, with a complex frontal system extending across the Nebraska-Kansas border and into central Iowa (Figure 2.9). Both supercells occurred on the same side of the frontal feature and within nearly identical distance from the front. Across the Nebraska-Kansas border during the mature stages of each supercell, MLCAPE values were around 2000 J kg^{-1} (Figure 2.10), and MLLCL heights ranged from 750 m on the cool side of the front in Nebraska to 1750 m on the Kansas side (Figure 2.11). Thus, from an operational viewpoint, the surrounding environment for these two supercells was nearly identical. As in the case study examined by Klees et al. (2016), it is likely that meso-gamma scale or smaller environmental heterogeneities existed in the vicinity of these supercells and that they were possibly responsible for the difference in tornado production.

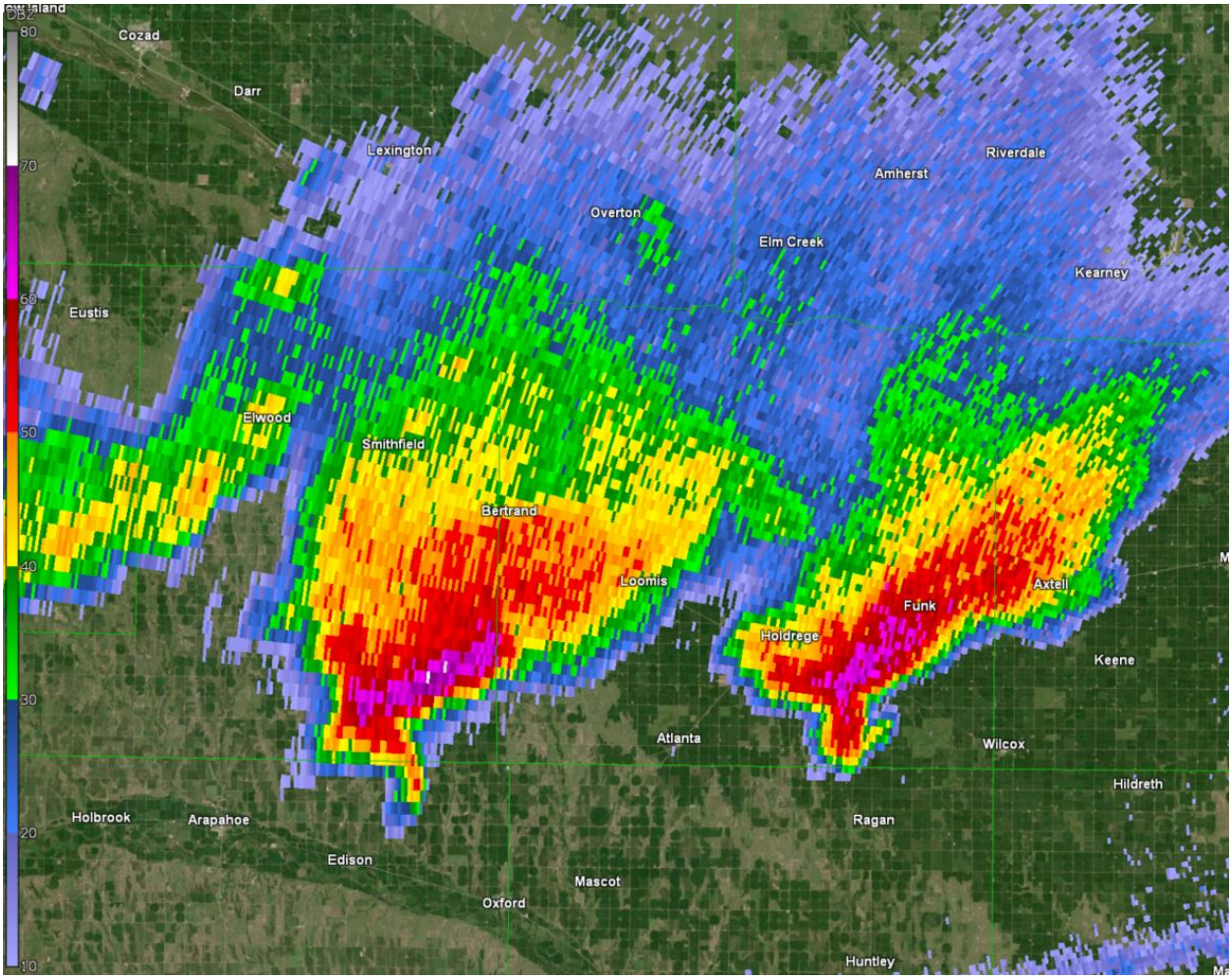

Figure 2.8: Radar image capture from the Hastings, Nebraska radar of the two proximity supercells at 2040 UTC (four minutes prior to tornadogenesis) 30 June 2018 in south-central Nebraska. City and town names are shown for geographical reference. Reflectivity scale is on the left of the image. The rightmost supercell became tornadic, while the leftmost supercell was non-tornadic its entire lifetime. Distance between the supercells at this time (measured from the center of the highest reflectivity in each storm) was 34.2 km.

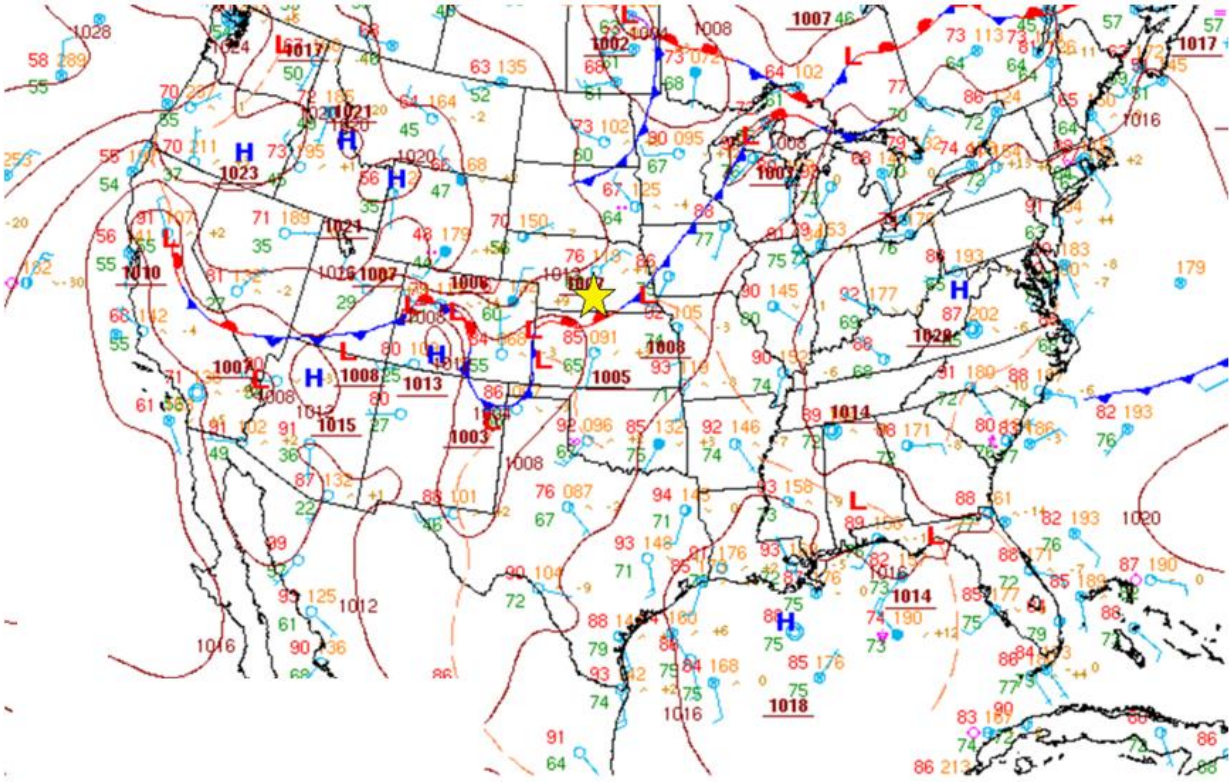

Figure 2.9: Surface map overview for 1800 UTC 30 June 2018, prior to initiation of the supercells in Figure 2.8. The yellow star indicates the approximate location of the supercells in Figure 2.8. Adopted from the Weather Prediction Center surface map analysis archive.

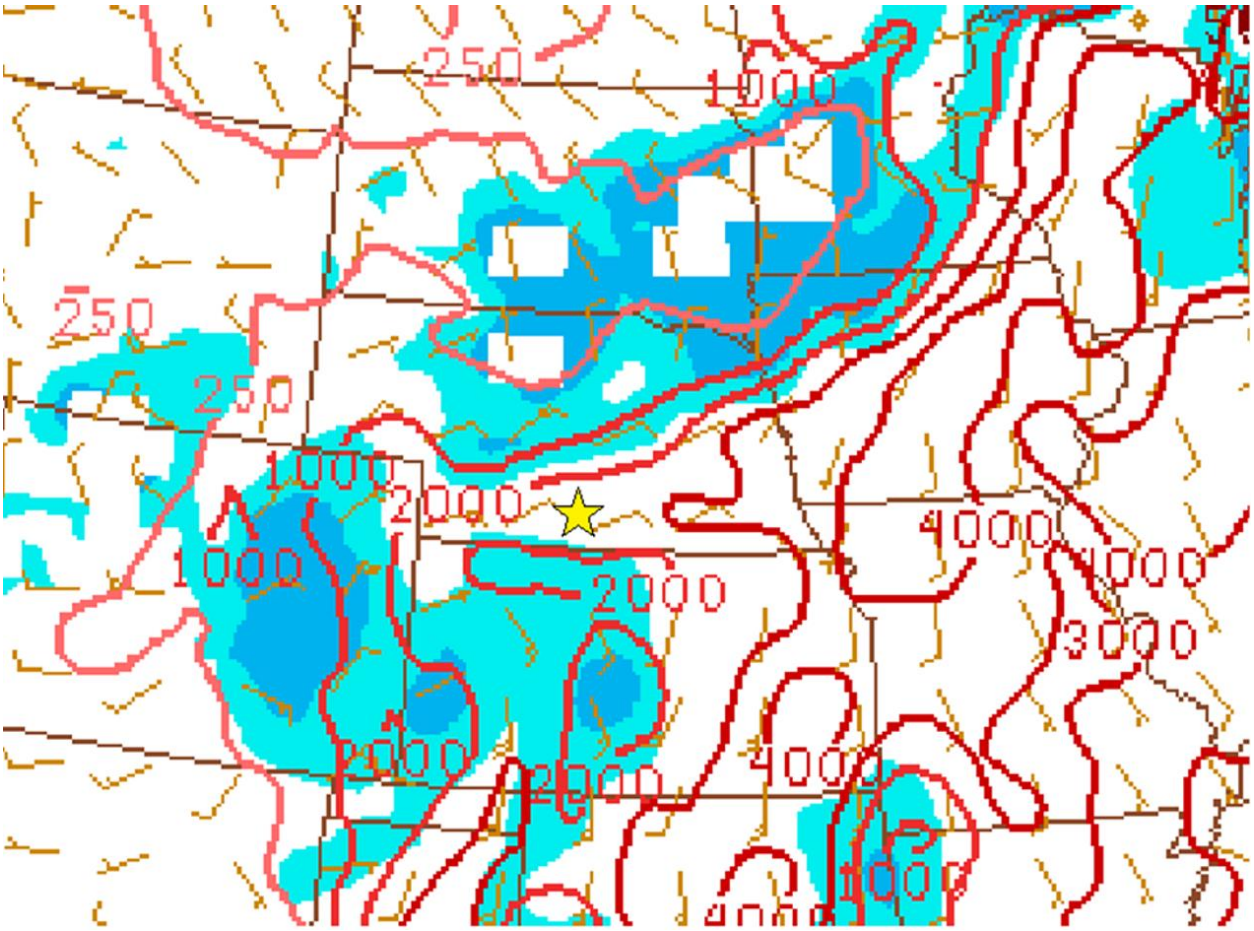

Figure 2.10: Storm Prediction Center (SPC) archived mesoscale analysis from 2000 UTC 30 June 2018 for MLCAPE and MLCIN. MLCIN values are contoured in blue and white. White values are ≤25 J kg^{-1} or missing data, light blue values are 26 – 100 J kg^{-1}, and dark blue values are ≥101 J kg^{-1}. Red contours represent MLCAPE values and are labeled. Approximate location of the proximate tornadic and non-tornadic supercells in Figure 2.8 is shown by the yellow star. Adopted from the SPC mesoscale analysis archive (https://www.spc.noaa.gov/exper/ma_archive/).

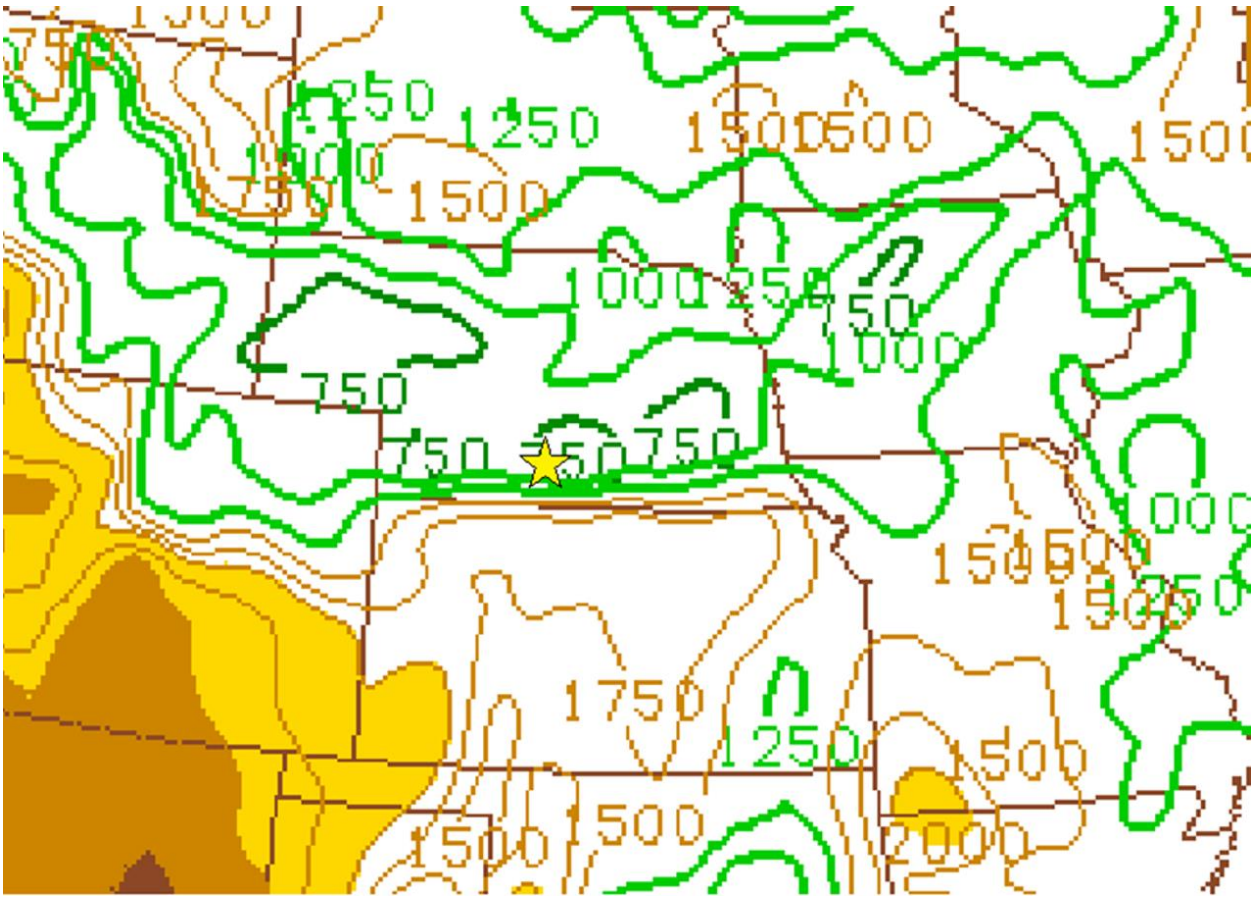

Figure 2.11: As in Figure 2.10., except for MLLCL heights. MLLCL heights 0 – 2000 m above ground level are white, 2001 – 3000 m are yellow, 3001 – 4000 m are light brown, and ≥4001 m are dark brown. Adopted from the SPC mesoscale analysis archive (https://www.spc.noaa.gov/exper/ma_archive/).

When tornadic and non-tornadic supercells occur in a similar environment, other factors likely influence differences in tornado production between storms, such as storm interactions (e.g., Weaver and Purdom 1995), differences in initiation characteristics (e.g., Houston and Niyogi 2007; Rousseau-Rizzi et al. 2017), modification of the near-storm environment by the storms themselves (e.g., Bunkers et al. 2022) and environmental heterogeneities smaller than the spatiotemporal scale of the observing network or model gridscale (Klees et al. 2016). These influences could cause differences in storm microphysics and structure which may ultimately explain why one supercell produces a tornado while a neighboring supercell does not (Van Den Broeke 2020). Therefore, in situations such as those presented above, using environmental variables to distinguish between tornadic and non-tornadic supercells becomes an unreliable method operationally due to the relatively coarse resolution scale of the observing network. This thesis will attempt to employ dual-pol radar to infer storm-scale characteristics of and differences between tornadic and non-tornadic supercells occurring in similar environments.

II: Dual-Polarization Radar and Dual-Polarization Signatures of Supercells

a. Dual-Polarization Radar

Dual-pol radar began to show value for meteorological applications in the late 20th century (e.g., Seliga and Bringi 1976; Illingworth et al. 1987; Balakrishnan and Zrnić 1990; Herzegh and Jameson 1992; Zrnić and Ryzhkov 1999). While conventional radar employs a single polarization of electromagnetic radiation, dual-pol radar employs two polarizations of electromagnetic radiation. Since dual-pol radar returns are received in two dimensions, this allows for inferences to be made about hydrometeor size, shape, and orientation within clouds

and storms (Balakrishnan and Zrnić 1990). By inferring hydrometeor characteristics, further inferences can then be made about microphysical processes and dynamics occurring within storms, such as size sorting (Kumjian and Ryzhkov 2008; Loeffler et al. 2020) and properties of storm updrafts and downdrafts (Seliga and Bringi 1976). Some variables from dual-pol radar that have shown value in meteorological applications and research include differential reflectivity (Z_{DR}), differential phase shift (Φ_{DP}) and its associate specific differential phase (K_{DP}), and the cross-correlation coefficient (ρ_{HV}). Differential reflectivity is the base-10 logarithmic of the ratio of reflectivity in the horizontal polarization to that in the vertical polarization (Seliga and Bringi 1976). Spherical hydrometeors have similar horizontal and vertical dimensions, therefore reflectivity in the horizontal component is similar to that in the vertical component. This results in a Z_{DR} close to zero, while more oblate hydrometeors with larger horizontal dimensions have larger values. Large raindrops produce high Z_{DR} values, and hail, particularly dry hail, will produce Z_{DR} values near zero. As such, areas of heavy rainfall will have large Z_{DR} values, while regions of hail will have Z_{DR} values closer to zero.

Φ_{DP} is the difference of phase between the horizontal and vertical polarization returning to the radar (Jameson 1994). As a beam of electromagnetic radiation from a dual-pol radar passes through a region of hydrometeors, the horizontally and vertically polarized beams will pass through different amounts of liquid or ice matter depending on the orientation and size of the hydrometeors relative to the beam. For example, large raindrops have a major axis orientated in the horizontal dimension; therefore, the horizontally polarized portion of the beam will pass through more liquid matter than the vertically polarized beam. This will cause the horizontally polarized beam to shift in phase more than the vertically polarized beam and

will result in increasing values of Φ_{DP}. The drawback to Φ_{DP} is that it measures accumulated phase shift along a given radial. Therefore, if a beam passes through a core of heavy precipitation close to the radar, high values of Φ_{DP} will be reported all along the radials that passed through the storm core. A more versatile parameter is specific differential phase (K_{DP}), which measures the change of Φ_{DP} along a radial and can therefore display specific regions of precipitation rather than accumulating values along the entire radial. As hail is generally spherical and falls in a tumbling fashion, K_{DP} is relatively unaffected by hail as both polarizations of the radar beam pass through similar amounts of ice and liquid matter. K_{DP} has been applied along with Z_{DR} to further classify hydrometeor types and has improved methods of estimating rainfall rates from a radar perspective (Brandes et al. 2001).

ρ_{HV} represents how similar hydrometeors are within a sample volume (Kumjian and Ryzhkov 2008). If all hydrometeors in a sample volume have the exact same size, shape, phase, and orientation, ρ_{HV} is exactly one. Generally, most hydrometeors within a sample volume are very similar in shape and orientation, therefore, for most meteorological scatterers, this value is close to one. However, regions of hailfall and mixed precipitation will have ρ_{HV} values closer to 0.9 or less. Non-meteorological scatterers, including insects, birds, and lofted debris can produce a ρ_{HV} value much less than one. This has further improved hydrometeor classifications within storm systems and has even presented meteorologists with a way to identify tornadic debris lofted high enough to be visible to the radar (Ryzhkov et al. 2005; Van Den Broeke 2015).

b. Dual-Polarization Signatures of Supercells

Dual-pol radar has been used in recent years to identify signatures and make inferences of microphysical processes within supercells which has provided new and valuable insight into supercell structure and development (Kumjian and Ryzhkov 2008; Romine et al. 2008; Van Den Broeke et al. 2008). Some repeatable dual-pol signatures identified within supercells include the Z_{DR} arc at low levels (Kumjian and Ryzhkov 2008; Dawson 2014; Wilson and Van Den Broeke 2021), the Z_{DR} column (Kumjian et al. 2014), hailfall signatures in the forward flank regions of the storm (Kumjian and Ryzhkov 2008), separation between the Z_{DR} arc and the K_{DP} foot (Loeffler et al. 2020), and the tornadic debris signature (TDS; Ryzhkov et al. 2005; Van Den Broeke and Jauernic 2014; Figure 2.12).

The Z_{DR} arc at low levels is found along the inflow edge of the supercell forward flank, and results from size sorting of hydrometeors in the storm-relative inflow (Kumjian and Ryzhkov 2008). Larger hydrometeors, particularly large raindrops, will fall out of the inflow earlier while smaller hydrometeors will be advected farther into the storm. As large raindrops result in higher Z_{DR} values, an enhanced region of Z_{DR} will generally be found along the inflow edge of the forward flank, where these large raindrops are falling. The separation distance between the region of high K_{DP} values within the storm (the K_{DP} foot) and the Z_{DR} arc also indicates size sorting processes in the storm (Figure 2.13), and larger separation distance and angles between these signatures are thought to be related to stronger storm-relative inflow (Loeffler and Kumjian 2018; Loeffler et al, 2020). Ryzhkov et al. (2005) suggested that high values in the Z_{DR} arc can be connected to strong mesocyclonic rotation within the supercell, and Kumjian and Ryzhkov (2007) showed that the strength (size, magnitude of Z_{DR} values) of the Z_{DR} arc is positively correlated to low-level SRH in the near-storm environment. The Z_{DR} arc has

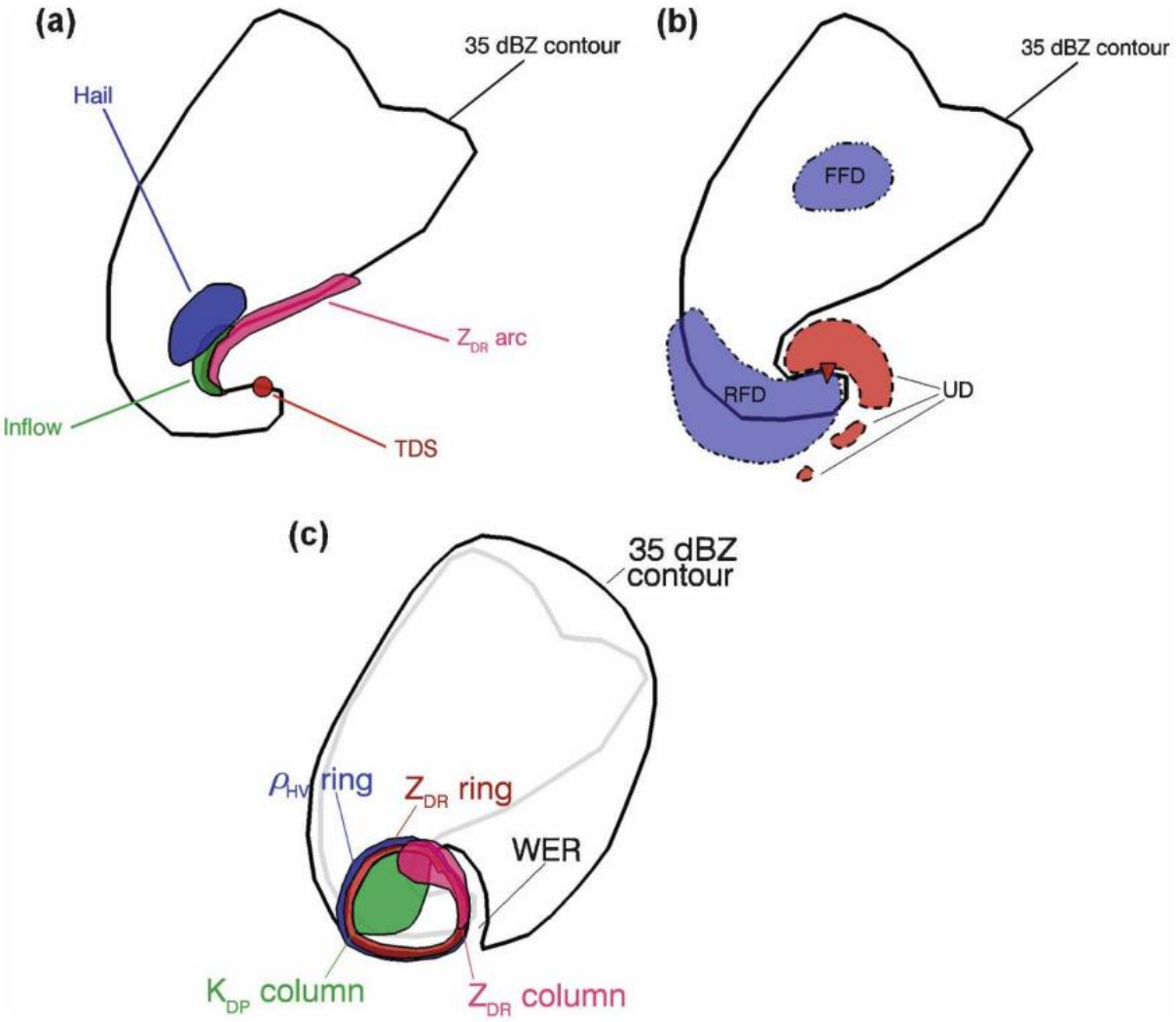

Figure 2.12: Schematics of dual-polarization radar signatures within supercells at (a) low-levels and (c) midlevels. (b) shows a typical supercell schematic, similar to Figure 2.1. In (c) "WER" refers to the weak-echo region (will not be referred to in this paper). [Figure 1 from Kumjian and Ryzhkov (2008)]

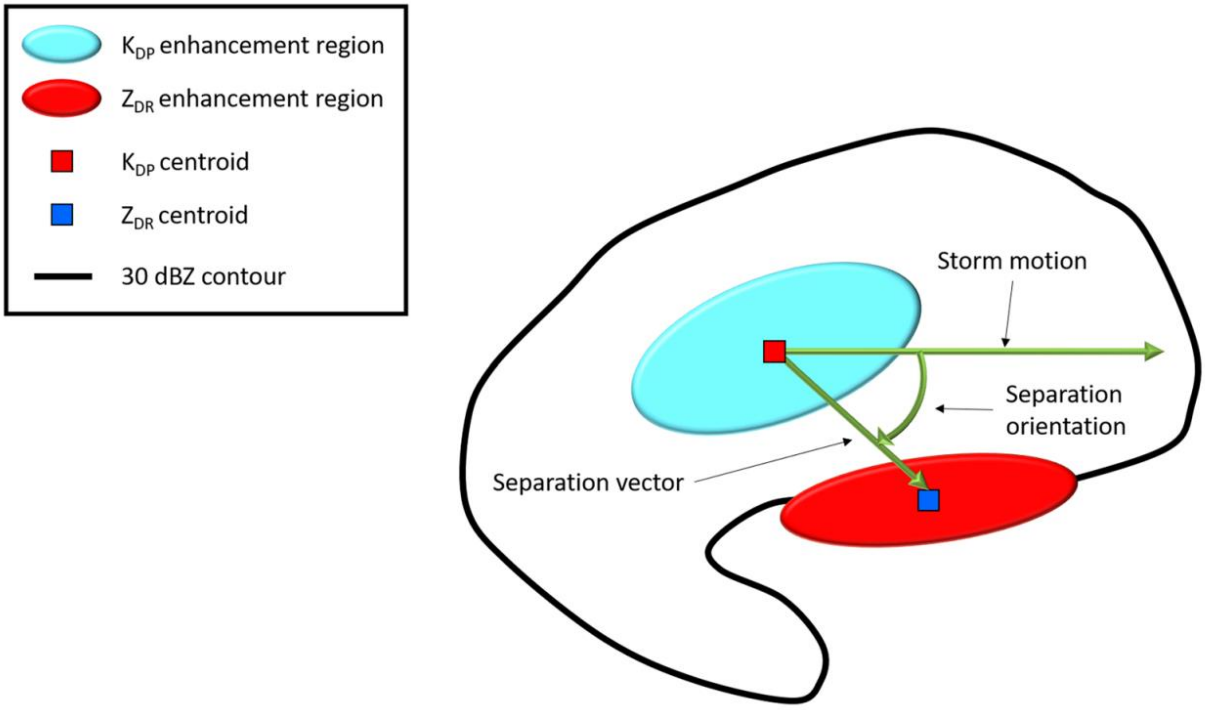

Figure 2.13: Schematic of the K_{DP} foot ("enhancement") region and the Z_{DR} arc ("enhancement region"), illustrating the separation angle and distance calculated and examined in supercells. [Figure 2 from Loeffler et al. (2020), adapted by those authors from Loeffler and Kumjian (2018)]

been hypothesized to have connections to environmental characteristics (Van Den Broeke 2016), tornado potential (Crowe et al. 2012), and tornado/mesocyclone lifecycles (Crowe et al. 2012; Van Den Broeke 2017). Characteristics of the Z_{DR} arc such as size and magnitude values within the arc have been hypothesized to have value in distinguishing between tornadic and non-tornadic supercells (Van Den Broeke 2020). In a relatively small sample size of pretornadic and non-tornadic supercells, Van Den Broeke (2020) found that Z_{DR} arcs within pretornadic supercells were generally larger, however more analysis is warranted as his findings were not statistically significant.

Z_{DR} columns are strongly correlated with the location of the storm updraft and represent a positive temperature perturbation (Kumjian and Ryzhkov 2008). Strong updrafts in supercells can loft large raindrops within the warm updraft to higher altitudes before they freeze. This results in a positive perturbation of Z_{DR} values at mid- to upper levels of the supercell, which well represents the updraft (Kumjian et al. 2010; Houser et al. 2015; Van Den Broeke 2016, 2017). Likewise, ρ_{HV} values aloft in the region of enhanced Z_{DR} will be diminished as hydrometeors usually become mixed-phase precipitation, with hydrometeors beginning to freeze at varying rates depending on size and composition of the particles. As with Z_{DR} arcs, characteristics of Z_{DR} columns have been examined for associations with tornado production and storm evolution (Van Den Broeke 2020). Thermodynamic properties of the atmosphere generally represent storm updraft potential, therefore characteristics of Z_{DR} columns such as size and depth are strongly correlated to CAPE and midlevel relative humidity (Van Den Broeke 2016). Z_{DR} columns had potential to distinguish pretornadic from non-tornadic supercells in a small sample size (Van Den Broeke 2020).

Hailfall regions can be identified through examination of Z_{DR} and conventional reflectivity fields. Large and/or water coated hail is very reflective and results in high (>55 dBZ) reflectivity values. However, due to their generally spherical shape and tumbling fall patterns, Z_{DR} values for large hail are near zero. Therefore, regions of collocated high reflectivity and low Z_{DR} often represent hailfall regions. ρ_{HV} has also been used to identify hailfall regions, as hail will often fall with varying sizes of raindrops, which produces a diminished ρ_{HV} value. Recent research suggests that hailfall regions in non-tornadic supercells are generally larger and more persistent than in tornadic supercells (Van Den Broeke 2020).

III: Hypotheses

As research continues to examine differences in dual-pol signatures between tornadic and non-tornadic supercells, there is value in assessing differences in these signatures between tornadic and non-tornadic supercells in similar environments. Based on prior literature, it is hypothesized that among a group of tornadic and non-tornadic supercells in a similar environment, tornadic supercells will have larger Z_{DR} columns (Sessa and Trapp 2020; Van Den Broeke 2020). Based on environmental similarity between a group of tornadic and non-tornadic supercells, it may be expected that Z_{DR} columns will show no difference between tornadic and non-tornadic supercells as Z_{DR} columns are strongly correlated to environmental conditions, particularly thermodynamic characteristics (e.g., Van Den Broeke 2016). However, it is further hypothesized that tornadic supercells have stronger mesocyclones (Brandes 1993; Naylor and Gilmore 2014), which may result in a stronger vertical pressure perturbation enhancing the updraft and Z_{DR} column signatures.

Building off the hypothesis that tornadic supercells have stronger mesocyclones, it is hypothesized that tornadic supercells have larger and more significant (larger magnitude) Z_{DR} arcs than non-tornadic supercells, particularly in the time leading up to tornadogenesis [defined as 30 minutes prior to the first tornado report (Van Den Broeke 2020)]. The presence of a stronger low-level mesocyclone will likely enhance size sorting of hydrometeors in the inflow, and therefore strengthen the Z_{DR} arc signature. Finally, it is hypothesized that a difference in hailfall exists between tornadic and non-tornadic supercells in a similar environment. Mean hailfall area is hypothesized to be larger in non-tornadic supercells. Hailfall area in tornadic supercells is hypothesized to be disrupted more repeatedly from stronger mesocyclone cycling and tornadogenesis processes (Van Den Broeke 2016, 2020), which would therefore decrease the mean hailfall area for the lifetime of a given tornadic supercell.

Emphasis will be placed on differences in characteristics of dual-pol signatures between tornadic and non-tornadic supercells in the 30 minutes prior to tornadogenesis and maximum low-level NROT in non-tornadic supercells. Significant findings would prove valuable for operational meteorologists as these signatures could be identified up to 30 minutes prior to tornadogenesis in a collection of supercells occurring in a similar spatiotemporal domain. Likewise, findings that support the above hypotheses could provide operational meteorologists with additional methods to anticipate tornadic from non-tornadic supercells on any given day that severe weather is anticipated.

Chapter III: Data and Methodology

I: Proximity Supercell Group Collection

To obtain a dataset of tornadic and non-tornadic supercells occurring in similar meso-beta scale environments, we searched the Storm Prediction Center (SPC) severe weather events archive (https://www.spc.noaa.gov/exper/archive/events/) for days on which at least one tornado was reported from 2017 through 2020. Archived radar images for those days were then examined to determine if the tornado report resulted from a supercell, multiple supercells coexisted in a similar region around the time of the tornado report(s), and that at least one supercell was not associated with a tornado report. This similar region was initially defined as storms being separated by less than 100 km and occurring nearly simultaneously (ideally within one hour of each other). Radar data from the nearest radar site(s) were then downloaded from the National Centers of Environmental Information (NCEI) Next-Generation Radar (NEXRAD) archive (https://www.ncdc.noaa.gov/nexradinv/map.jsp) for examination in Gibson Ridge Analyst-2 software (gxlevel.com).

Gibson Ridge Analyst-2 software was used to confirm the presence of multiple supercells in the region of the tornado report. Storms were identified as supercellular if they possessed persistent mesocyclonic rotation as described by Thompson et al. (2003) and one or more previously identified reflectivity characteristics associated with supercells (i.e., hook echo, tight reflectivity gradient on the inflow side, “flying-V”; Lemon 1977; Stumpf et al. 1998; Thompson et al. 2003). Supercells were also required to be within 100 km of the radar to obtain quality low-level radar data. All identified supercells were classified as tornadic or non-tornadic

based on the NCEI storm events database (https://www.ncdc.noaa.gov/stormevents/) which is believed to be the most accurate severe weather events archive available. However, this database may still be unreliable for confirming if a supercell was non-tornadic, as it is possible that a brief tornado could have been produced and not recorded in the database for a multitude of reasons (e.g., lack of spotters, no damage reported, tornado occurred at night, etc.). If at least one tornadic and non-tornadic supercell were confirmed to be present in a similar spatial and temporal domain and within 100 km of a radar site, all supercells meeting these requirements were grouped and retained for environmental assessment. This initially provided 55 groups of proximity supercells, containing a total of 210 supercells (Table 1).

Table 1: All 210 supercells within the 55 proximity supercell groups initially collected. Asterisks are placed beside group numbers that were ultimately not included in analysis due to environmental similarity being too low within those groups.

Date	Group #	# Of Tornadic Storms (n = 104)	# Of Non-Tornadic Storms (n = 107)	Radars Within 100 km Of At Least One Storm.
26 March, 2017	1	1	2	KFWS and KTLX
9 May, 2017	2	2	3	KFDX and KLBB
16 May, 2017	3	2	1	KAMA, KDDC, and KFDR
18 May, 2017	*4	2	1	KFDR and KVNX
12 June, 2017	5	2	1	KCYS
28 June, 2017	6	3	1	KDMX
1 May, 2018	7	1	2	KOAX and KUEX
2 May, 2018	8	1	2	KFDR and KTLX
29 May, 2018	9	1	3	KDDC
8 June, 2018	*10	1	2	KMVX
19 June, 2018	11	1	3	KCYS and KFTG
19 June, 2018	12	1	1	KUEX
30 June, 2018	13	1	1	KUEX
29 July, 2018	*14	2	1	KCYS
3 March, 2019	15	1	2	KEOX and KMXX
14 March, 2019	16	4	5	KBMX and KDGX
24 March, 2019	17	1	2	KLSX
30 April, 2019	18	4	1	KSGF and KSRX
5 May, 2019	19	1	1	KDDC
7 May, 2019	20	2	4	KAMA and KLBB
20 May, 2019	21	4	3	KFDR, KLBB, KLTX, and KMAF
22 May, 2019	22	7	2	KINX, KTLX, and KSGF
23 May, 2019	23	2	4	KAMA and KLBB
25 May, 2019	24	2	3	KAMA, KLBB, and KMAF
27 May, 2019	25	7	2	KILN, KIND, KIWX, and KLOT
28 May, 2019	26	2	6	KBGM, KCCX, and KPBZ
28 May, 2019	*27	2	2	KICT, KTWX, and KUEX
30 May, 2019	28	1	1	KLWX
18 March, 2020	29	2	3	KDYX, KFDR, and KFWS
24 March, 2020	30	2	1	KGWX and KHTX
29 March, 2020	31	1	1	KDVN

Table 1 (continued): All 210 supercells within the 55 proximity supercell groups initially collected. Asterisks are placed beside group numbers that were ultimately not included in analysis due to environmental similarity being too low within those groups.

Date	Group #	# Of Tornadic Storms (n = 104)	# Of Non-Tornadic Storms (n = 107)	Radars Within 100 km Of At Least One Storm.
29 March, 2020	32	1	1	KHPX and KVWX
8 April, 2020	33	1	2	KNQA and KPAH
12 April, 2020	34	2	2	KDGX
5 May, 2020	35	1	1	KCAE
12 May, 2020	36	2	2	KEWX
14 May, 2020	37	3	1	KTWX
17 May, 2020	38	4	2	KLCH and KPOE
19 May, 2020	39	1	1	KPUX
22 May, 2020	*40	1	2	KFDR
22 May, 2020	41	3	1	KSRX
23 May, 2020	42	3	1	KDVN
23 May, 2020	43	1	2	KILX and KLOT
23 May, 2020	44	1	2	KAMA and KLBB
6 June, 2020	45	2	2	KMLB and KTBW
8 June, 2020	46	1	2	KMVX
8 June, 2020	47	2	4	KLNX
20 June, 2020	48	1	2	KABR
20 June, 2020	*49	1	2	KLNX
27 June, 2020	*50	1	1	KLSX
28 June, 2020	51	1	1	KARX
1 August, 2020	52	1	1	KFCX
13 August, 2020	*53	1	1	KLNX
1 September, 2020	*54	1	3	KAMA and KLBB
11 October, 2020	55	2	1	KLTX

II: Defining Similar Environments for a Group of Supercells

a. Qualitative Environmental Assessment

As the primary purpose of this study is to compare tornadic and non-tornadic supercells that coexist in similar environments, proximity supercell groups were required to exhibit similar environmental characteristics to be retained for analysis. To control for environment, both qualitative and quantitative assessment of the environments of each proximity supercell group were performed. The purpose of qualitative assessment was primarily to ensure that any atmospheric boundaries (if any existed) in the region of the supercells did not separate one supercell from the others in the group. The purpose of quantitative assessment was to provide further confidence that the environments supporting each supercell in the group were similar.

Qualitative assessment was performed by examining archived SPC hourly mesoscale analysis maps for the region in which the supercells occurred. Supercell proximity groups passed qualitative assessment if the group of storms appeared to have similar thermodynamic and kinematic environmental characteristics across the entire time the supercells existed. Focus was placed on environmental variables that can typically distinguish supercell from non-supercell environments (e.g., MLCAPE and 0-6 km BWD; Thompson et al. 2003, 2012), and variables with potential for distinguishing between tornadic and non-tornadic environments (e.g., 0-1 km SRH and LCL height; Parker 2014; Wade et al. 2018; Coniglio and Parker 2020). Further, no atmospheric boundaries separating one or more supercells from the rest of the group could be present, ensuring that all supercells occurred in the same meso-beta scale air mass. If the group of proximity supercells appeared to exhibit similar environmental

characteristics based on archived mesoscale analysis maps, the group was retained for more rigorous quantitative assessment.

When possible, archived observed soundings were examined across the location to assess whether the group of supercells appeared to exist in a region consisting of similar atmospheric vertical profiles of temperature, moisture, and wind. Archived observed soundings were only used when the region in which the group of supercells occurred spanned across or near to at least two upper-air stations, and within one hour of when an observed radiosonde launch occurred. All proximity supercell groups except for six occurred nearest to just one upper-air station, therefore, only one observed sounding could be used for the entire group (at least two, each from different locations or times, would be needed to observationally assess if the environment is similar across the group). For those six proximity supercell groups, observed soundings were examined for the region across which those groups spanned. All 55 proximity supercell groups passed qualitative environmental assessment.

b. Developing a Method for Quantitatively Assessing Degree of Environmental Similarity

Quantitatively defining degree of environmental similarity for a group of supercells has not yet been performed to our knowledge. Therefore, the following is a simple method developed to meet the needs of this study which may be altered or enhanced for other situations following additional work. Limitations to this method will be discussed later in this section. First, a Rapid Refresh (RAP) model sounding was collected in the inflow region of each supercell across the entire dataset. The RAP model replaced the RUC model in 2012 and included a larger model domain and an improved data assimilation method. The RAP model

includes a horizontal resolution of 13 km and 51 vertical levels, a significant improvement from the RUC model that operated with 40 km horizontal resolution and only 40 vertical levels. Forecasting skill improved significantly in the RAP model, particularly for short-range events such as convective forecasting, which also made the RAP model more valuable for convective storm research (Benjamin et al. 2016). Biases for RAP model soundings are discussed briefly in the environmental comparisons section of Chapter 4. For each tornadic supercell, the time of the RAP model sounding was at the hour closest to the first reported tornado. If the first reported tornado occurred halfway between the hour (25 minutes to 35 minutes after the hour), a RAP model sounding was collected at the bottom and the top of the hour surrounding the tornado report. Environmental parameters from each RAP sounding were then averaged to estimate the environmental conditions halfway through the hour. For each non-tornadic supercell, the procedure was similar except using the time of maximum low-level rotation in the supercell, measured by NROT at the lowest radar elevation scan, as the time at which the model sounding would be collected. NROT calculates the difference of maximum inbound and outbound velocities within a rotation couplet and normalizes this by range from the radar. The result gives values of NROT ranging from -5 to 5, with values over 1 being significant for mesocyclonic rotation (Cooper and Vorst 2016). All cases were checked as thoroughly as possible to ensure that the most representative NROT value was used for each mesocyclone.

To determine the location of the RAP sounding, a marker was placed on the tight reflectivity gradient signature of each supercell at the time of the tornado report or maximum low-level rotation. The tight reflectivity gradient has been shown to represent areas near to the updraft, where air is rapidly accelerating upward and into the storm and suspending large

hydrometeors. This signature is generally accepted to represent size-sorting processes by the updraft and storm-relative inflow. Larger hydrometeors with greater terminal fall velocities will fall out quicker than smaller hydrometeors and will therefore not be advected very far into the storm and fall out to the surface. Progressively smaller hydrometeors will travel farther into the storm from the inflow before falling to the surface. This results in high reflectivity nearest to the updraft and storm-relative inflow entrance region and progressively decreasing reflectivity into the storm. The updraft region generally has little to no reflectivity at low levels, therefore the rapid change from little to high reflectivity results in a tight reflectivity gradient signature (Duda and Gallus 2010; MetEd UCAR – Radar Signatures Training: https://www.meted.ucar.edu/radar/severe_signatures/print_LLRG.htm#page_4.0.0). Therefore, along the tight reflectivity gradient it can be assumed that air is moving up and being ingested into the storm. If a tight reflectivity gradient was not readily visible at this time, the marker was placed along the inflow side of the supercell, based on supercell motion (e.g., a northeastward-moving storm generally has an inflow region to the south-southeast of the storm).

An initial RAP sounding was then collected 15 km away from this marker perpendicular to the tight reflectivity gradient (or perpendicular to the estimated tight reflectivity gradient). From this initial RAP sounding, the effective inflow layer depth and the pressure-weighted mean wind direction within this layer were recorded (Thompson et al. 2007, 2012; Nowotarski et al. 2020). Once the effective inflow layer pressure-weighted mean wind direction was determined, a backwards trajectory was followed 40 km (Potvin et al. 2010) away from the marker on the tight reflectivity gradient, following the direction of the effective inflow layer

mean wind direction. Based on previous literature, 40 km away from the storm in the inflow region well represents the inflow environment that is not contaminated or altered by the storm itself and that is not too far from the storm such that it may no longer represent inflow environmental air (the "Goldilocks" zone for supercell inflow; Potvin et al. 2010; Wade et al. 2018). At this location 40 km away from the supercell, the RAP model sounding was collected that would be used to represent the environment for the given supercell. Figure 3.1 shows a schematic example of how this was performed. Note that this method assumes this model sounding is representative of the environment that the storm will be ingesting. Factors such as storm motion, storm interactions, and changes in the environment that occur below the spatiotemporal scale of the RAP model, could result in the storm ingesting air that is not entirely represented by this model sounding. Furthermore, alterations of the near-storm environment by the storm itself will also likely result in the storm ingesting air that is not represented by the model sounding. However, for our purposes, we assume the model sounding 40 km away from the storm in the inflow sector to largely capture the background mesoscale environment the storm will experience during a large portion of its life (Potvin et al. 2010; Wade et al. 2018).

All soundings were checked for convective contamination. If a sounding exhibited vertical accelerations stronger than typical synoptic-scale vertical accelerations (e.g., Durran and Snellman 1987), and if the sounding was saturated through most of the atmosphere, it was considered convectively contaminated. This was not observed for any of our supercell soundings. In four soundings, vertical accelerations were approaching values greater than synoptic-scale accelerations, and the atmosphere appeared mostly saturated. For these cases,

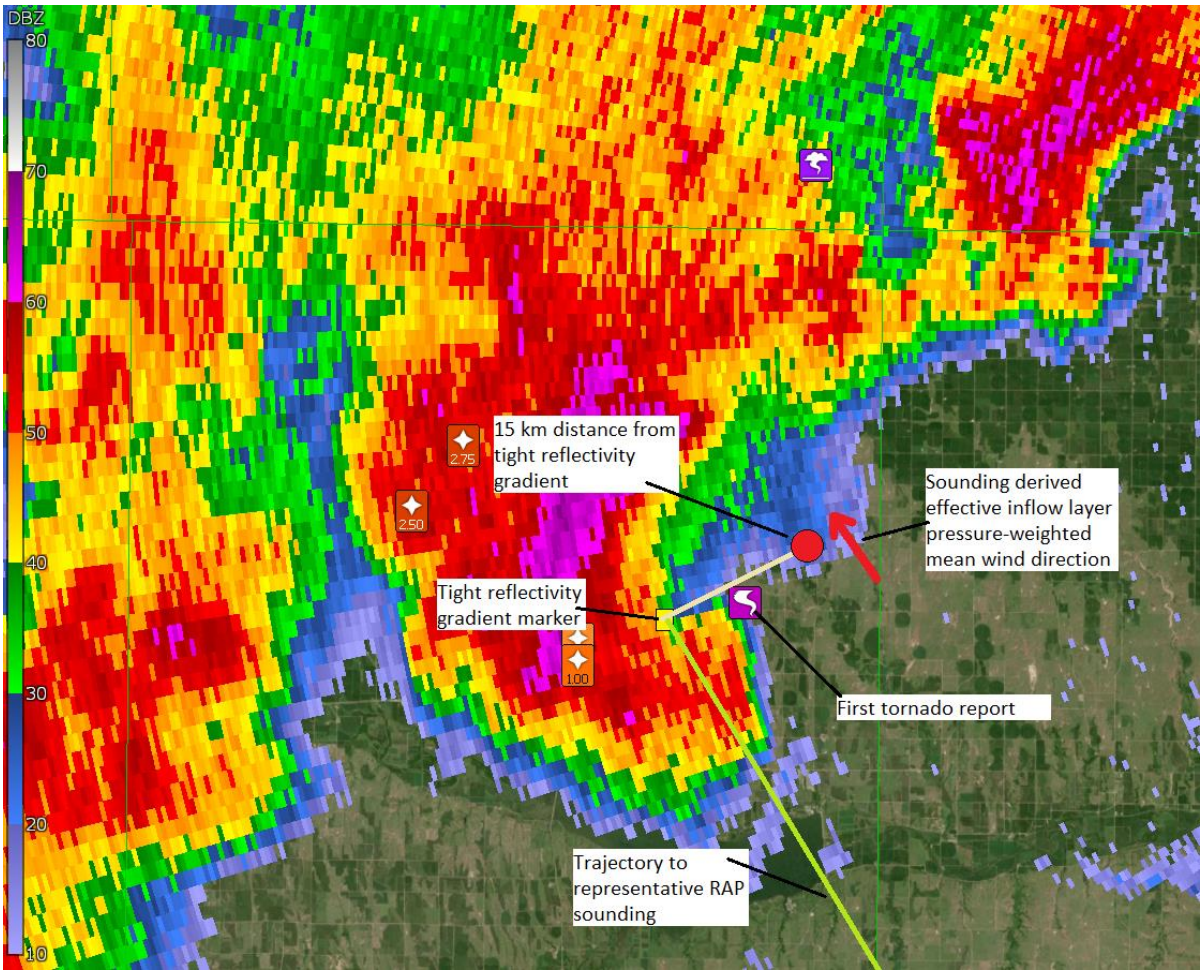

Figure 3.1: Example of how a representative RAP model sounding was collected for a supercell. The background radar image is from a tornadic supercell in group 12 in Table 1. The yellow square indicates the location of the tight reflectivity gradient, and the tan line is roughly perpendicular to this gradient and the red dot is ~15 km away (not to scale in this example). The red arrow would represent the effective inflow layer wind direction (an example just for illustration, not the actual wind direction in this case), and the green line follows this direction 40 km away in a backwards trajectory to the location of the representative model sounding (outside the image). This is done at the time of the tornado report or maximum low-level rotation.

additional soundings were collected at locations where no convection was occurring at the exact time of the model initialization (i.e., at an exact hour). These soundings were ensured to be far enough away from storms that they would not be convectively contaminated (e.g., >40 km from the storms). For each sounding in these four cases, it appeared that the overall background environment was saturated on these days, and vertical accelerations were similar. Therefore, we assumed those soundings were not convectively contaminated. In four of our total 210 supercell soundings, there appeared to be convection occurring between the supercell and the sounding location 40 km away from the storm, which may have caused misrepresentation of the supercell inflow environment for those cases. However, because this issue was very limited throughout the dataset, no additional measures were taken to account for these situations.

While 15 km away from the supercell is an arbitrary distance to use for obtaining the effective inflow layer mean wind direction for a given supercell, altering this distance by any amount less than the RAP model grid spacing of 13 km would have minimal change on the wind direction. A wind direction change of a few degrees would change the resulting location for the sounding representing the supercell environment, although it will be shown later in the methodology that such a change would be inconsequential to the results of this project. It also needs to be noted that no quality control methods were applied to check for contamination of the effective inflow layer wind direction by parameterizations within the model, therefore it is possible that some error exists in these estimated wind directions.

As shown in previous literature, environmental variables that have particular importance for supporting supercell environments include MLCAPE, most unstable CAPE

(MUCAPE), CIN, LCL heights, BWD, and SRH. MLCAPE, MUCAPE, and CIN represent the thermodynamic conditions supporting supercell updrafts (e.g., Thompson et al. 2003). Significant differences in these values between supercells could result in large differences in updraft properties, which have implications for storm longevity, severity, and influence on the surrounding environment. LCL heights, allowing inference of cloud base heights, also reflect low-level moisture in the surrounding environment (French et al. 2015; Coniglio and Parker 2020). Lower LCL heights may result in less negatively buoyant downdrafts which may support tornadogenesis. This may explain why tornadic supercells have been found to more often have lower LCL heights (Parker 2014; Coniglio and Parker 2020). BWD and SRH directly reflect the atmospheric vertical wind profile, with SRH also reflecting the connection between expected storm motion and the low-level vertical wind profile (Kerr and Darkow 1996; Esterheld and Giuliano 2008; Parker 2014; Wade et al. 2018; Coniglio and Parker 2020). While 0-6 km BWD has been more commonly used to diagnose supercell environments and has connections to updraft potential (Thompson et al. 2003; Gilmore et al. 2004), 0-1 km BWD and 0-1 km SRH have been used to assess low-level mesocyclogenesis potential (Esterheld and Giuliano 2008). Higher values generally correlate well to low-level mesocyclogenesis potential and strength, and tornadic supercells have been found to have higher values of 0-1 km SRH (Wade et al. 2018; Coniglio and Parker 2020).

As the goal of this research is to control for environment and each of the aforementioned variables have some influence on supercell development and behavior, each variable was recorded to be used in quantitative environmental comparison. From each RAP sounding associated with each supercell across the dataset, MLCAPE, MUCAPE, CIN, LCL

heights, 0-1 km BWD, 0-6 km BWD, and 0-1 km SRH were recorded. CIN and LCL heights were calculated using a lowest 100-hPa mixed-layer approach, therefore, MLCIN and MLLCL height will be used hereafter. 0-1 km SRH was calculated using a Bunkers storm motion estimate (Bunkers et al. 2000). It was found after collection of all supercell soundings that MLCAPE and MUCAPE, and 0-1 km BWD and 0-1 km SRH, were strongly correlated (r = 0.852, and r = 0.869, respectively). Therefore, MUCAPE and 0-1 km BWD were not recorded for each supercell environment to avoid overrepresenting thermodynamic and kinematic conditions. The former variables (MLCAPE and 0-1 km SRH) have been referenced more frequently in the literature for supercell environments, thus those variables were retained. To additionally account for low-level moisture/saturation, which may have implications on entrainment and low-level thermodynamics (French et al. 2015), the average relative humidity from 1 to 3 km above ground level was recorded. Finally, the height of the freezing level was recorded for each supercell environment. While this variable is not currently thought to be critical for supercell or tornado development, it well represents larger scale environmental conditions which can confirm that a group of supercells are coexisting in a similar air mass if they possess similar freezing level heights in their inflow regions. Additionally, the height of the freezing level is important for certain dual-pol radar signatures, such as Z_{DR} columns and hailfall area (Van Den Broeke 2016). Therefore, if differences in Z_{DR} columns and hailfall area exist between tornadic and non-tornadic supercells despite freezing level heights being similar, other mechanisms are likely responsible for the difference in signatures.

To assess environmental similarity between supercells in our dataset, each supercell sounding (base) was compared to every other supercell sounding in the dataset (comparison)

using a percent difference approach. Percent differences were calculated for each of the collected variables between all supercells (below, MLCAPE is only listed as an example; this same calculation was done for all other variables):

$$(1) \quad MLCAPE\ \%diff = \frac{|MLCAPE\ (\boldsymbol{base}) - MLCAPE(\boldsymbol{comparison})|}{MLCAPE(\boldsymbol{base})} x100\%$$

The above equation and methodology described thus far show that altering the distance of the initial RAP sounding to collect the effective inflow layer mean wind direction would likely result in an inconsequential difference when comparing proximity supercells. This is best illustrated through a simple example. For a comparison of two proximate supercell environments, suppose the effective inflow layer mean wind direction 15 km away from the base supercell was from the southeast, at 160 degrees (180 degrees being directly south). For the comparison supercell, suppose the wind direction was found to be 165 degrees. We then would follow that direction associated with each supercell 40 km away from the respective storm and collect the representative environmental sounding. Now, say that we alter the initial RAP sounding distance from the supercell to be only 13 km away from the storm, and in this case the effective inflow layer mean wind directions for the base and comparison supercells are 155 and 163 degrees, respectively. Following this direction 40 km away from the storms will result in different locations for the representative environmental soundings, however the calculation of percent differences between variables will likely be relatively unchanged. Changing the trajectory, and therefore the values of the environmental variables collected for one storm will also be done for the other storm, and it is very likely that the percent difference will remain very similar. This is especially true given that all supercell proximity groups passed qualitative

assessment, and therefore are in large-scale similar environments. Therefore, any difference that would arise from changing the distance from the storm of the initial sounding and the identified trajectory would likely be inconsequential for this methodology.

An equation was then created to assess environmental similarity based on all percent differences calculated. Inputs for this equation are the percent differences of each environmental variable from a comparison of a pair of supercell environments. Next, weighting values were assigned to each environmental variable based on their potential to distinguish between tornadic and non-tornadic supercell environments. Based on previous literature, 0-1 km SRH and MLLCL height are the two variables collected in our study that have the most potential to distinguish between tornadic and non-tornadic environments. Therefore, these variables were assigned a weighting value of two, while the other variables were assigned a weighting value of one. Table 2 presents all variables collected along with their associated weighting values. Each environmental variable percent difference was then subtracted from one and multiplied by the weighting value assigned to that variable. A 0% difference in the environmental variable between two soundings would result in a value equal to the weighting value for that variable, while a 100% difference would result in a value of 0. If the percent difference was greater than 100% for a particular variable, that value was set to 0. All values were then added together and normalized by the highest possible similarity score (9). A result of 1 indicates a perfectly similar environment between two supercells (all percent differences = 0%):

(2) $Environmental\ Similarity$

$$= [(1 - \%diff\ MLCAPE) + (1 - \%diff\ MLCIN)$$
$$+ [2 * (1 - \%diff\ MLLCL)] + (1 - \%diff\ 1 - 3\ km\ RH)$$
$$+ [2 * (1 - \%diff\ 0 - 1\ km\ SRH)] + (1 - \%diff\ 0 - 6\ km\ BWD)$$
$$+ (1 - \%diff\ 0℃\ Z)]/9$$

Table 2: Environmental variables collected from the representative RAP model soundings for each supercell and their weighting values for environmental similarity calculations.

Variable Type	**Variable (units)**	**Weighting Value**
Thermodynamic	MLCAPE (J kg^{-1})	1
	MLCIN (J kg^{-1})	1
	MLLCL (m)	2
	Freezing Level Height (m)	1
	1-3 km Relative Humidity (%)	1
Kinematic	0-6 km BWD (m s^{-1})	1
	0-1 km SRH (m^2 s^{-2})	2

The above equation was used to compare each supercell to all other supercells in the dataset. This resulted in 21,945 ([210*209]/2) environmental similarity values. These values were normally distributed, and the mean and median values were 0.5615 and 0.5636, respectively (Figure 3.2).

Assigning higher weighting values to 0-1 km SRH and MLLCL height increases the requirement for those variables to be similar between supercells if we are controlling for environment. For example, if all variables between two supercell soundings showed high similarity based on a percent difference approach, however one supercell possessed 0-1 km SRH of 300 $m^2 s^{-2}$ and an MLLCL height of 800 m while the other possessed only 50 $m^2 s^{-2}$ of 0-1 km SRH and an MLLCL of 1500 m, the first supercell would be expected to be more likely to become tornadic (Coniglio and Parker 2020). Therefore, to remove the ability of environmental variables to distinguish between tornadic and non-tornadic supercell environments, it is critical that these two variables in particular remain as similar as possible between proximate tornadic and non-tornadic supercells. From equation (2), we can see that if the percent difference is high in 0-1 km SRH and MLLCL height, the resulting environmental similarity value will be much lower than if the percent difference was just as high for MLCAPE and 1-3 km RH, for example. Therefore, this higher weighting for 0-1 km SRH and MLLCL height places more emphasis on those variables being similar in a supercell environment comparison.

From the distribution of environmental similarity values obtained for the entire dataset, an environmental similarity threshold value was then selected that would be used to quantitatively confirm if a pair of supercell environments were similar. We selected the 75^{th} percentile of the distribution to represent the environmental similarity threshold: 0.6571

(Figure 3.2). If a pair of supercell environments compared using the above methodology produce an environmental similarity value greater than 0.6571, they are assumed to have a quantitatively similar environment.

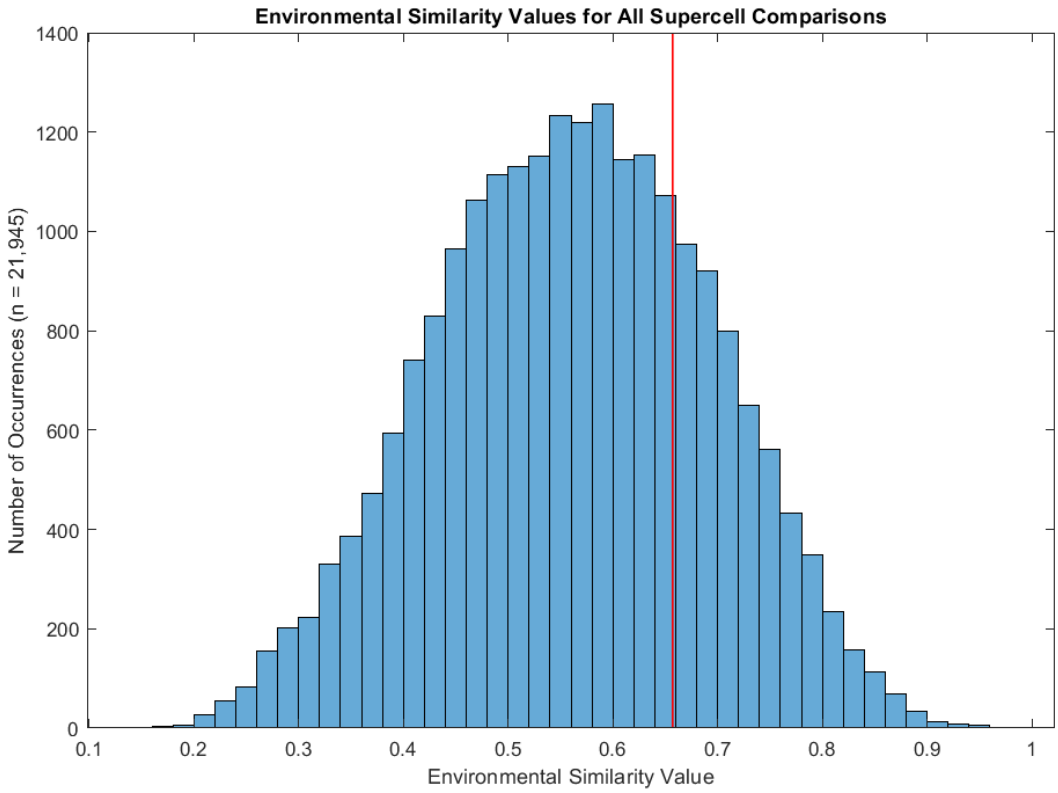

Figure 3.2: Distribution of all environmental similarity values from all possible supercell pair comparisons in our dataset (n = 21,945). The 75th percentile (0.6571) is shown with the red line.

c. Limitations to the Quantitative Environmental Similarity Method

Following qualitative and quantitative environmental assessment, it may be assumed that a pair of supercells within a group are coexisting in a similar environment. However, environmental heterogeneities often occur on very small spatial and temporal scales which can cause two adjacent supercells to ingest different environmental air (Klees et al. 2016). These environmental heterogeneities are rarely captured by observational or model grid scales, and therefore remain unresolved in environmental assessments. Furthermore, individual supercells are known to alter their near inflow environment through mechanisms such as deviating their motion and enhancing low-level SRH (Bunkers et al. 2000; Parker 2014). Another example is cold pool generation which can alter low-level thermodynamic profiles and generate additional horizontal vorticity in the near-storm environment, which could be tilted and stretched into the storm updraft (Davies-Jones 1984).

The method developed to quantitatively assess degree of environmental similarity does not, and cannot, account for these environmental heterogeneities occurring beneath observational and model grid scales. Therefore, it is entirely possible that a tornadic supercell, shown to have a high degree of environmental similarity with neighboring non-tornadic supercells based on the above method, has either altered its near-inflow environment or is ingesting a pocket of air unresolved by models or observations that may be providing the additional ingredient(s) necessary for tornadogenesis. The same may be true for a non-tornadic supercell occurring amongst a group of tornadic supercells, though in this case the additional ingredients necessary for tornadogenesis may be withheld from this supercell.

If a group of supercells coexist across a similar spatial and temporal domain, it is very likely that some degree of storm interaction is occurring (e.g., Bluestein and Weisman 2000; Hastings and Richardson 2010). Storm interactions have been documented in recent literature and are still an area of active research (e.g., Bunkers et al. 2006; Tanamachi et al. 2015). Outflow boundaries generated by each storm could interact with nearby storms and could support or inhibit tornadogenesis. Additional streamwise vorticity could be added to the near-storm environment upon interaction, or the outflow characteristics could be too cold and negatively buoyant, therefore cutting off warm, moist inflow to the storm. Hydrometeor seeding could be occurring at mid- to upper levels as one storm downstream of another could be receiving hydrometeors aloft from the storm trailing it. This could enhance precipitation loading and influence thermodynamics of the downstream storm all the way to the generation of its cold pool.

Once again, the methodology developed herein cannot account for these types of storm interactions. These interactions often occur on spatial and temporal scales too small to be resolved by the model grid scale used in this study. Further, it is still an active area of research examining how these storm interactions influence supercell evolution; therefore, the result of storm interactions is still somewhat unknown. It is possible that these storm interactions may be responsible for differences in tornado production within a group of proximate supercells. While it may be possible to infer storm-scale interactions and small-scale environmental heterogeneities using dual-pol radar and other methods, it is currently unknown if those are reliable methods for the observational network to resolve such small-scale influences on storm evolution.

Selecting the 75th percentile of the distribution of environmental similarity values to represent the quantitative environmental similarity threshold needs to be considered carefully. Rather than using this threshold value to state that two supercells being compared are in a quantitatively similar environment, a more realistic statement would be that the two supercells being compared are in a *seemingly* similar environment, according to the model grid scale. Furthermore, it is possible to have a situation where two supercells have similar environmental values for all variables except 0-1 km SRH, and still produce an environmental similarity value greater than 0.6571. It is also possible to perform the above methodology for two supercells that occurred on different dates and in different regions, and still produce an environmental similarity value greater than 0.6571. Therefore, it is recommended that this methodology as currently described be used cautiously when comparing supercells that occurred on different days and/or in different regions.

III: Selecting Storm Pairs

This methodology was then applied to each proximity supercell group in Table 1 to assess degree of environmental similarity within the group. Comparisons of environments here were only performed between tornadic and non-tornadic supercells within the same group (tornadic – tornadic or non-tornadic – non-tornadic comparisons were not performed). Therefore, if in a given proximity supercell group only one tornadic supercell was present, that supercell environment was set as the base environment for comparison (all environmental differences were calculated according to that environment). This was also done if in a given proximity supercell group only one non-tornadic supercell was present, with the non-tornadic supercell environment set as the base for comparison. In many situations, proximity supercell

groups consisted of multiple tornadic and non-tornadic supercells. For these groups, multiple comparisons were performed between each possible pair of tornadic – non-tornadic supercells, with the tornadic supercell environment always being used as the base environment for comparison.

Once comparisons within each group were performed, it was then ensured that at least one tornadic – non-tornadic supercell pair within each group produced an environmental similarity value greater than 0.6571. Nine groups did not have any environmental similarity value greater than 0.6571 and were no longer included in our dataset (Table 1). Next, in the remaining 46 proximity supercell groups with sufficient environmental similarity values, we selected the tornadic – non-tornadic supercell pair that exhibited the highest degree of environmental similarity to be used for comparison and analysis of their respective dual-pol signatures. One tornadic – non-tornadic supercell pair was selected that did not have the highest environmental similarity value in the group. This was to preferentially select the more intense tornadic supercell (EF-3 vs EF-0). The environmental similarity value for the EF-0 tornadic supercell compared to the non-tornadic supercell was 0.8085, while the environmental similarity value for the EF-3 tornadic supercell compared to the same non-tornadic supercell was 0.8054. Therefore, both comparisons resulted in similarly high degrees of environmental similarity (0.38% difference). As a comparison between more high impact tornadic supercells and non-tornadic supercells in similar environments will likely be more valuable, we preferentially selected the EF-3 tornadic supercell to be used for this particular pair. This process of pair selection resulted in 46 pairs of tornadic and non-tornadic supercells (92 total

supercells – 46 tornadic, 46 non-tornadic) in seemingly similar environments to be used for comparison of dual-pol radar signatures (Table 3).

Table 3: The 46 pairs of tornadic and non-tornadic supercells in similar environments retained for polarimetric analysis and comparison. The first column indicates the group number from which the pair originates in Table 1. For the time column, the time in parenthesis indicates the time of maximum low-level rotation in the non-tornadic supercell of the pair.

Group # of Origin	Time of tornadogenesis (max NROT; UTC)	Nearest Radar(s)	Environmental Similarity Value
1	0018 (0016)	KFWS and KTLX	0.8429
2	0232 (0458)	KFDX and KLBB	0.7293
3	2249 (0002)	KDDC and KFDR	0.8742
5	2250 (2123)	KCYS	0.6639
6	2303 (2232)	KDMX	0.8367
7	2246 (2208)	KUEX	0.7974
8	2138 (2242)	KFDR	0.7833
9	2150 (2235)	KDDC	0.9276
11	2019 (1906)	KFTG	0.7943
12	2242 (2307)	KUEX	0.8719
13	2044 (2112)	KUEX	0.9480
15	2000 (2006)	KEOX and KMXX	0.7249
16	2319 (1919)	KBMX and KDGX	0.8536
17	2131 (2317)	KLSX	0.7858
18	2215 (2348)	KSGF and KSRX	0.8338
19	2320 (2252)	KDDC	0.7728
20	2127 (2047)	KAMA and KLBB	0.8704
21	2223 (2334)	KLBB and KMAF	0.8005
22	0145 (0244)	KINX and KSGF	0.9298
23	2314 (2223)	KAMA	0.9652
24	2257 (2252)	KAMA and KLBB	0.8487
25	2356 (2351)	KIWX	0.8054
26	1945 (2027)	KCCX and KPBZ	0.9211
28	1848 (1906)	KLWX	0.7802
29	0615 (2256)	KDYX	0.7180
30	2233 (0007)	KGWX	0.8093
31	0043 (0052)	KDVN	0.7659
32	0058 (0014)	KHPX and KVWX	0.7934
33	0052 (2346)	KPAH and KNQA	0.6894
34	2145 (2246)	KDGX	0.9252

Table 3 (continued): The 46 pairs of tornadic and non-tornadic supercells in similar environments retained for polarimetric analysis and comparison. The first column indicates the group number from which the pair originates in Table 1. For the time column, the time in parenthesis indicates the time of maximum low-level rotation in the non-tornadic supercell of the pair.

Group # of Origin	Time of tornadogenesis (max NROT; UTC)	Nearest Radar(s)	Environmental Similarity Value
35	2232 (0016)	KCAE	0.7144
36	1412 (1515)	KEWX	0.7944
37	0150 (0130)	KTWX	0.8382
38	2241 (0052)	KPOE	0.8189
39	0215 (0058)	KPUX	0.8512
41	0232 (0144)	KSRX	0.9002
42	1929 (1727)	KDVN	0.8038
43	1856 (2046)	KILX	0.8658
44	2215 (2359)	KAMA and KLBB	0.7015
45	2326 (2135)	KMLB and KTBW	0.7271
46	2117 (1952)	KMVX	0.8409
47	2350 (0033)	KLNX	0.9533
48	2225 (0103)	KABR	0.7192
51	0139 (0038)	KARX	0.7641
52	2235 (1734)	KFCX	0.7258
55	2019 (1944)	KLTX	0.7769

IV: Quantifying Dual-Polarization Radar Signatures

Each tornadic and non-tornadic supercell pair was then analyzed using the Supercell Polarimetric Observation Research Kit (SPORK), an algorithm developed at the University of Nebraska-Lincoln for tracking and quantifying dual-pol radar signatures within storms (Wilson and Van Den Broeke 2021). The SPORK algorithm ingests radar data and identifies storms within a radar volume by contouring reflectivity values greater than 45 dBZ. Any closed contour of 45 dBZ is then set as a storm object and assigned an ID for tracking purposes. Storm objects larger than 300 km^2 are divided into multiple storm objects using a second, higher-reflectivity contour of 50 dBZ. These contour thresholds are customizable, and thus can be lowered for tracking smaller or elevated supercells or increased for large or embedded storms. To track storm objects from one radar scan to the next, the algorithm uses a radius from the storm centroid to determine if a new storm ID will be assigned or if a previous storm ID will be kept for that storm object in the next scan. Storm centroids in successive radar scans are compared with previous storm centroids in its assigned radius. If a storm centroid from the previous scan is detected in that radius, the storm ID of the previous centroid is maintained for the new centroid. If no storm centroid is detected, the new storm centroid is assigned a new storm ID. This radius is initially set as 10 km however is also customizable and therefore can be adjusted for fast-moving storms.

The SPORK algorithm quantitatively analyzes dual-pol signatures associated with each storm object: Z_{DR} arcs, K_{DP} feet, regions of hailfall, and Z_{DR} columns (Wilson and Van Den Broeke 2021). Figure 3.3 shows an example of SPORK output images used to track storm objects, and Table 4 shows all polarimetric signatures analyzed. Prior to performing these calculations, the

Z_{DR} field is calibrated by analyzing Z_{DR} 1.5 km above the sounding-derived freezing level. The calibration value is subtracted from the Z_{DR} field at all levels to correct Z_{DR} bias. Table 4 summarizes all polarimetric signatures and metrics calculated and the threshold values used to identify each signature within the algorithm.

This process was performed for each radar scan across the analysis period of each storm. Analysis periods were defined as 30 minutes prior to tornadogenesis (the time of the first tornado report) for tornadic supercells to 30 minutes after tornadogenesis. The analysis period was the same for non-tornadic supercells, except surrounding the time of maximum low-level NROT. Then, average and median values for each metric were recorded for: 1) the entire analysis period, 2) the pretornadic/pre-maximum NROT analysis period, and 3) the post-tornadic/post-maximum NROT analysis period. Because of factors such as variations in radar scanning techniques from radar to radar (resulting in more or fewer scans within the 30-minute time prior to tornadogenesis for different cases), for storms developing and becoming tornadic quickly (within less than 30 minutes following initiation), or storms losing supercell characteristics shortly after the first tornado report, the number of scans for each storm analysis period varied. Each storm was required to have at least three scans for pretornadic (or pre-maximum NROT) analysis times, which ensured at least 15 minutes of data prior to tornadogenesis. The same requirement was made for post-tornadic (or post-maximum NROT) analysis times. All except for two storms had sufficient scans for every section of the analysis period. One non-tornadic storm had only two scans prior to maximum NROT, therefore that storm and its tornadic counterpart were not included in pre-tornadogenesis comparisons. This storm pair was still included in post-tornadogenesis comparisons however, as sufficient scans

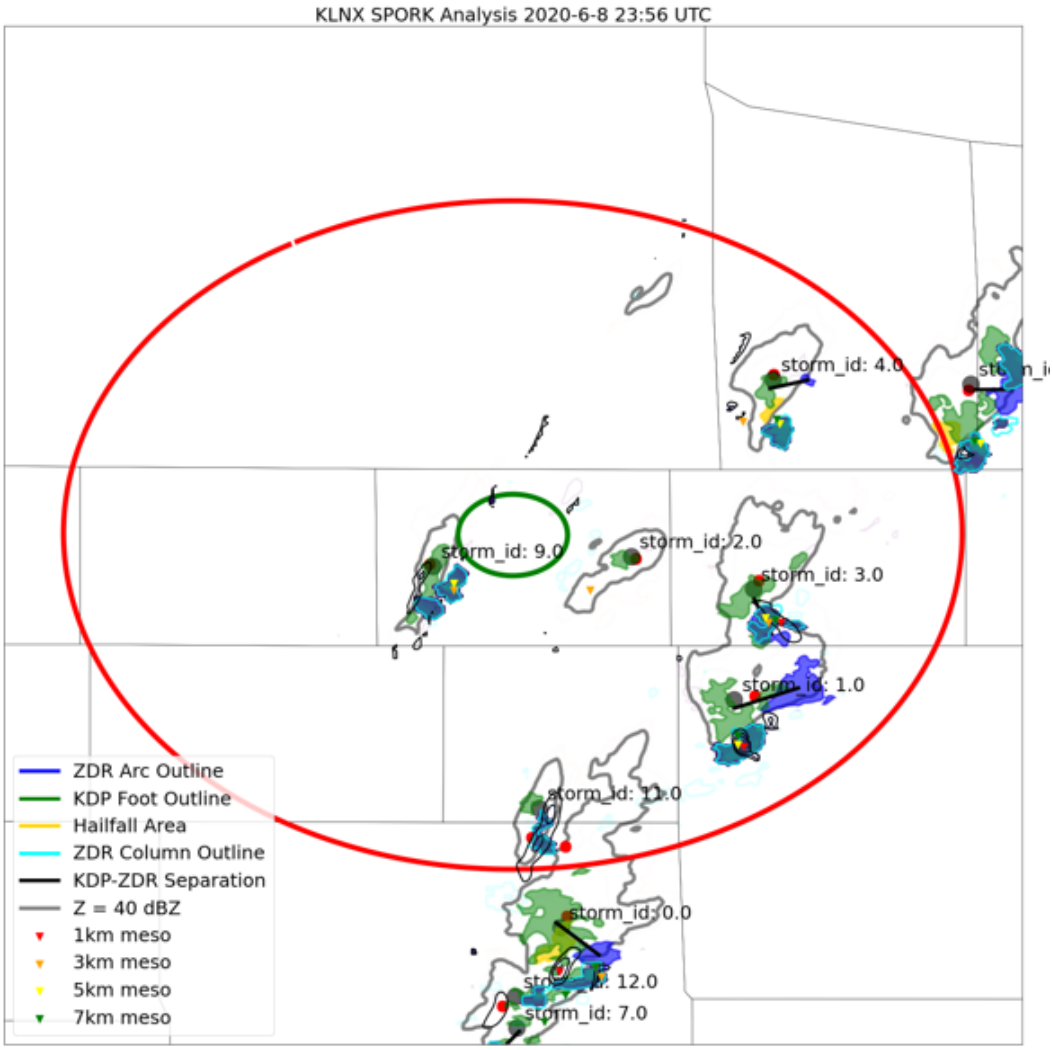

Figure 3.3: An example SPORK output image used to track and identify convective cells from 8 June 2020 (group 47 in Table 1). Grey dots are placed at storm centroids. Grey lines outline areas of >40 dBZ. Blue shaded areas show Z_{DR} arcs, green shaded areas show K_{DP} feet, and yellow areas show hailfall areas. Light blue lines outline Z_{DR} columns. Black lines show the separation between the K_{DP} foot and the Z_{DR} arc. Different colored triangles indicate areas of mesocyclonic rotation, as indicated in the legend. The radar is at the center of the green circle at the image center.

Table 4: Polarimetric variables and metrics collected from the SPORK algorithm and compared between tornadic and non-tornadic storms. The third column from the left indicates the threshold value used in the algorithm to contour the given polarimetric signature. Variables that replaced zeros with "NaNs" are indicated in the rightmost column.

Signature	**Metric (units)**	**Threshold**	**Replaced Zeros with "NaNs"?**
Z_{DR} Arc	Area (km^2)	3.25 dB	No
	Maximum Value (dB)	--	Yes
	Mean Value (dB)	--	Yes
	10 Maximum Values (dB)	--	Yes
	Median Value (dB)	--	Yes
Hailfall	Area (km^2)	≥50 dBZ collocated with Z_{DR} ≥1 dB	No
K_{DP} Foot	Area (km^2)	1.5 ^{o} km^{-1}	No
	Maximum Value (deg km^{-1})	--	Yes
Reflectivity	Area (km^2)	35 dBZ	No
	Maximum Value (dBZ)	--	No
	Core Average (dBZ)	--	No
K_{DP}-Z_{DR} Separation	Distance (km)	--	Yes
	Angle (deg)	--	Yes
Z_{DR} Column	Area (km^2)	0.5 dB above 0^{o}C height	No
	Maximum Depth (km)	# Of grid points meeting Z_{DR} column area threshold above 0^{o}C height	No
	Mean Depth (km)	As for column maximum depth	No

were present for that analysis period. One tornadic storm had only two scans after tornadogenesis, therefore that storm and its non-tornadic counterpart were excluded from post-tornadogenesis comparisons. This storm pair was still included in pre-tornadogenesis comparisons however, as sufficient scans were present for that analysis period.

When calculating average and median values for each metric, the option was available to either include zeros in the calculation or set all zeros to "NaN" (Not a Number), thus removing them from the calculation. This may be desired for metrics where a value of exactly zero is unrealistic, such as separation angle. An exact separation angle of zero degrees between the K_{DP} foot and the Z_{DR} arc is unrealistic, however the SPORK algorithm does not record very small, non-zero values. Therefore, for situations where the separation angle is very small and non-zero, that metric value is set to zero in the algorithm. This is largely a result of the observational network resolution not being able to capture the minute details of metric observations at times. Therefore, for certain variable metrics where an exact value of zero is unlikely, we replaced those zeros with "NaN" for calculation purposes. These metrics were separation angles and K_{DP}-Z_{DR} separation distances (Table 4). Additionally, for all Z_{DR} arc metrics other than the arc area, values of zero were replaced with "NaN". This is due to Z_{DR} arc metrics being reported as zero even if no arc signature is present. For example, if no arc signature is present, the algorithm would report an arc area of zero km^2 (which is reasonable to include), yet an arc maximum value of zero dB also. This is an incorrect value to include, since with no arc present, there should be no arc maximum value at all. Therefore, for the Z_{DR} arc maximum value, mean value, the 10 maximum values, and median value, zeros were replaced with "NaNs". By the same argument, for K_{DP} foot maximum values zeros were replaced with "NaNs"

(Table 4). For all other variable metrics zeros were included in calculations, as a value of zero for any of these metrics is reasonable and important to record (e.g., if a storm has no hailfall area, this is an important point when comparing storms). Zeroes were also included for metrics where zeros never occur in the dataset for those metrics (e.g., a value of zero for reflectivity maximum and average does not occur in supercells).

Trend analysis was also performed for each metric within each storm. This was performed by subtracting the metric mean value in the pretornadic/pre-maximum NROT analysis period from the metric mean value in the post-tornadic/post-maximum NROT analysis period for the same storm. Thus, a negative value indicated a decrease in that metric across the analysis period, while a positive value indicated an increase in that metric. For statistical purposes (which will be discussed in the following section), the direction of subtraction for trend analysis resulted in the same outcome either way. As an additional assessment of how the degree of environmental similarity between two supercells relates to differences in dual-pol signatures, correlations between dual-pol metric differences and environmental similarity values were examined. Finally, to test the hypothesis that tornadic mesocyclones are stronger than non-tornadic mesocyclones, low-level maximum NROT values within the analysis period were recorded for tornadic supercells as well. This was done manually in Gibson Ridge Analyst-2 software.

V: Statistical Comparisons

To test for statistically significant differences in metrics, a Mann-Whitney U-test (Wilcoxon rank sum test) at the 5% significance level was used to test for differences between

the 46 tornadic and the 46 non-tornadic supercells as their own populations (i.e., this test for differences does not account for similar environments, rather is merely comparing the tornadic dataset to the non-tornadic dataset separately). The Mann-Whitney U-test does not assume a Gaussian distribution. This test was performed for all metric comparisons and mesocyclone strength comparisons. Comparisons were performed between the 46 tornadic and 46 non-tornadic supercells for the entire analysis period, the pretornadic/pre-maximum NROT analysis period, and the post-tornadic/post-maximum NROT analysis period.

To test for statistically significant differences between pairs of tornadic and non-tornadic supercells in similar environments (pairwise comparisons), the Wilcoxon signed rank test and the paired t-test were used at the 5% significance level. The Wilcoxon signed rank test does not assume a Gaussian distribution in the differences between two datasets, while the paired t-test does assume a Gaussian distribution. Therefore, the Shapiro-Wilk normality test was performed on each distribution of differences for each metric between tornadic and non-tornadic supercells. If the distribution of differences for a metric was normally distributed, the paired t-test was used. If the distribution was not normally distributed, the Wilcoxon signed rank test was used.

Unfortunately, since "NaN" replaced zeros for several dual-pol metrics, several storms no longer met the scan requirement to be included *only for those dual-pol metric calculations*. This resulted in many storms being removed from calculations for: Z_{DR} arc metrics (other than arc area), K_{DP} foot maximum value, and K_{DP}-Z_{DR} arc separation distances and angles. For these particular metrics, the sample size used in the statistical calculations was less than 30 for

several metrics, which is shown in Tables 5 and 6. Therefore, results for these particular metrics and analysis periods are not as statistically robust.

Table 5: Sample sizes for tornadic – non-tornadic population comparisons of polarimetric features where zeros were replaced with "NaN". These sample sizes were used for individual population comparisons between tornadic and non-tornadic supercells only for these variables. Asterisks denote sample sizes that may not produce statistically robust results for those particular variables (n < 30).

Variable	**Tornadic Sample Size**	**Non-Tornadic Sample Size**
Full Analysis Period		
K_{DP}-Z_{DR} Separation Distance	35	40
K_{DP}-Z_{DR} Separation Angle	33	38
Z_{DR} Arc Maximum, Mean, Median, and 10 Maximum Values	36	42
K_{DP} Foot Maximum Value	46	46
Pre-tornadogenesis – Pre-Maximum NROT Period		
K_{DP}-Z_{DR} Separation Distance	31	32
K_{DP}-Z_{DR} Separation Angle	*28	*27
Z_{DR} Arc Maximum, Mean, Median, and 10 Maximum Values	32	32
K_{DP} Foot Maximum Value	46	45
Post-Tornadogenesis – Post-Maximum NROT Period		
K_{DP}-Z_{DR} Separation Distance	*29	30
K_{DP}-Z_{DR} Separation Angle	*29	*29
Z_{DR} Arc Maximum, Mean, Median, and 10 Maximum Values	30	30
K_{DP} Foot Maximum Value	45	44

Table 6: As in Table 5, except for pairwise comparisons of tornadic and non-tornadic supercells in similar environments for the same variables. Note that in these comparisons, if one supercell of the pair had too few scans for the particular variable being compared, that complete pair had to be removed – therefore, these sample sizes are much smaller than in Table 5. Asterisks denote sample sizes that are likely too small to produce statistically robust results for those particular variables (n < 30).

Variable	**Pairwise Sample Size**
Full Analysis Period	
K_{DP}-Z_{DR} Separation Distance	34
K_{DP}-Z_{DR} Separation Angle	31
Z_{DR} Arc Maximum, Mean, Median, and 10 Maximum Values	35
K_{DP} Foot Maximum Value	46
Pre-tornadogenesis – Pre-Maximum NROT Period	
K_{DP}-Z_{DR} Separation Distance	*23
K_{DP}-Z_{DR} Separation Angle	*18
Z_{DR} Arc Maximum, Mean, Median, and 10 Maximum Values	*24
K_{DP} Foot Maximum Value	45
Post-Tornadogenesis – Post-Maximum NROT Period	
K_{DP}-Z_{DR} Separation Distance	*21
K_{DP}-Z_{DR} Separation Angle	*21
Z_{DR} Arc Maximum, Mean, Median, and 10 Maximum Values	*22
K_{DP} Foot Maximum Value	44

Chapter IV: Results

I: Comparisons of Tornadic and Non-Tornadic Environments

To compare the findings of this study to previous work on supercell environments, one tornadic sounding and one non-tornadic sounding were taken from each proximity group to be used in comparisons of tornadic and non-tornadic environments. Only two soundings from a group were taken for these comparisons to avoid overrepresenting the group environment. In cases where multiple tornadic and/or non-tornadic supercells existed in a group, a random number generator was used to select the tornadic and non-tornadic soundings to be used. This resulted in 55 tornadic and non-tornadic soundings. The tornadic soundings were divided up as seven significant tornadic environments, and 48 weakly tornadic environments. Comparing environments of tornadic and non-tornadic supercells tended to agree with findings from Thompson et al. (2003) where significant tornadic environments had higher 0-1 km SRH and lower MLLCLs (Figures 4.1 and 4.2), however it is important to recognize the small sample size of significant tornadic environments in this study. No statistical tests were performed between significant tornadic and non-tornadic environments due to the small sample size of significant tornadic cases, yet 0-1 km SRH and MLLCL were not statistically different between tornadic environments collectively and non-tornadic environments ($p = 0.570$ and $p = 0.862$, respectively). MLCAPE seemed to trend towards higher values in tornadic supercells (Figure 4.3), however this result was not statistically significant ($p = 0.205$). Figures 4.1, 4.2, and 4.3 show the median value of 0-1 km SRH and MLCAPE was greater than the median values found by Thompson et al. (2003), and the median value of MLLCL is less than the median value found by Thompson et al. (2003). This may be because non-tornadic supercells in this study shared

environments with tornadic supercells in proximity, suggesting that the non-tornadic supercells were skewed more towards environments favorable for tornadic supercells.

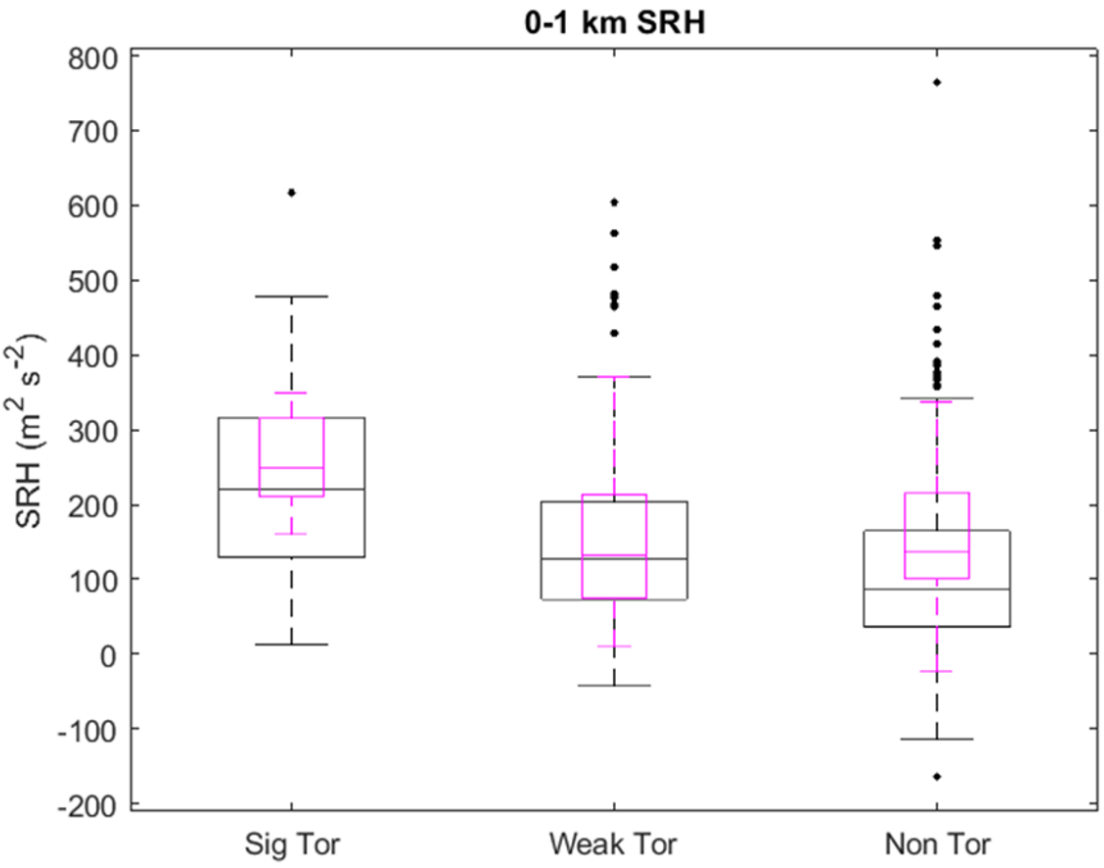

Figure 4.1: Box and whiskers plots of the distributions of 0-1 km SRH for significant tornadic environments, weakly tornadic environments, and non-tornadic environments from this study and the study by Thompson et al. (2003). The black box and whiskers plots are distributions from Thompson et al. (2003), and the purple box and whiskers plots are from this study. The boxes contain values from the 25th percentile to the 75th percentile, with the median value denoted by a horizontal line in the box. Whiskers extend to the nonoutlier minimums and maximums, and outliers are denoted by black dots for the Thompson et al. (2003) data, and red crosses for the data from this study.

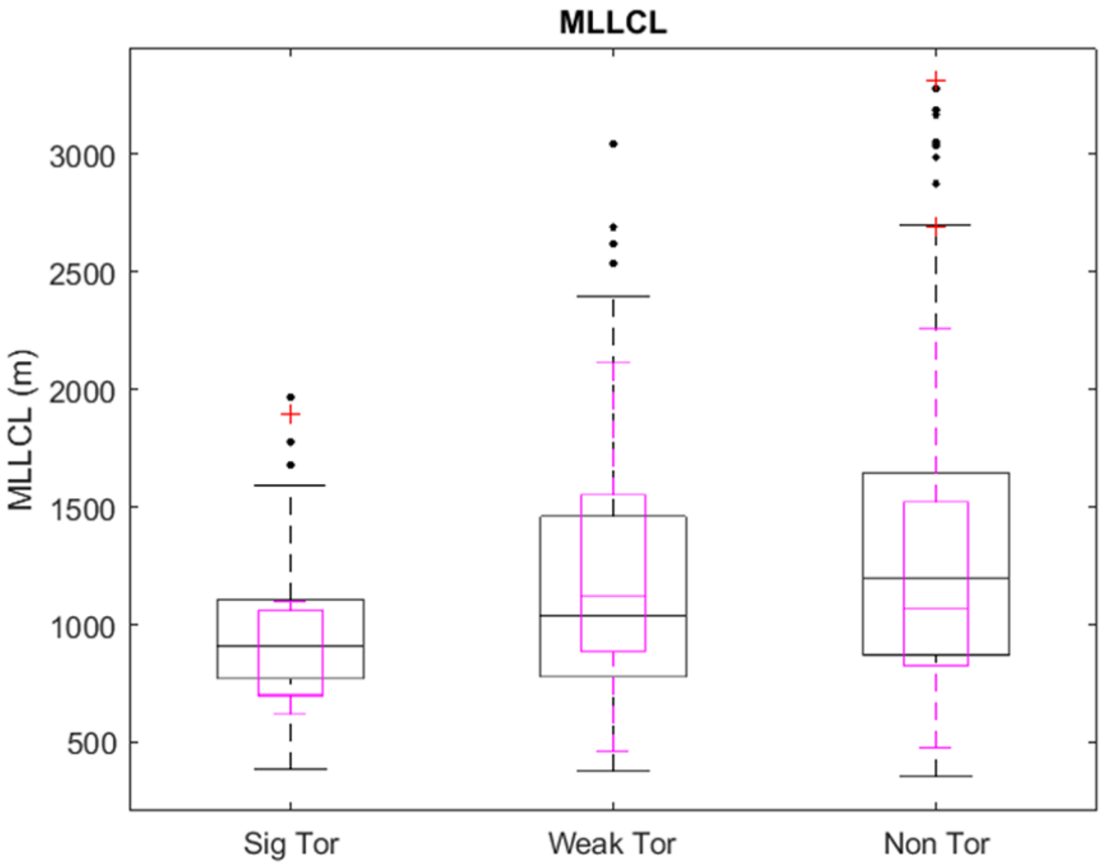

Figure 4.2: As in Figure 4.1., except for MLLCL.

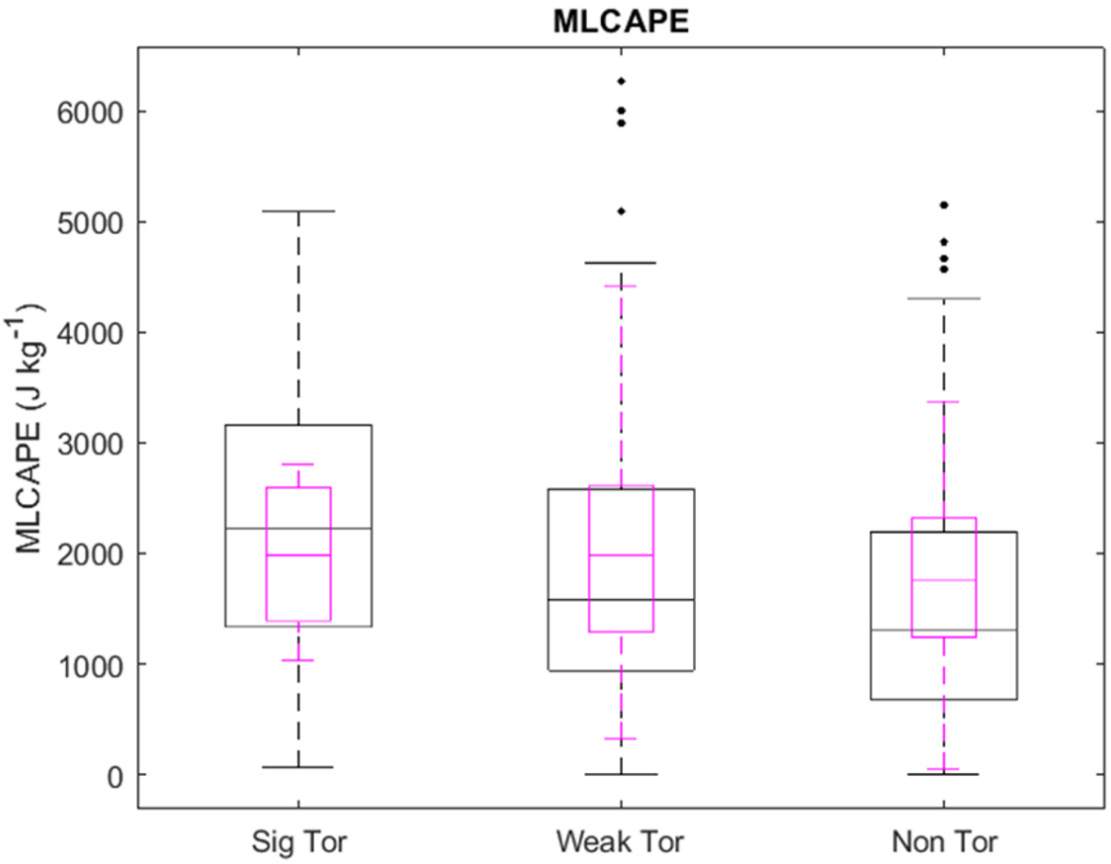

Figure 4.3: As in Figure 4.1., except for MLCAPE.

II: Environmental Similarities Between Proximate Tornadic and Non-Tornadic Supercells

Comparing environments of proximate supercells was found to produce much higher similarity on average than comparing environments of all supercells within the dataset to one another. The mean and median environmental similarity values from comparisons within proximity supercell groups (n = 212) were 0.7149 and 0.7265, respectively. Furthermore, it was found that environmental similarity within proximity supercell groups increased as supercells were closer together in space and time. Proximity supercell comparisons that did not meet the threshold environmental similarity value of 0.6571 were on average 188.3 km apart and separated by 2.2 hours (from the time the soundings were taken). Comparisons that were in the upper 75th percentile of environmental similarities were on average 105.4 km apart and separated by only 1.3 hours. And in the upper 90th percentile the average distance and time between supercell soundings was 96.5 km and 0.8 hours, respectively. The correlation between environmental similarity percentile and distance and time between supercell soundings was strongly negative (r = -0.933 and r = -0.917, respectively. Figures 4.4 and 4.5).

The above results suggest that as supercells occur on more similar spatial and temporal domains, their corresponding background environments become increasingly similar, according to the observational and model spatiotemporal gridscale. This suggests that the ability of environmental characteristics to distinguish between tornadic and non-tornadic supercells decreases in these situations, as more overlap in environmental variables will occur. Therefore, radar methods to discriminate supercells become more reliable. This further motivates this and other research for using radar avenues to assess tornadic potential. This also motivates other

avenues of research examining the effect of small-scale environmental heterogeneities on supercell development and tornado dynamics, and storm interactions.

Model soundings from the RAP may have a warm and dry bias near the surface (Weygandt et al. 2015; Wade et al. 2018). This must be considered for the individual magnitudes of environmental variables such as MLLCL and MLCIN, which are largely impacted by low-level thermodynamics. MLCAPE may also be impacted by this bias, as low-level temperature and moisture can largely influence the overall stability of the atmosphere. While this needs to be considered when using these model soundings, the method used herein comparing two individual soundings is likely unaffected. Any biases would become irrelevant in comparison purposes, as the comparison magnitude would likely be similar if biases were corrected. Figure 4.6 presents the distributions of environmental differences within the proximity group comparisons. MLCIN differed the most in environmental comparisons, with non-tornadic supercell environments usually having greater MLCIN (Figure 4.7); the median MLCIN percent difference was 71.2%. Height of the freezing level was the most consistent environmental variable throughout proximity comparisons, with a median percent difference of 3.5%. 0-6 km BWD was also generally consistent for proximity supercell comparisons. The median percent difference was 10.5%, with the maximum percent difference only 45.0%. MLCAPE, MLLCL, and 0-1 km SRH had variable degrees of environmental similarity between proximate supercells. The median percent difference for MLCAPE was 24.9%, for MLLCL was 21.5%, and for 0-1 km SRH was 28.2%.

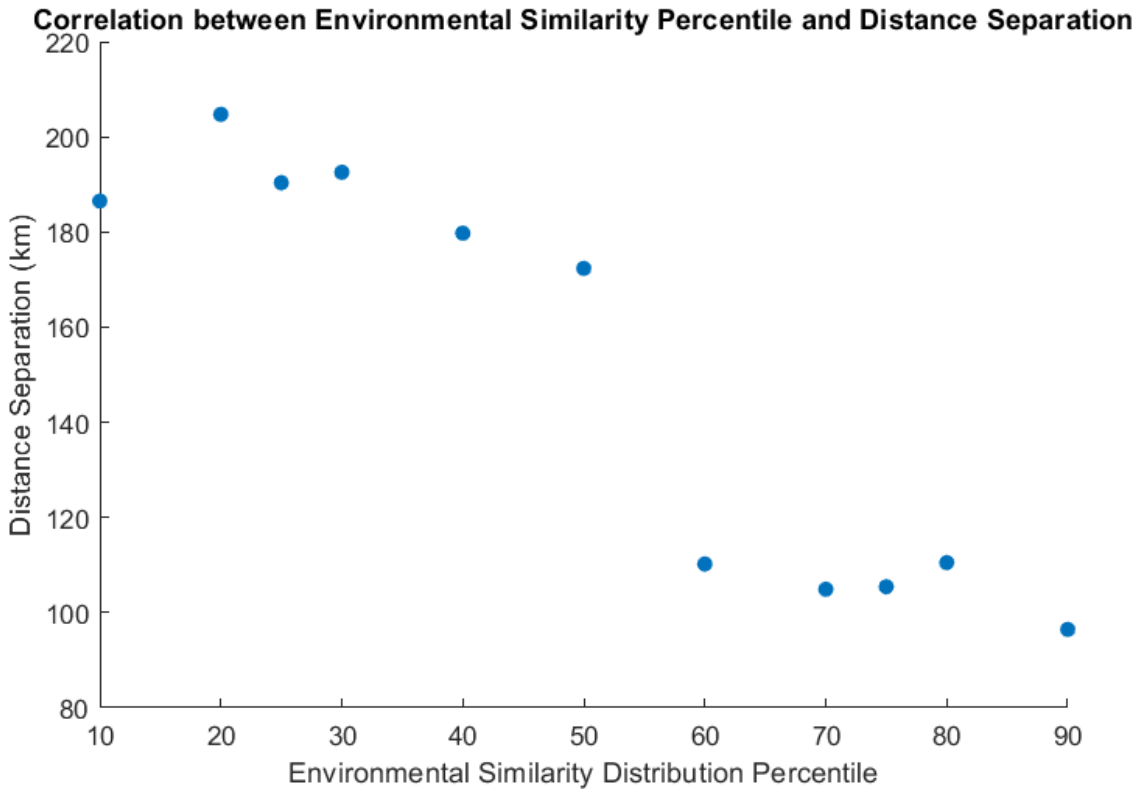

Figure 4.4: Scatterplot of environmental similarity distribution percentile values against distance separation between soundings for comparisons (*r* = -0.933).

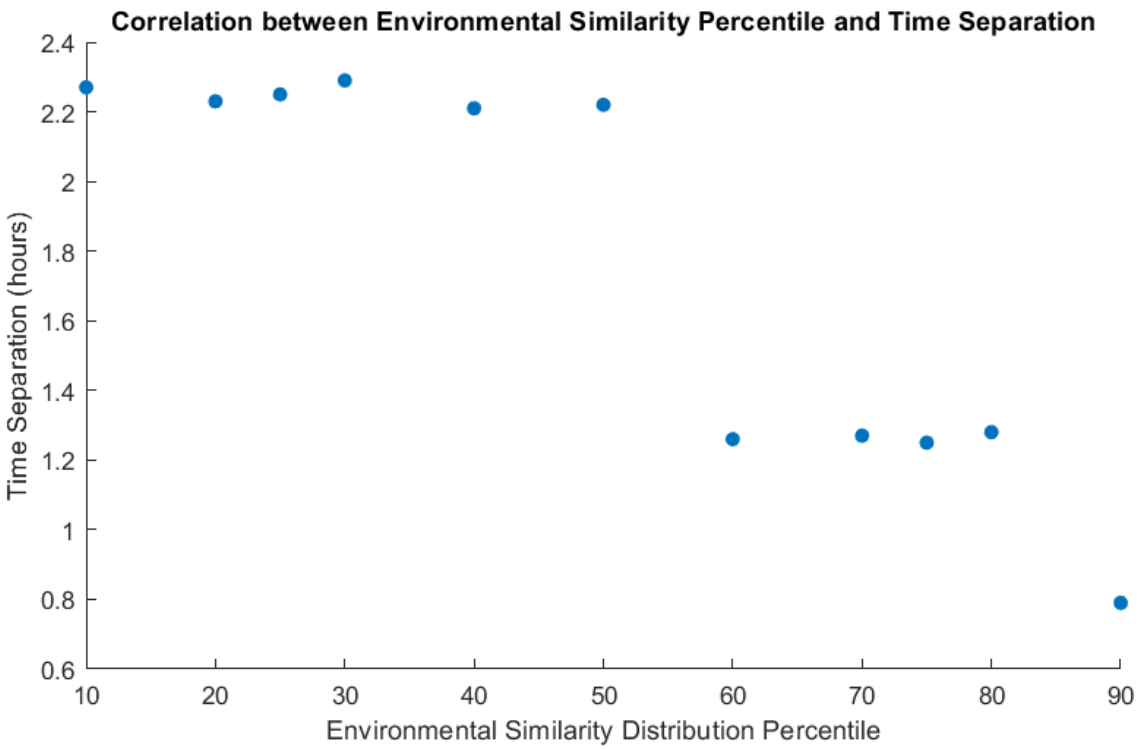

Figure 4.5: As in Figure 4.4., except for environmental similarity distribution percentiles against time between soundings for comparisons (r = -0.917).

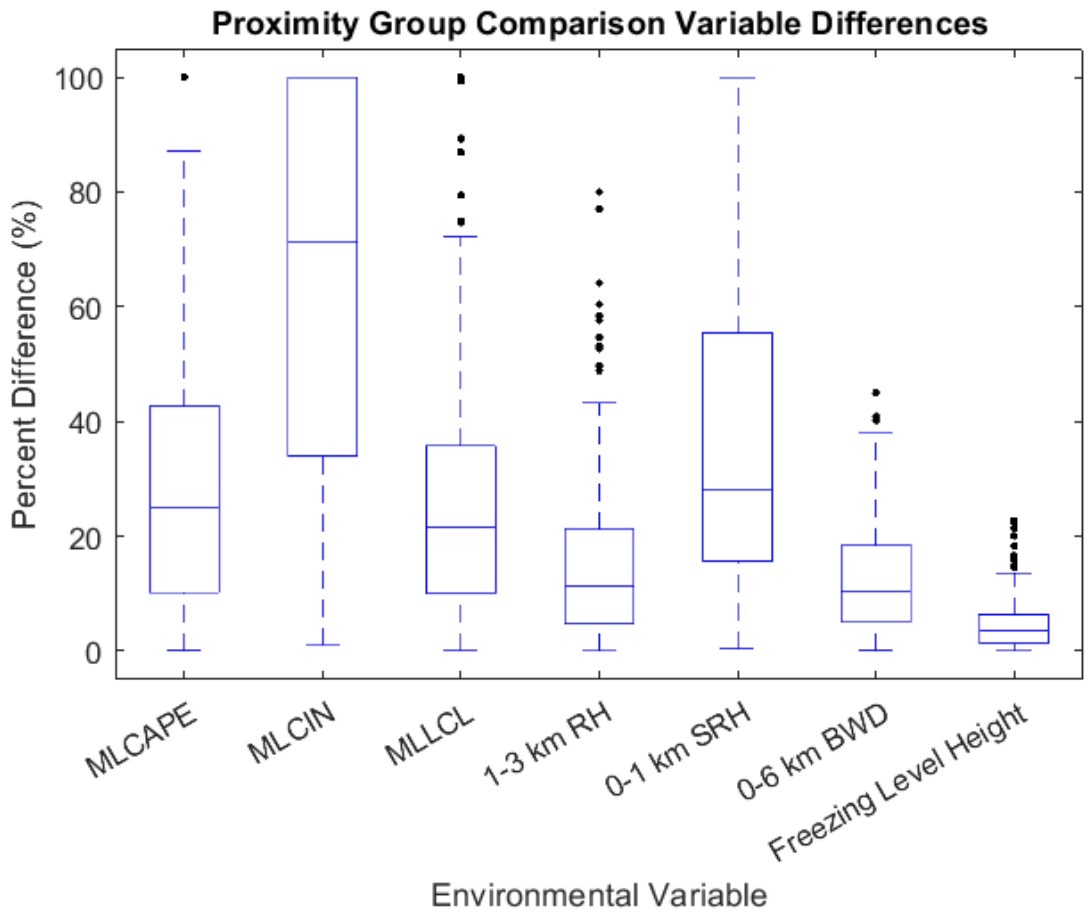

Figure 4.6: Box and whiskers plot of the percent differences for each environmental variable used in comparisons of proximity supercells. The above shows the distribution of percent differences for all comparisons done within the 55 proximity groups initially collected, in Table 1 (total number of comparisons = 212). Box and whiskers distributions are as in Figure 4.1, except black dots denote outliers for this data.

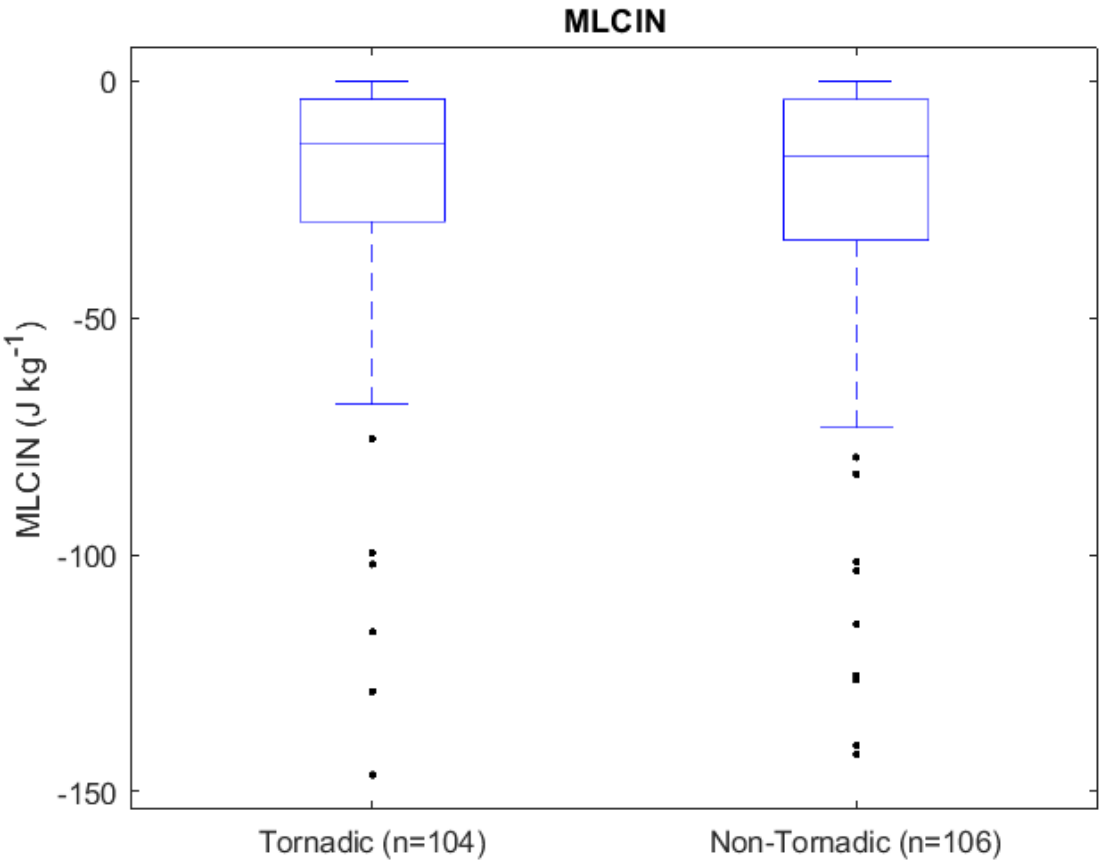

Figure 4.7: Box and whiskers plot of the distribution of MLCIN for the tornadic environments compared to the non-tornadic environments. Box and whisker distributions are as in Figure 4.6.

However, this does not completely disregard the ability of environmental variables to distinguish between tornadic and non-tornadic supercells even when in proximity. Nine groups were collected that had tornadic and non-tornadic supercells in proximity, however had no tornadic – non-tornadic pair that exhibited a high enough degree of environmental similarity for our study. In those nine groups, the median percent difference for MLCAPE, MLCIN, MLLCL, and 0-1 km SRH all increased substantially (Figure 4.8). It is likely due to the large differences between MLLCL and 0-1 km SRH that these groups were excluded and may also explain the differences in tornado production within those groups. Furthermore, in exactly half of our proximity pairs that were retained for this research (23/46), the tornadic supercell did have greater 0-1 km SRH. Therefore, some may argue that 0-1 km SRH would still be a discriminating factor in those cases. On the other hand, some non-tornadic supercells had greater 0-1 km SRH than the corresponding tornadic counterpart. Therefore, in some scenarios, environmental variables may still prove valuable to assess tornadic potential within groups of supercells. For most cases, supercells in proximity can be assumed to have seemingly similar environments at the scale of the observational and model gridscale, and radar methods are preferred to distinguish between likely storm outcomes.

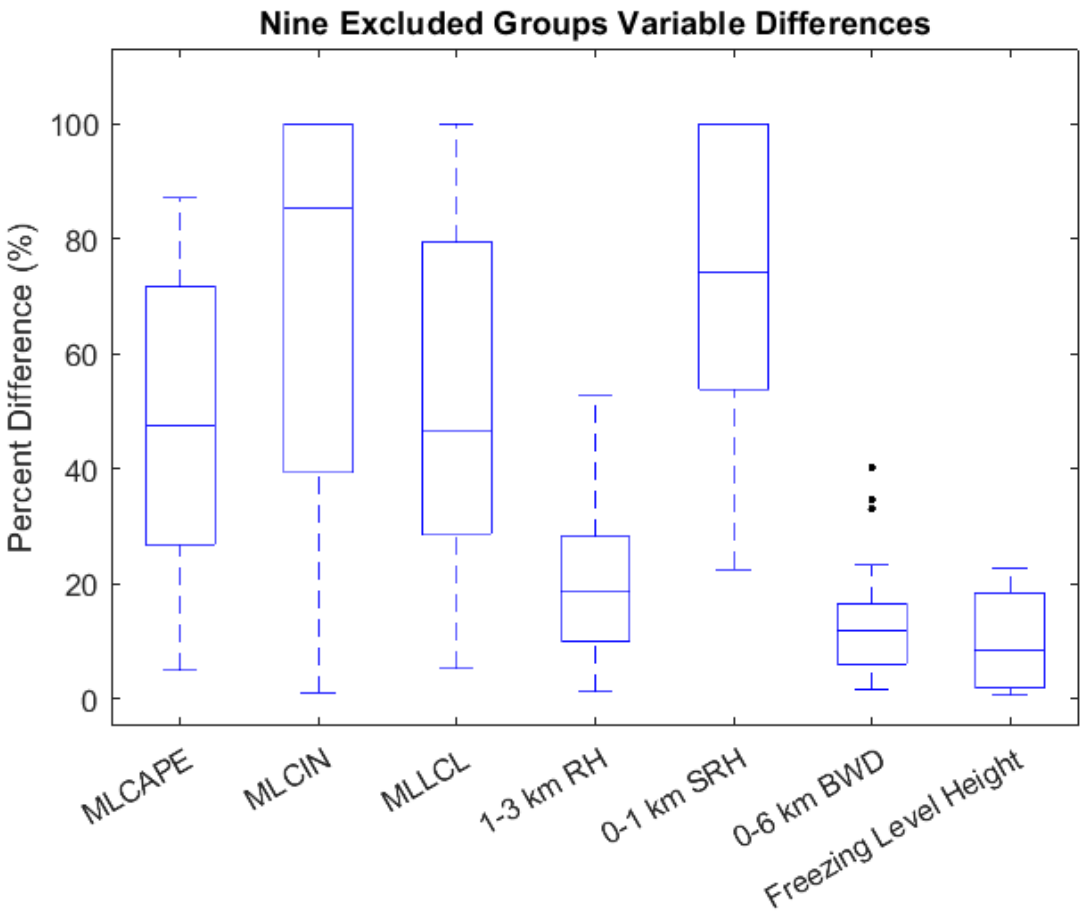

Figure 4.8: Box and whiskers plot of the percent differences for each environmental variable for the comparisons performed within the nine proximity groups that did not meet the threshold of 0.6571. The box and whiskers distributions are as in Figure 4.6.

Comparisons of environmental variables clearly showed that deep-layer environmental variables, such as 0-6 km BWD and height of the freezing level, are less variable. This result is not surprising, as freezing level height is largely a synoptic-scale environmental variable and typically varies over large distances or between different air masses. As all proximity supercell groups were shown to each be within a same air mass, freezing level heights were expected to be very similar. The high degree of similarity in 0-6 km BWD is likely due to the same reason. Increases in 0-6 km BWD are linked to passages of upper-level synoptic features and jet streaks. Therefore, supercells in proximity were unlikely to experience large differences in 0-6 km BWD.

Variables confined to lower levels of the atmosphere and that primarily represent mesoscale environments (e.g., MLCIN, MLLCL, and 0-1 km SRH) tend to have much higher variability. This is particularly intriguing as low-level mesocyclogenesis and tornadogenesis are thought to be largely dependent on low-level environmental conditions (e.g., Thompson et al. 2003; Coniglio and Parker 2020). This may be because low-level environmental parameters are more heavily influenced by terrain characteristics and friction. Diurnal heating at low-levels is also much more variable through the lower atmosphere, which could influence the low-level environmental conditions more so than in the mid- to upper-levels of the atmosphere. Despite no statistical differences in MLLCL and 0-1 km SRH occurring between tornadic and non-tornadic supercells in this dataset, it may be worth considering that even small differences in these variables may result in tornado production in some supercells, while not in others within a group. This may be particularly true for 0-1 km SRH, as Bunkers et al. (2022) found that for tornadic and non-tornadic supercells in proximity, the tornadic storm tended to deviate more to the right of forecast storm motion (Bunkers et al. 2000). This extra rightward deviation would

enhance 0-1 km SRH in the near inflow environment and could therefore support tornadogenesis. This also may suggest that the higher degree of 0-1 km SRH variability between proximate storms may not be entirely due to different wind profiles in the lower atmosphere, but also from differences in storm motion. For two identical hodographs, differences in storm motion would result in variations of 0-1 km SRH. Therefore, modifications of the near-storm environment by the storm itself may be more critical for assessing tornadic potential than examining the background storm environment by itself.

Within the 46 proximate supercell pairs, the median percent difference for all variables decreased substantially (Figure 4.9). All median percent differences except for MLCIN were ≤20%. The 75th percentile of MLLCL, 1-3 km RH, 0-6 km BWD, and height of the freezing level were all below 20%. The median percent difference of MLCIN decreased substantially to 41.0%. Since much research has found that tornadic supercell environments typically possess larger 0-1 km SRH and lower LCLs, we checked for statistically significant differences in these variables in the 46 proximate supercell pairs. Using a Mann-Whitney U-test to compare tornadic and non-tornadic populations separately, no statistically significant differences were found for either variable (Figures 4.10 and 4.11). Furthermore, pairwise comparisons of MLLCL and 0-1 km SRH were performed to determine if in our 46 pairs these variables could distinguish between the tornadic and non-tornadic supercell environment. Pairwise comparisons resulted in no statistically significant differences. (p = 0.9 for 0-1 km SRH and p = 0.581 for MLLCL; Figure 4.12).

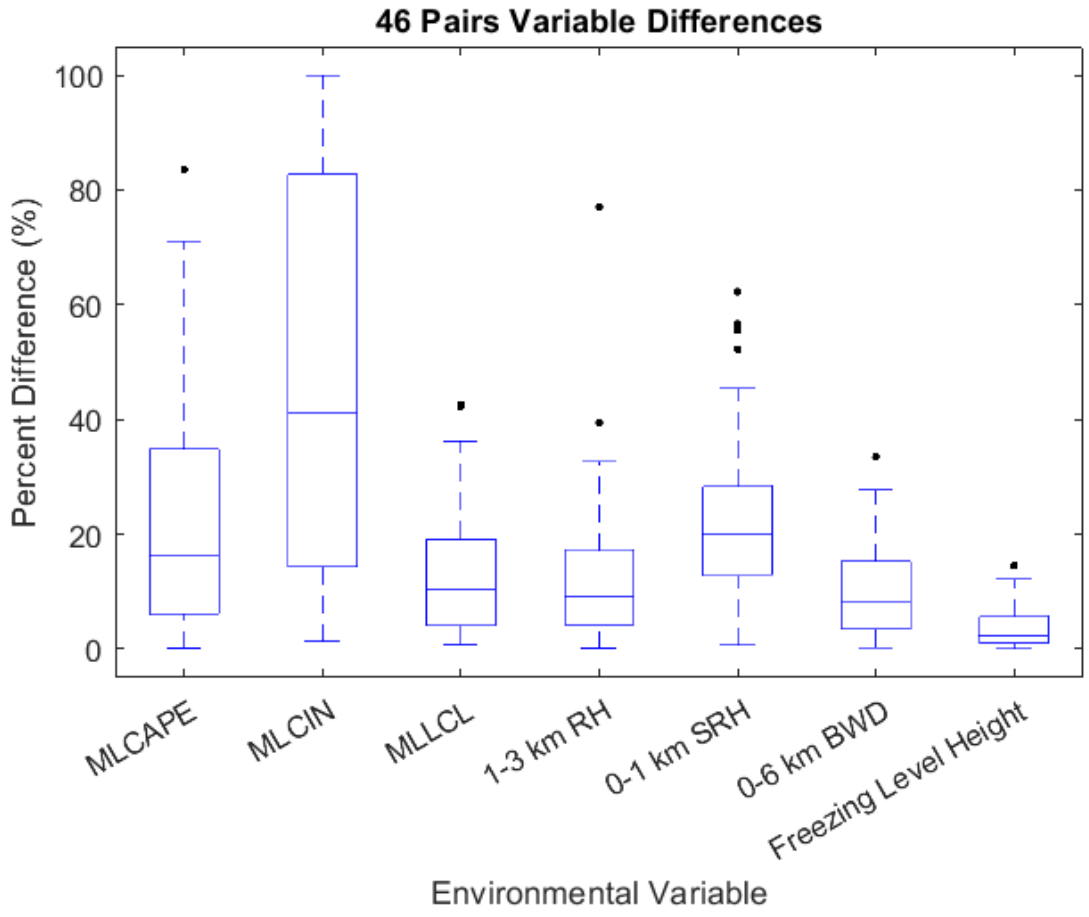

Figure 4.9: As in Figure 4.6., except only for the comparisons of environments of the 46 tornadic – non-tornadic supercell pairs ultimately retained for analysis in this study, shown in Table 2.

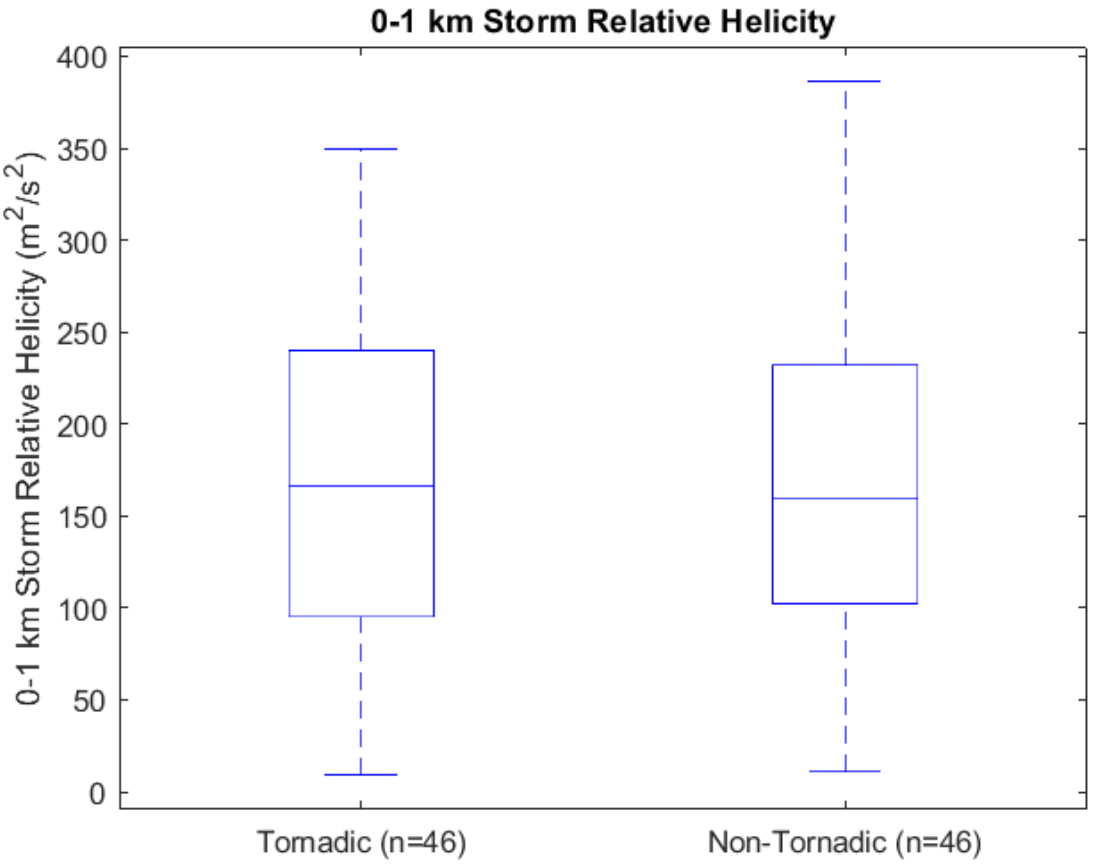

Figure 4.10: Box and whiskers plot for 0-1 km SRH of all 46 tornadic supercells and all 46 non-tornadic supercells ultimately used in the analysis, shown in Table 2. Box and whiskers distributions are as in Figure 4.6.

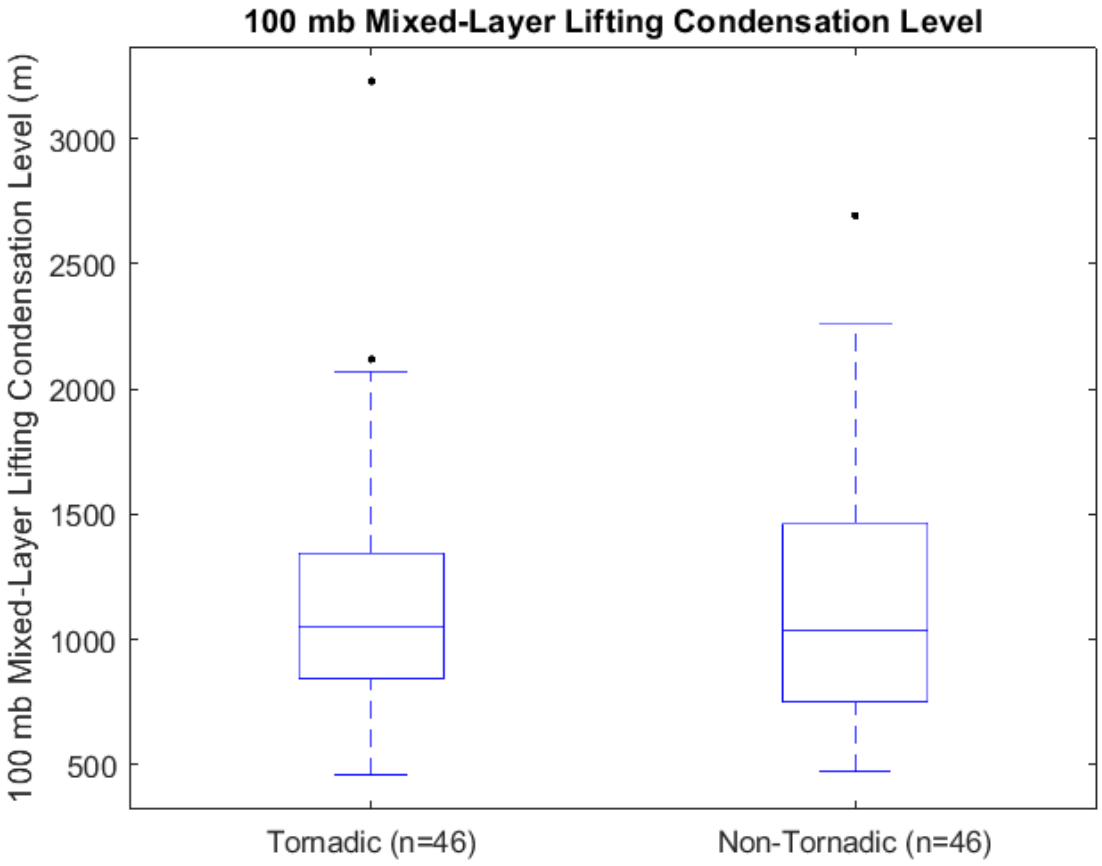

Figure 4.11: As in Figure 4.10., except for MLLCL. Box and whiskers distributions are as in Figure 4.6.

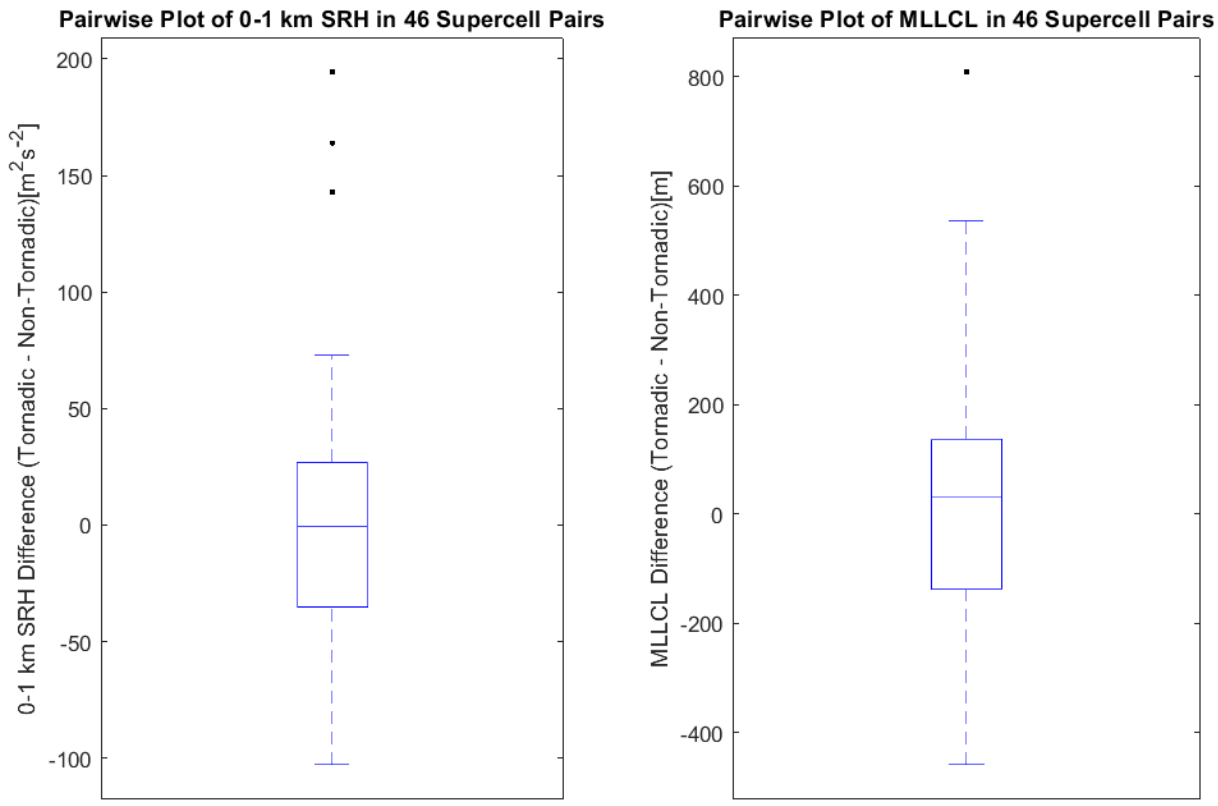

Figure 4.12: Pairwise plot of 0-1 km SRH (left) and MLLCL (right) between the 46 tornadic and non-tornadic supercells in similar environments, shown in Table 2. Values plotted are equal to the tornadic environment variable minus the non-tornadic environment variable, such that values above zero indicate the tornadic supercell environment had a greater value. Box and whiskers distributions are as in Figure 4.6.

The significant decrease in environmental variable percent differences within the 46 pairs used for analysis is encouraging. This shows that within our initial dataset of 55 groups and 210 supercells, these 46 pairs generally had the most similar environments. Additionally, differences in MLLCL and 0-1 km SRH between tornadic and non-tornadic supercells within these 46 pairs were not statistically significant. Therefore, the ability for those variables to distinguish between tornadic and non-tornadic environments as found by prior studies (e.g., Coniglio and Parker 2020; and many others) was somewhat removed. This is encouraging for polarimetric signature comparisons in this study, as external forcing from the background environment was highly controlled for within these pairs. However, as mentioned previously, a potential area of research using proximity supercells could assess whether even small magnitude differences (i.e., less than 10% difference) in MLLCL or 0-1 km SRH could result in tornadogenesis in some cases.

III: Mesocyclone Comparisons

Prior to comparing low-level mesocyclone strength between tornadic and non-tornadic supercells, we checked for any correlation between NROT values and distance from the radar and elevation of the mesocyclone. This was to ensure that the strength of mesocyclones according to NROT are not under- or overestimated depending on distance from the radar and height above the ground. We found that distance from the radar had a very weak correlation with NROT (r = 0.198 for tornadic mesocyclones and r = 0.231 for non-tornadic mesocyclones; Figure 4.13). Elevation of the mesocyclone also had a very weak correlation with NROT (r = 0.142 for tornadic mesocyclones and r = -0.109 for non-tornadic mesocyclones; Figure

4.14). Therefore, distance from the radar and elevation of the mesocyclone were not a concern for measuring mesocyclone strength with NROT.

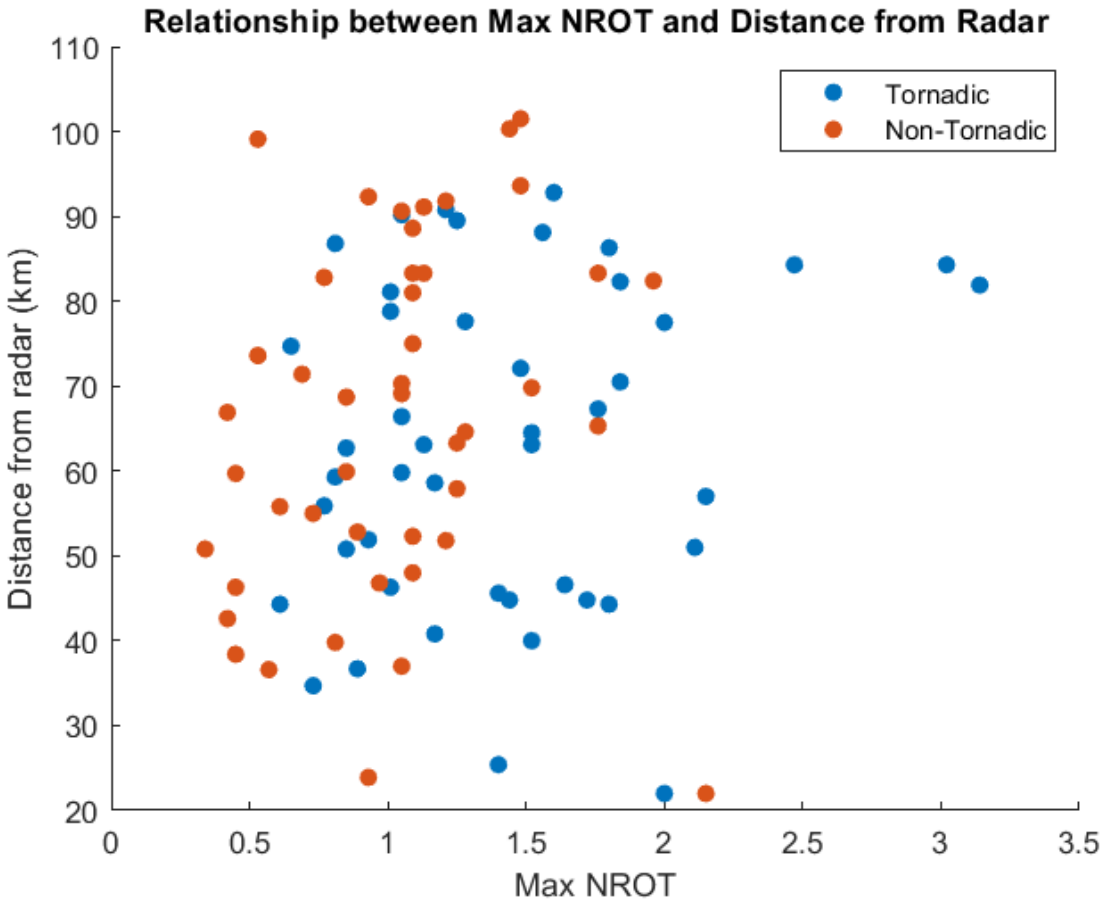

Figure 4.13: Scatterplot of tornadic and non-tornadic mesocyclone maximum NROT values against distance from the radar (r = 0.198 for tornadic storms, r = 0.231 for non-tornadic storms).

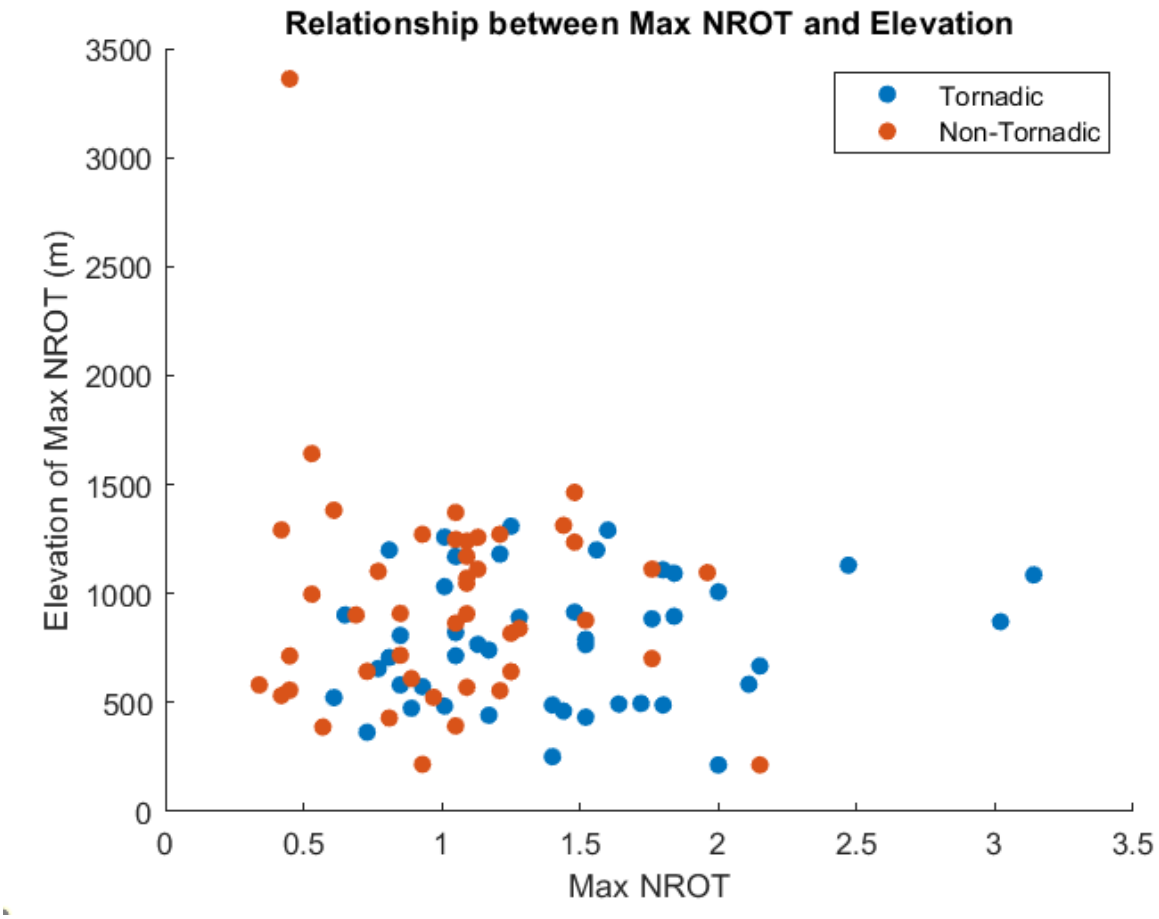

Figure 4.14: As in Figure 4.13., except against elevation of the maximum NROT value for tornadic and non-tornadic mesocyclones (r = 0.142 for tornadic storms, r = -0.109 for non-tornadic storms).

One non-tornadic supercell passed extremely close to the radar during the estimated peak NROT period (within <10-15 km from the radar). Therefore, an accurate value of maximum NROT for this supercell was not able to be obtained, as NROT values close to the radar are difficult to interpret. The analysis period for this particular supercell surrounded the estimated time of peak NROT, however, for mesocyclone comparisons, this storm was removed. According to NROT, tornadic mesocyclones were found to be significantly stronger than non-tornadic mesocyclones (p = 0.0009; Figure 4.15). The median NROT value for tornadic mesocyclones was 1.4, and the median NROT value for non-tornadic mesocyclones was 1.1. The 25th percentile NROT value for tornadic supercells was 1.0, nearly at the median value for non-tornadic mesocyclones. Pairwise comparisons of mesocyclones also showed that tornadic mesocyclones are statistically stronger than non-tornadic mesocyclones even when in similar environments (p = 0.0001; Figure 4.16). It is not surprising that tornadic mesocyclones were stronger than non-tornadic mesocyclones; this agrees with much prior literature (e.g., Brandes 1993; Naylor and Gilmore 2014) and motivates additional research to assess external controls on mesocyclone strength.

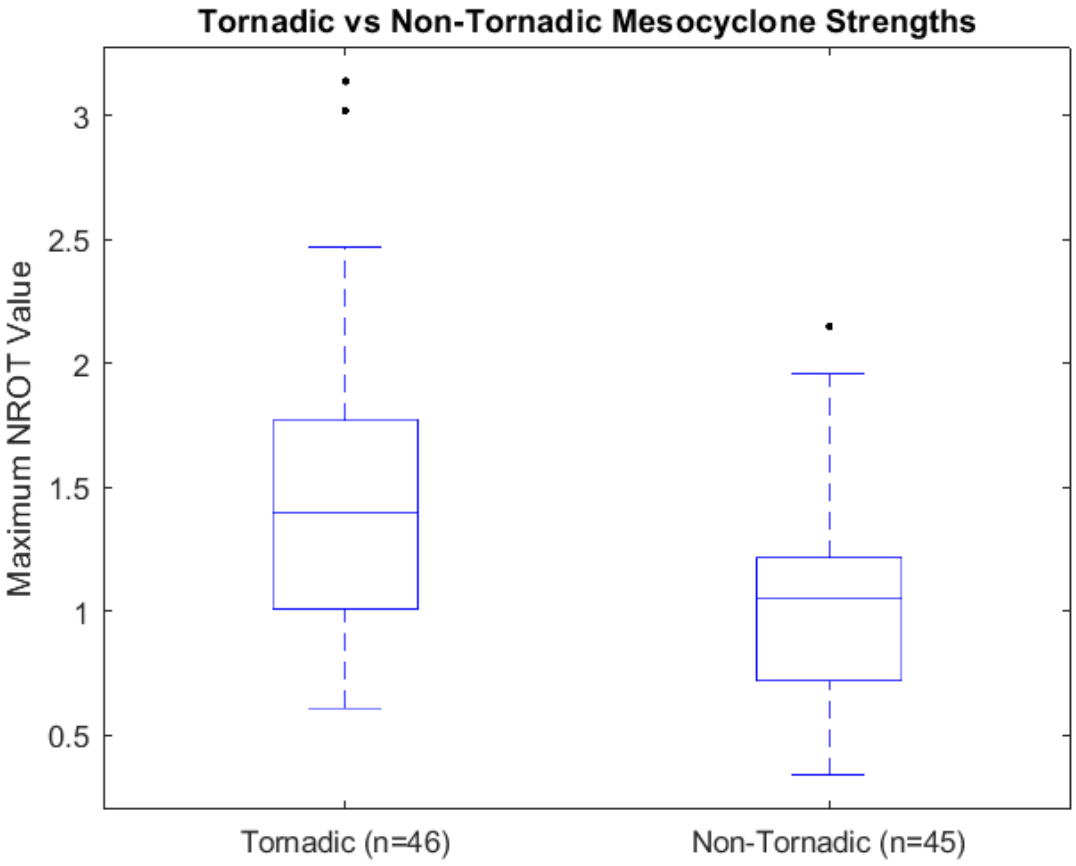

Figure 4.15: Box and whiskers plot of the distributions of tornadic and non-tornadic mesocyclone maximum NROT values. Box and whiskers distributions are as in Figure 4.6.

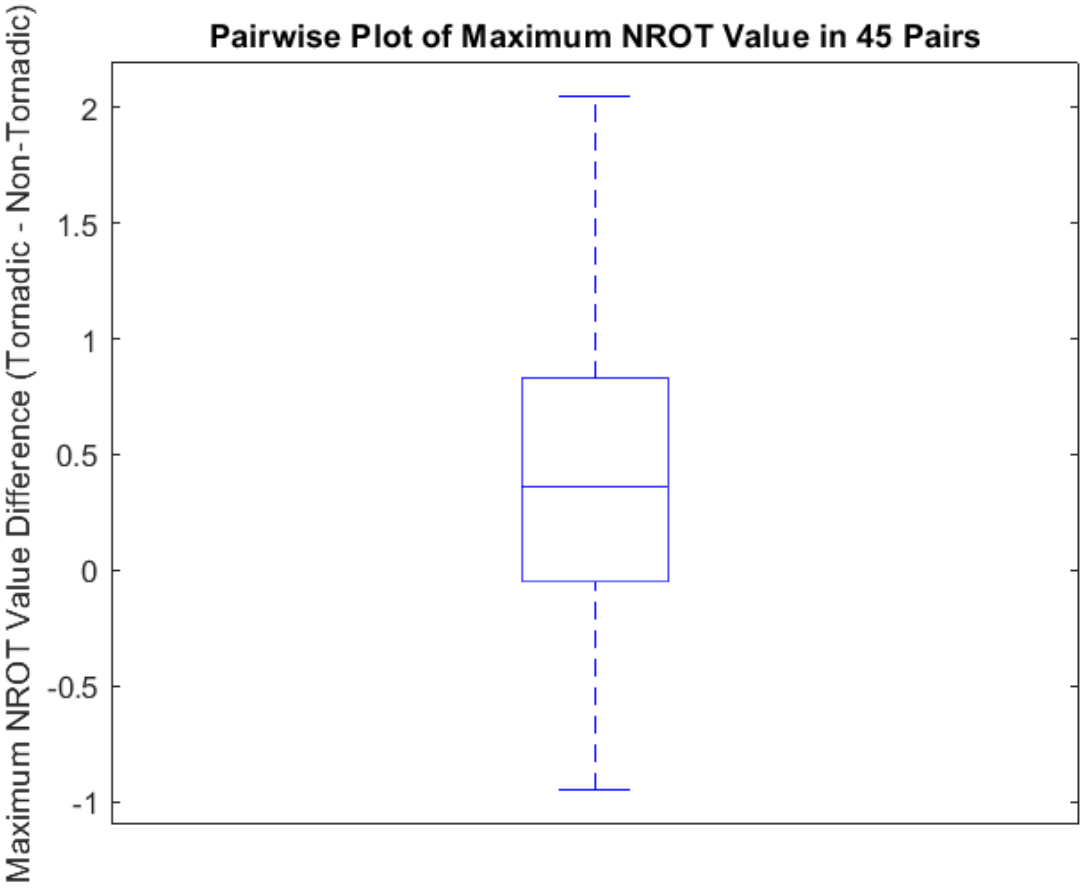

Figure 4.16: Pairwise plot of maximum NROT between the 45 tornadic and non-tornadic supercells in similar environments, shown in Table 2. One pair was removed from this comparison as the non-tornadic supercell did not have a reliable NROT value. Values plotted are equal to the maximum tornadic NROT value minus the maximum non-tornadic NROT value, such that values above zero indicate the tornadic supercell had a larger NROT value. Box and whiskers distributions are as in Figure 4.6.

IV: Comparing Polarimetric Signatures Between Tornadic and Non-Tornadic Populations

For the full analysis period, tornadic supercells were found to have a larger K_{DP}-Z_{DR} separation distance than non-tornadic supercells, when compared as individual populations and not controlling for environments (Table 7 and Figure 4.17). Previous findings on K_{DP}-Z_{DR} separation are mixed. Loeffler et al. (2020) found that the K_{DP}-Z_{DR} separation distance was relatively similar between tornadic and non-tornadic supercells, however the separation angle was more perpendicular to storm motion in tornadic supercells. Homeyer et al. (2020) also found that the orientation of the separation angle was more perpendicular to storm motion in tornadic supercells and that separation distance was similar. Contrary to these findings, Crowe et al. (2012) found the separation distance was larger in tornadic supercells, however this was done qualitatively and with a very small sample size. Findings from this research agree more with those of Crowe et al. (2012) – separation angles were not statistically different, however the separation distance was larger in tornadic supercells. Loeffler and Kumjian (2018) found that maximum separation distance between the K_{DP} foot and the Z_{DR} arc occurred just prior to tornadogenesis in nonsupercell tornadic storms. They hypothesized that this maximized separation may be the result of a strengthening updraft prior to tornadogenesis, which would subsequently enhance the low-level storm-relative inflow. This enhanced storm-relative inflow would then be manifested through increased size-sorting of hydrometeors and a greater separation distance. While no Z_{DR} column metrics were found to be statistically different, Z_{DR} column area was nearly statistically larger in pretornadic supercells. This result may align with the hypothesis by Loeffler and Kumjian (2018), as a larger updraft (inferred through Z_{DR} column area) would enhance the low-level storm-relative inflow and increase the K_{DP}-Z_{DR} separation

distance. Further investigation on the K_{DP}-Z_{DR} separation is warranted, as these results along with many others suggest that this signature may distinguish between tornadic and non-tornadic supercells.

Table 7: *P*-values from statistical comparisons of all polarimetric variable and metric median values between tornadic and non-tornadic supercells as individual populations (not controlling for environment). Analysis periods are denoted in the top row. Values in parenthesis show *p*-values from mean value comparisons. Values in boldface are statistically significant at the 5% significance level.

Variable	**Analysis Period**		
	Full Analysis	**Pre-tornadogenesis – Pre-Maximum NROT**	**Post-Tornadogenesis – Post-Maximum NROT**
Z_{DR} Arc Area	0.785 (0.821)	0.360 (0.611)	0.915 (0.909)
Z_{DR} Arc Maximum Value	0.571 (0.437)	0.056 (**0.049**)	0.739 (0.599)
Z_{DR} Arc Mean Value	0.677 (0.592)	0.286 (0.095)	0.620 (0.796)
Z_{DR} Arc 10 Maximum Values	0.861 (0.791)	0.073 (0.092)	0.935 (0.842)
Z_{DR} Arc Median Value	0.798 (0.806)	0.424 (0.251)	0.982 (0.899)
Hailfall Area	0.559 (0.850)	0.337 (0.986)	0.527 (0.965)
K_{DP} Foot Area	0.228 (0.266)	0.283 (0.349)	0.248 (0.191)
K_{DP} Foot Maximum Value	0.424 (0.571)	0.772 (0.858)	0.139 (0.236)

Table 7 (continued): *P*-values from statistical comparisons of all polarimetric variable and metric median values between tornadic and non-tornadic supercells as individual populations (not controlling for environment). Analysis periods are denoted in the top row. Values in parenthesis show *p*-values from mean value comparisons. Values in boldface are statistically significant at the 5% significance level.

Variable	**Analysis Period**		
	Full Analysis	**Pre-tornadogenesis – Pre-Maximum NROT**	**Post-Tornadogenesis – Post-Maximum NROT**
Reflectivity Area greater than 35 dBZ	0.152 (0.069)	0.092 (0.117)	0.119 (0.090)
Reflectivity Maximum	0.818 (0.676)	0.753 (0.646)	0.704 (0.634)
Reflectivity Core Average	0.553 (0.529)	0.463 (0.439)	0.723 (0.669)
K_{DP}-Z_{DR} Separation Angle	0.867 (0.858)	0.979 (0.926)	0.913 (0.889)
K_{DP}-Z_{DR} Separation Distance	**0.028** (**0.015**)	0.087 0.199	**0.041** **0.029**
Z_{DR} Column Area	0.264 (0.088)	0.072 (0.098)	0.108 (0.069)
Z_{DR} Column Maximum Depth	0.677 (0.410)	1 (0.654)	0.335 (0.160)
Z_{DR} Column Mean Depth	0.907 (0.659)	0.815 (0.878)	0.560 (0.441)

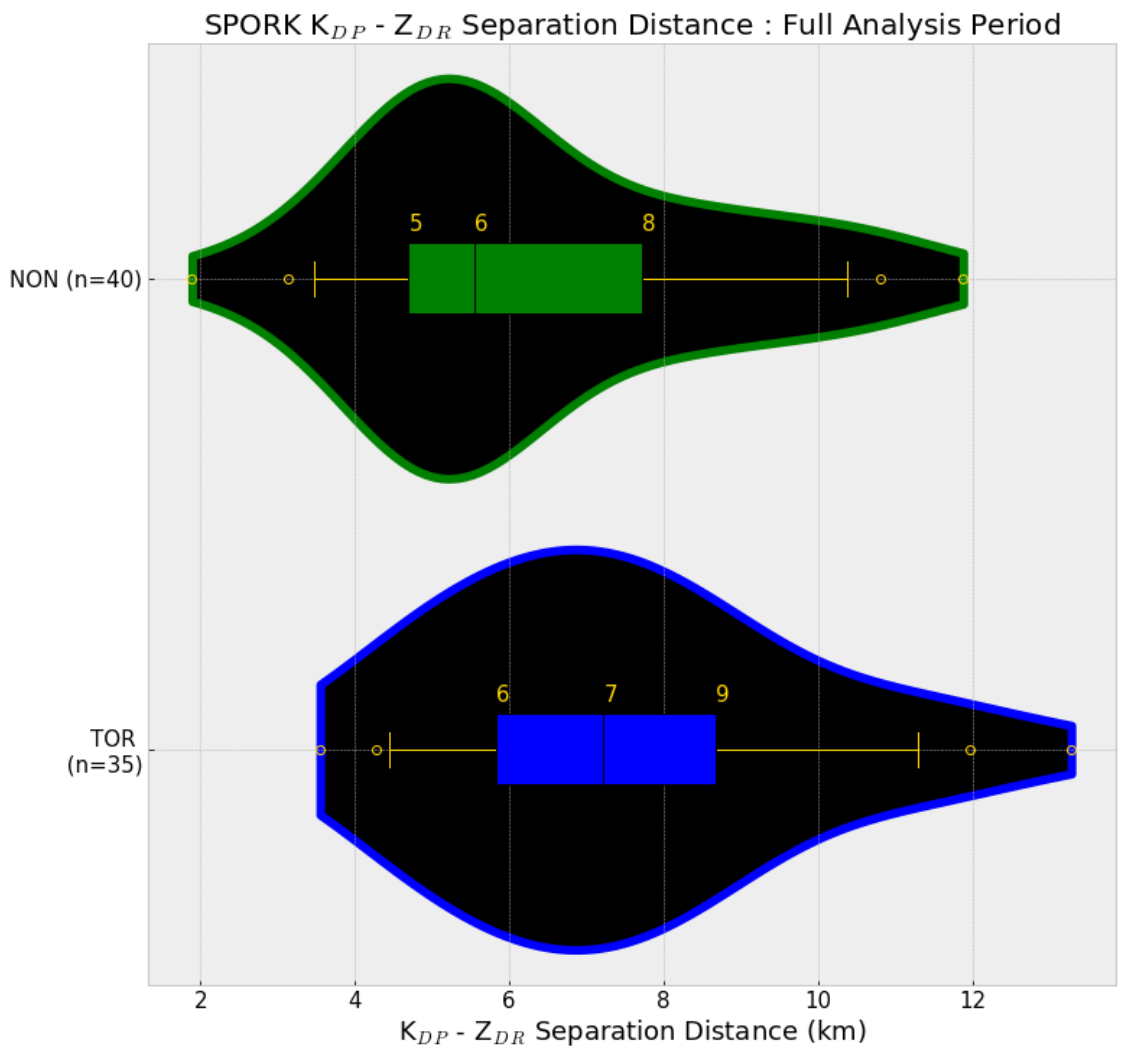

Figure 4.17: Violin and box and whiskers plots for median K_{DP}-Z_{DR} separation distance for tornadic and non-tornadic supercells in this study. Boxes enclose values from the 25th percentile to the 75th percentile, and the median value is denoted with a black line. The 25th percentile, median, and 75th percentile are denoted in gold numbers. Whiskers extend to the nonoutlier minimum and maximum values; outliers are denoted in gold circles (p = 0.028).

Additionally, for pretornadic – pre-maximum NROT times, the mean maximum value in the Z_{DR} arc was statistically different, with non-tornadic supercells having a larger Z_{DR} arc maximum value. This same metric was close to being statistically different for the median Z_{DR} arc maximum value (Table 7 and Figure 4.18). This disagrees with previous findings by Crowe et al. (2012) who were able to discriminate between tornadic and non-tornadic supercells using a 6 dB threshold in 11 out of 20 of their cases, with tornadic supercells having larger values. This also disagrees with Van Den Broeke (2020) who suggested that the maximum value in the arc may be larger in tornadic supercells. Therefore, additional results on the Z_{DR} arc maximum value are needed to determine if this characteristic is useful in distinguishing between storms. Van Den Broeke (2020) also found that the size of the Z_{DR} arc was not successful in discriminating between pretornadic and non-tornadic supercells in a relatively small sample size. While Z_{DR} arcs were larger for pretornadic supercells in his study, this was not statistically significant. Findings from this study show that there was no statistical difference in Z_{DR} arc size, which agrees with Van Den Broeke (2020), and suggests that this signature may not be useful in discriminating between tornadic and non-tornadic storms. No other signatures were statistically different, however Z_{DR} column area was statistically different at the 10% significance level for the pretornadic times (Figure 4.19). In the post-tornadogenesis time, only K_{DP}-Z_{DR} separation distance was statistically different, again with tornadic supercells having a larger separation (Figure 4.20).

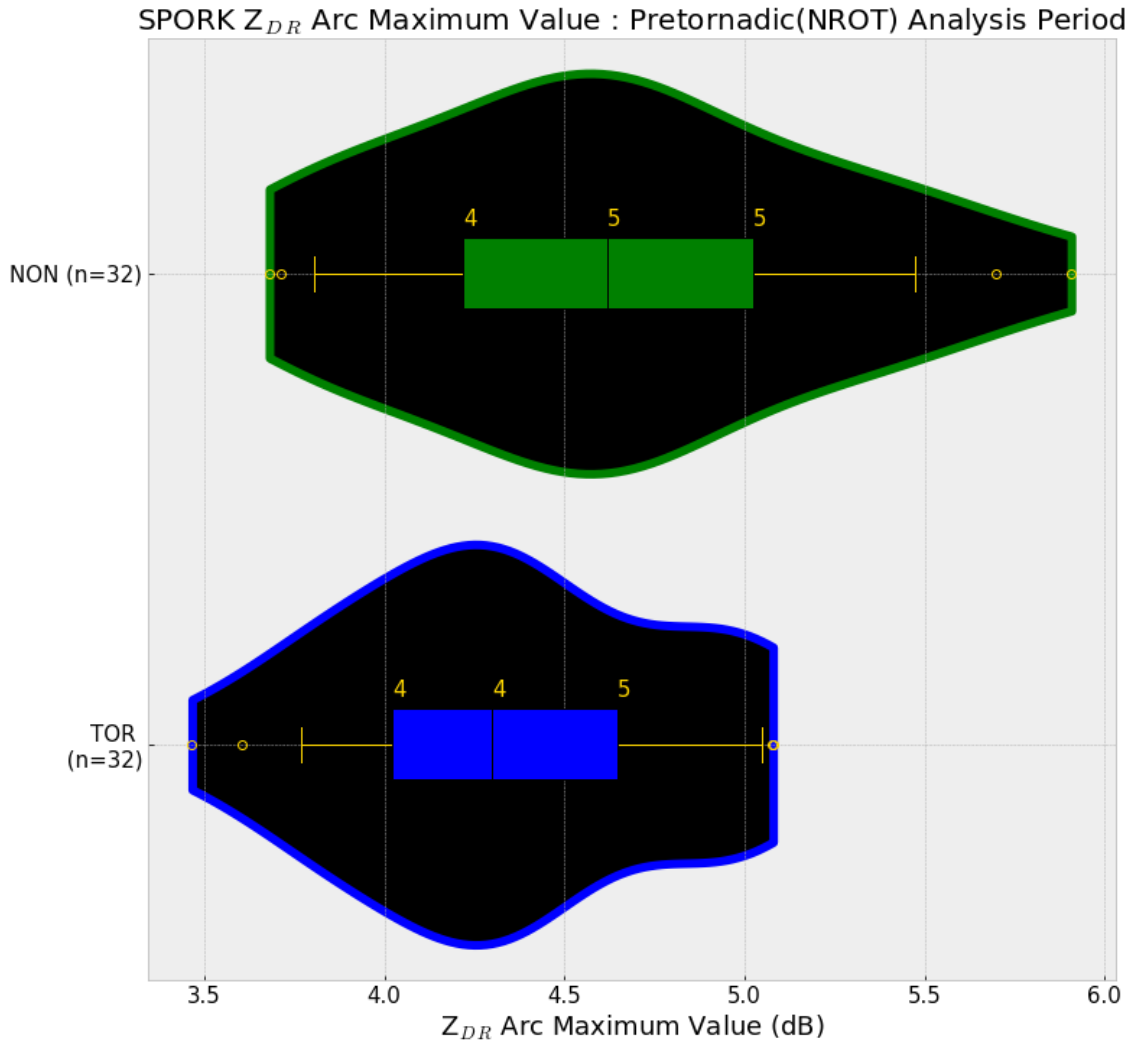

Figure 4.18: As in Figure 4.17., except for median Z_{DR} arc maximum value in the pretornadic – pre-maximum NROT analysis period (p = 0.056).

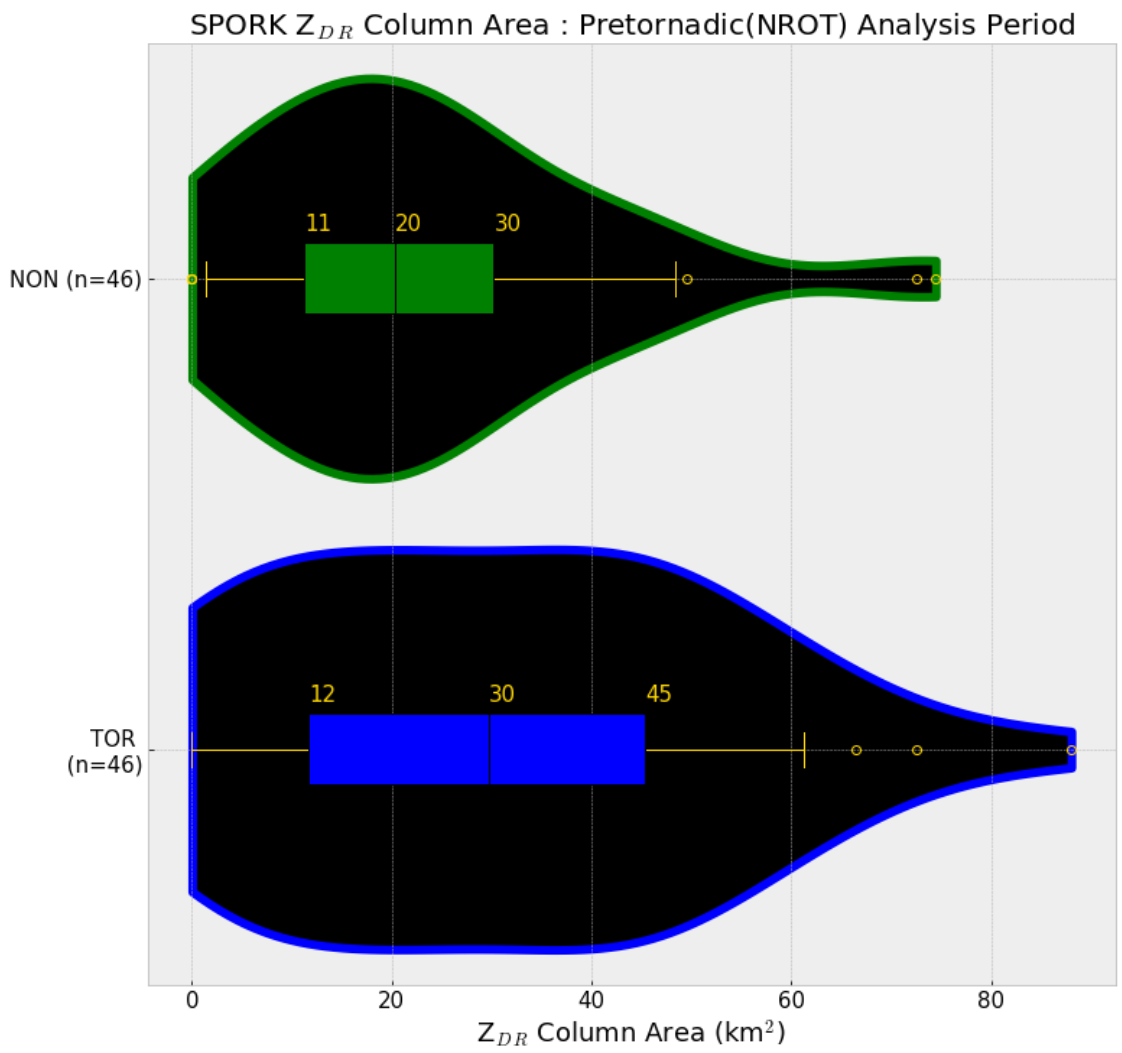

Figure 4.19: As in Figure 4.17., except for median Z_{DR} column area in the pretornadic – pre-maximum NROT analysis period (p = 0.072).

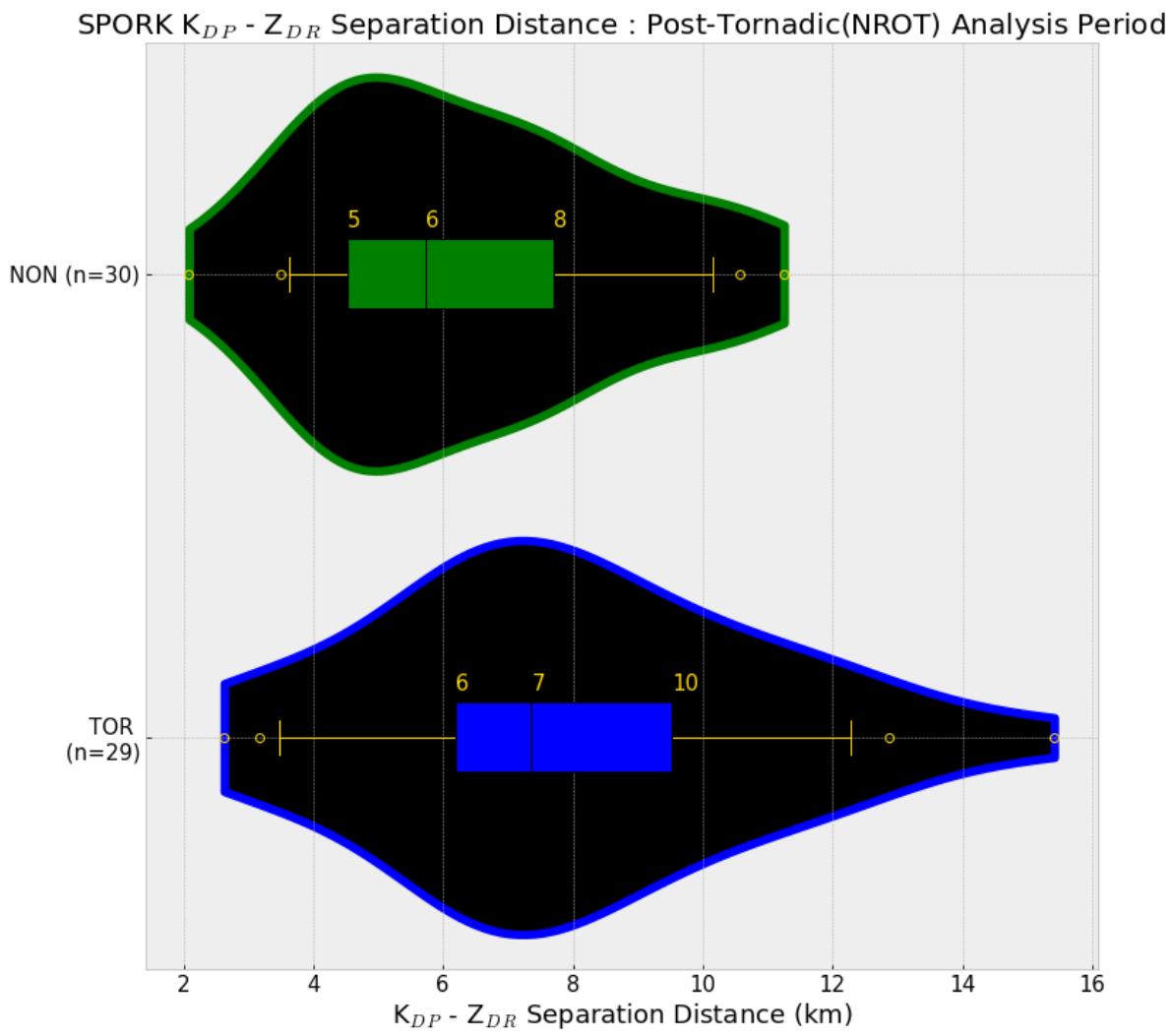

Figure 4.20: As in Figure 4.17., except for median K_{DP}-Z_{DR} separation distance in the post-tornadogenesis – post-maximum NROT analysis period (p = 0.041).

V: Comparing Polarimetric Signatures Between Tornadic and Non-Tornadic Supercells in Similar Environments

a. Full Analysis Comparisons

In pairwise comparisons of tornadic and non-tornadic supercells in similar environments, K_{DP} foot area was statistically larger in tornadic supercells when comparing across the entire analysis period (Table 8 and Figure 4.21). K_{DP}-Z_{DR} separation distance was statistically different, with tornadic supercells having a larger separation distance (Table 8 and Figure 4.22). Mean Z_{DR} column area was statistically larger in tornadic supercells (Figure 4.23). No Z_{DR} arc metrics were statistically different between tornadic and non-tornadic supercell pairs; in fact, the results for Z_{DR} arc comparisons were far from statistically significant for all metrics (Figure 4.24 shows Z_{DR} arc area as an example). Hailfall area was also not statistically different (Figure 4.25). Table 8 presents all statistical *p*-values from full analysis pairwise comparisons.

Table 8: *P*-values from pairwise comparisons of all polarimetric variables between tornadic and non-tornadic supercells in similar environments for the full analysis period. Values in boldface are significant at the 5% significance level.

Variable	Median Comparison	Mean Comparison
Z_{DR} Arc Area	0.946	0.735
Z_{DR} Arc Maximum Value	0.224	0.172
Z_{DR} Arc Mean Value	0.451	0.394
Z_{DR} Arc 10 Maximum Values	0.257	0.288
Z_{DR} Arc Median Value	0.694	0.719
Hailfall Area	0.412	0.411
K_{DP} Foot Area	**0.026**	**0.031**
K_{DP} Foot Maximum Value	0.258	0.781
Reflectivity Area greater than 35 dBZ	0.085	0.063
Reflectivity Maximum	0.294	0.122
Reflectivity Core Average	0.129	0.072
K_{DP}-Z_{DR} Separation Angle	0.888	0.835
K_{DP}-Z_{DR} Separation Distance	**0.012**	**0.003**
Z_{DR} Column Area	0.105	**0.012**
Z_{DR} Column Maximum Depth	0.371	0.452
Z_{DR} Column Mean Depth	0.479	0.721

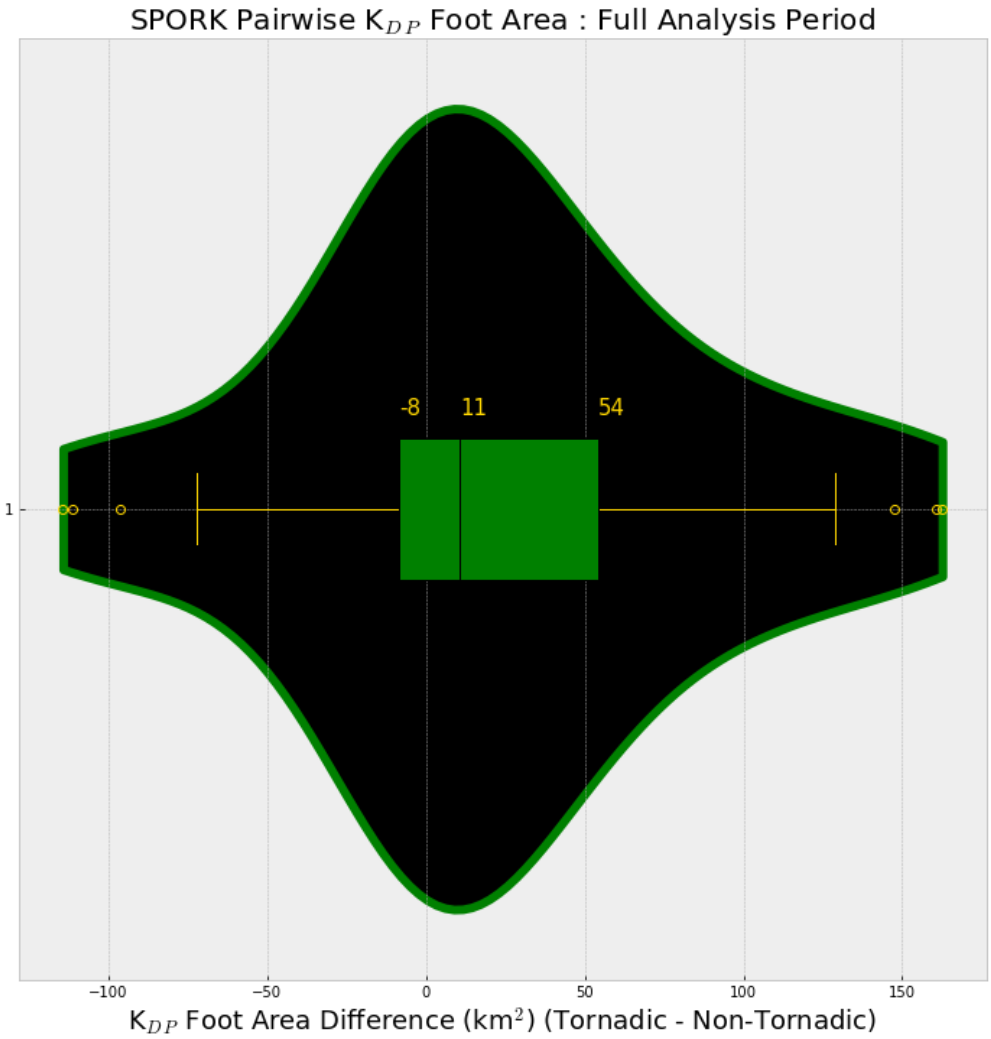

Figure 4.21: Pairwise plot depicting median tornadic K_{DP} foot area minus median non-tornadic K_{DP} foot area for the full analysis period for the 46 tornadic – non-tornadic supercell pairs in Table 2. Positive values indicate the tornadic supercell had a larger K_{DP} foot area than the non-tornadic supercell counterpart. Box and whiskers distributions are as in Figure 4.16 (n = 46; *p* = 0.026).

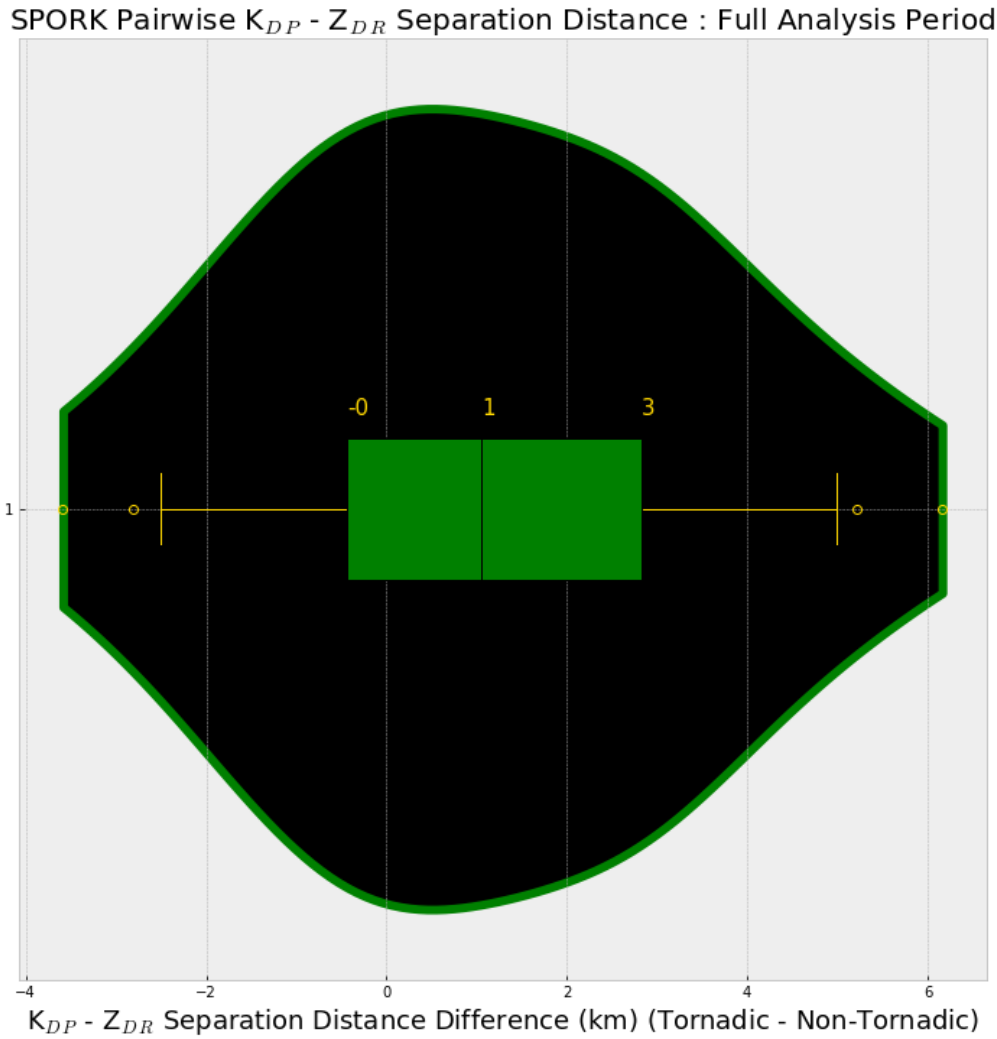

Figure 4.22: As in Figure 4.21., except for median tornadic K_{DP}-Z_{DR} separation distance minus median non-tornadic K_{DP}-Z_{DR} separation distance for the full analysis period (n = 34; *p* = 0.012).

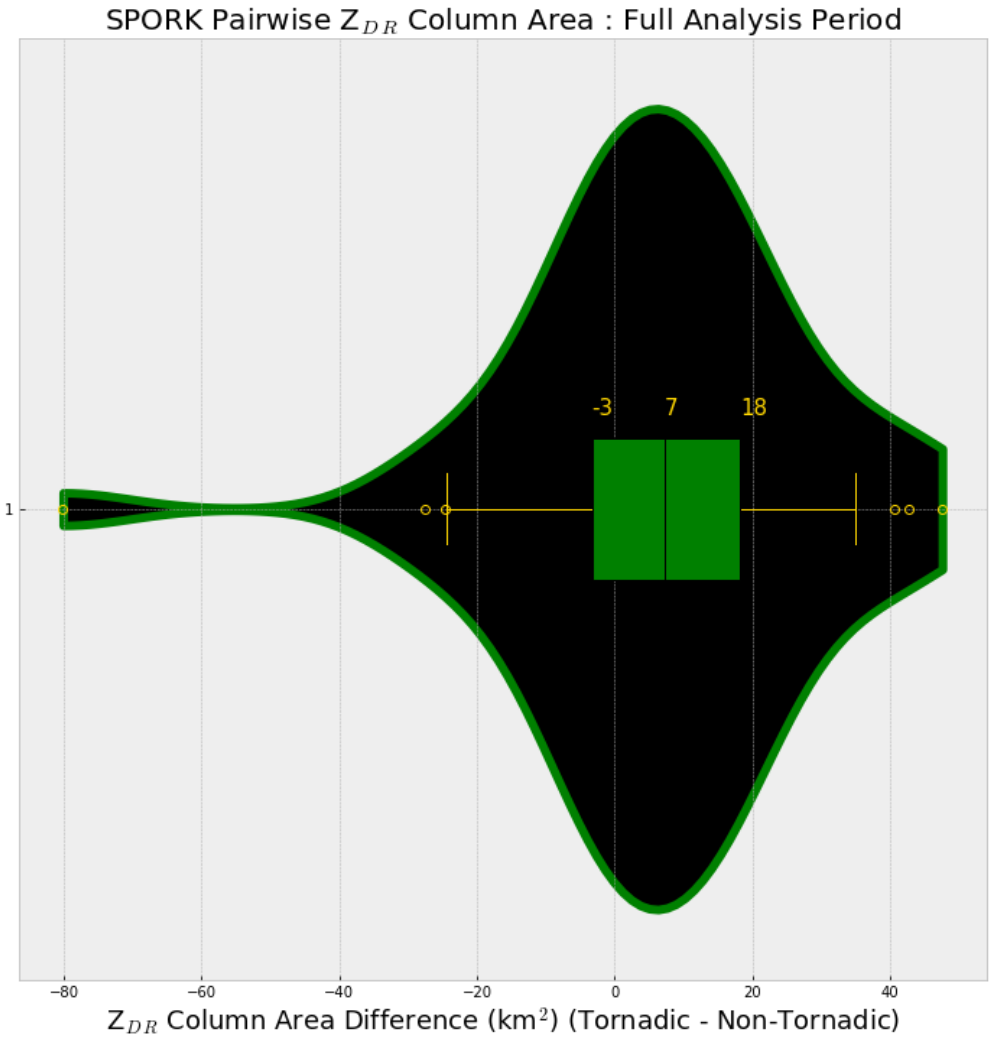

Figure 4.23: As in Figure 4.21., except for mean tornadic Z_{DR} column area minus mean non-tornadic Z_{DR} column area for the full analysis period (n = 46; *p* = 0.012).

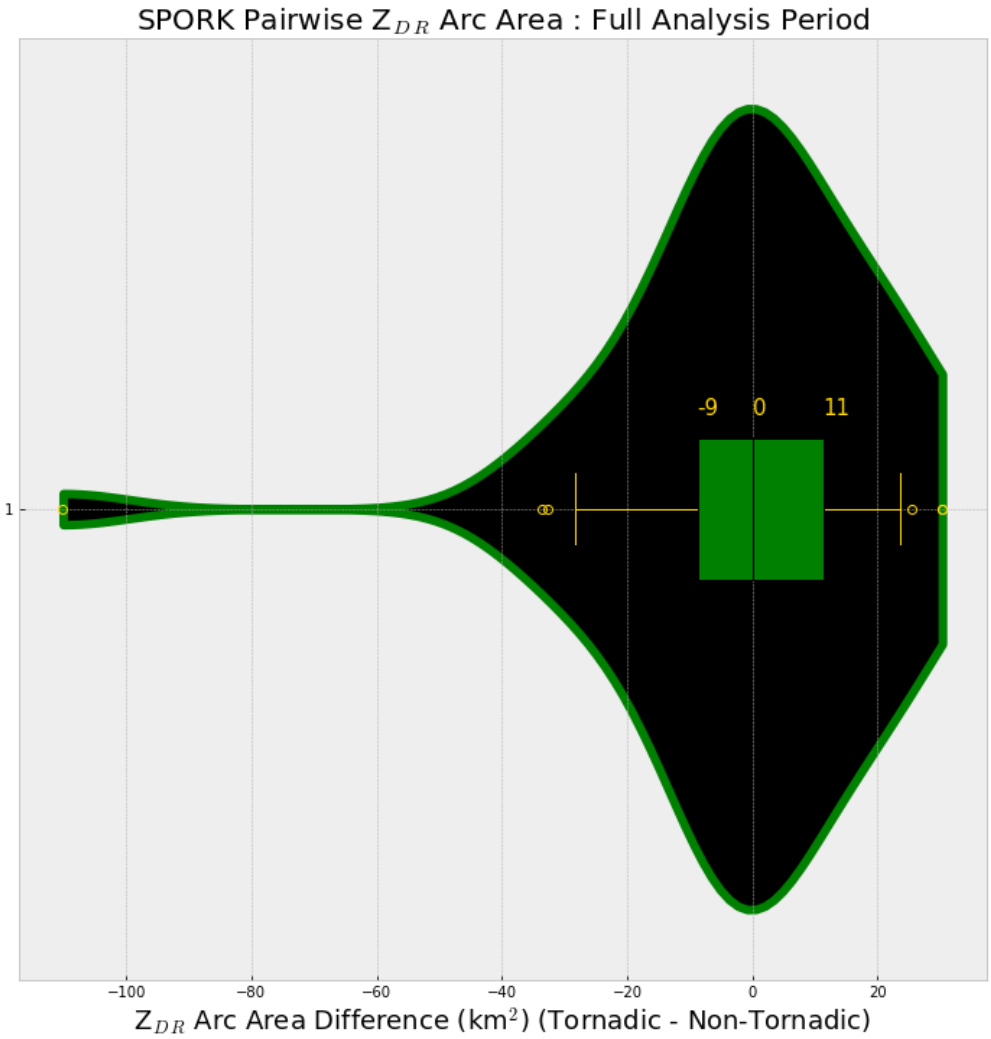

Figure 4.24: As in Figure 4.21., except for median tornadic Z_{DR} arc area minus median non-tornadic Z_{DR} arc area for the full analysis period (n = 46; *p* = 0.946).

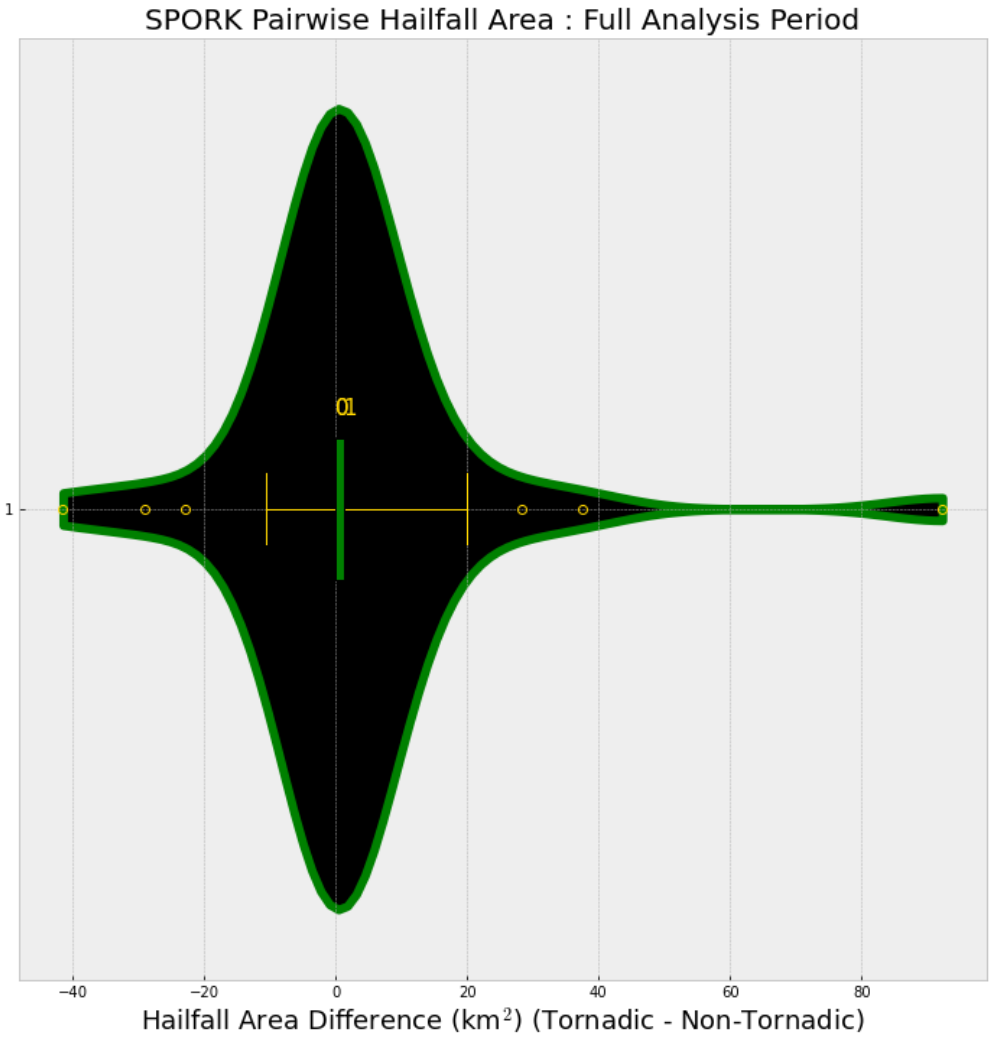

Figure 4.25: As in Figure 4.21., except for median tornadic hailfall area minus median non-tornadic hailfall area for the full analysis period (n = 46; *p* = 0.412).

b. Pre-tornadogenesis/Pre-Maximum NROT Comparisons

For pretornadic – pre-maximum NROT comparisons, hailfall area was found to be statistically different, and larger in *pretornadic* supercells (Table 9 and Figure 4.26), against the hypothesized expectation. Z_{DR} column area was found to be statistically different, with pretornadic supercells having larger Z_{DR} column areas than non-tornadic supercells (Figure 4.27). In about two-thirds (31/46) of similar environment supercell pairs, the pretornadic supercell had a larger Z_{DR} column area than the non-tornadic supercell counterpart. The only other statistically significant result for this period was the median Z_{DR} arc maximum value being larger in non-tornadic supercells (Figure 4.28; this was almost statistically significant using a mean calculation also, see Table 9). However, for this comparison only 24 cases were able to be used, as only 24 pairs of pretornadic and non-tornadic supercells *both* had an identifiable Z_{DR} arc in the pretornadogenesis – pre-maximum NROT times. Therefore, this result is likely not as statistically robust. No other statistically significant differences were found in the Z_{DR} arc signature. Table 9 presents all statistical values from pretornadic – pre-maximum NROT pairwise comparisons.

Table 9: *P*-values from pairwise comparisons of all polarimetric variables between tornadic and non-tornadic supercells in similar environments for the pretornadic – pre-maximum NROT period. Values in boldface are statistically significant at the 5% significance level.

Variable	Median Comparison	Mean Comparison
Z_{DR} Arc Area	0.315	0.449
Z_{DR} Arc Maximum Value	**0.037**	0.051
Z_{DR} Arc Mean Value	0.130	0.123
Z_{DR} Arc 10 Maximum Values	0.093	0.108
Z_{DR} Arc Median Value	0.262	0.193
Hailfall Area	**0.030**	**0.028**
K_{DP} Foot Area	0.089	0.115
K_{DP} Foot Maximum Value	0.765	0.569
Reflectivity Area greater than 35 dBZ	0.059	0.054
Reflectivity Maximum	0.433	0.275
Reflectivity Core Average	0.134	0.080
K_{DP}-Z_{DR} Separation Angle	0.646	0.829
K_{DP}-Z_{DR} Separation Distance	0.122	0.084
Z_{DR} Column Area	**0.010**	**0.007**
Z_{DR} Column Maximum Depth	0.799	0.666
Z_{DR} Column Mean Depth	0.744	0.608

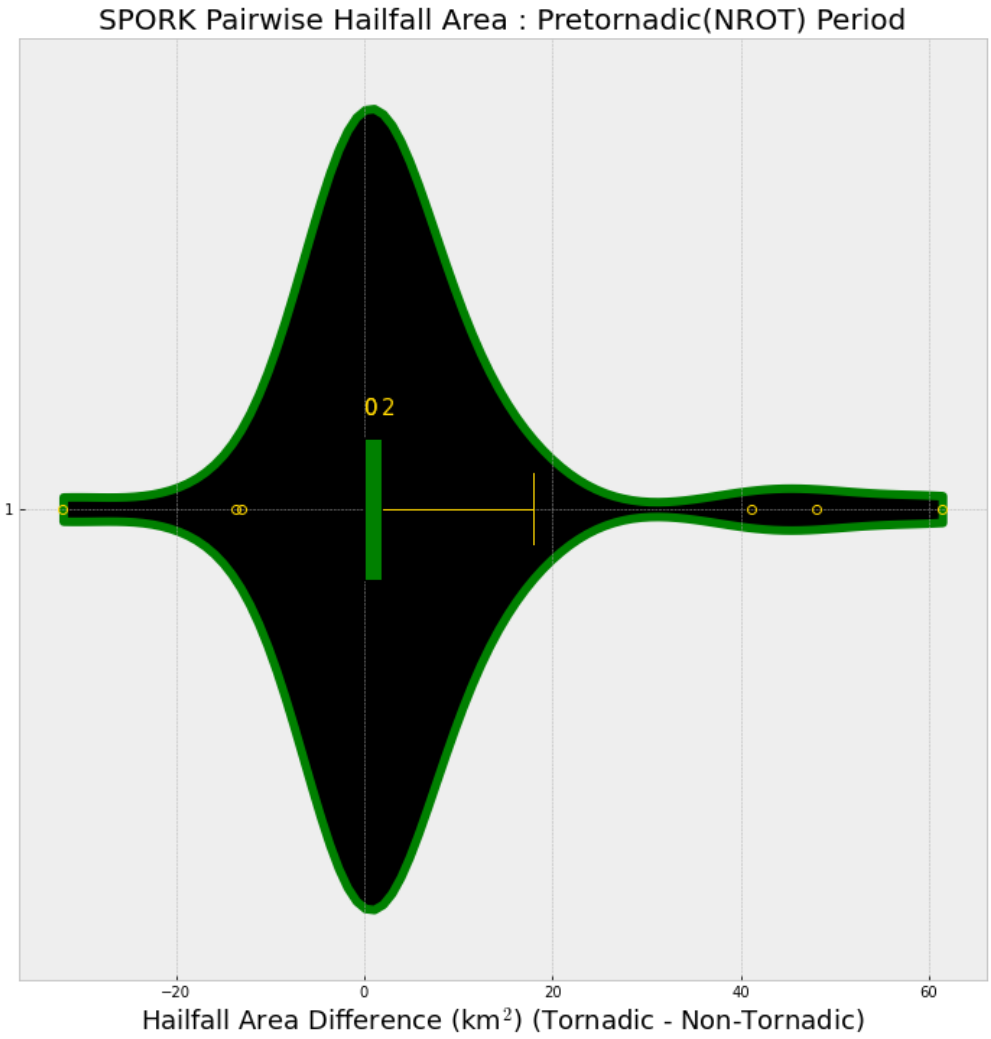

Figure 4.26: As in Figure 4.21., except for median tornadic hailfall area minus median non-tornadic hailfall area for the pretornadic – pre-maximum NROT analysis period (n = 46; *p* = 0.030).

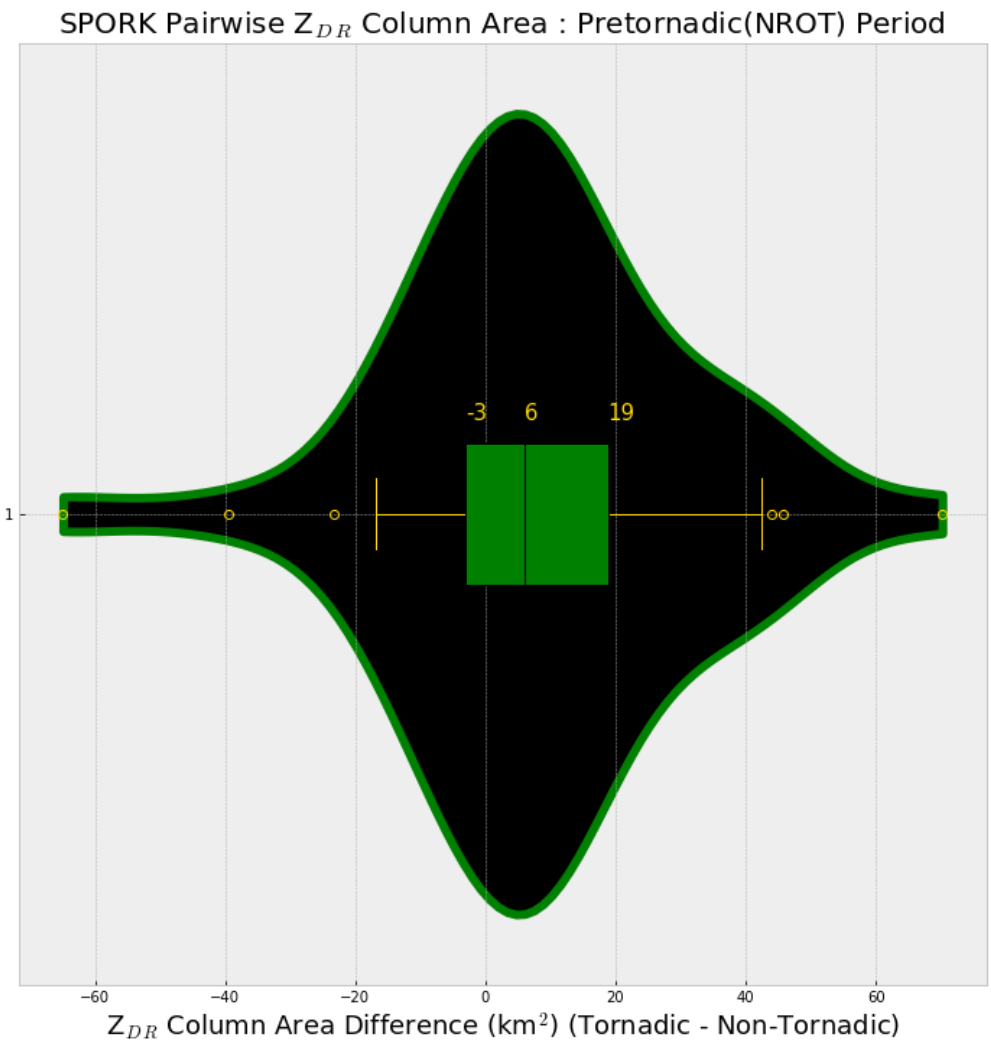

Figure 4.27: As in Figure 4.21., except for median tornadic Z_{DR} column area minus median non-tornadic Z_{DR} column area for the pretornadic – pre-maximum NROT analysis period (n = 46; *p* = 0.010).

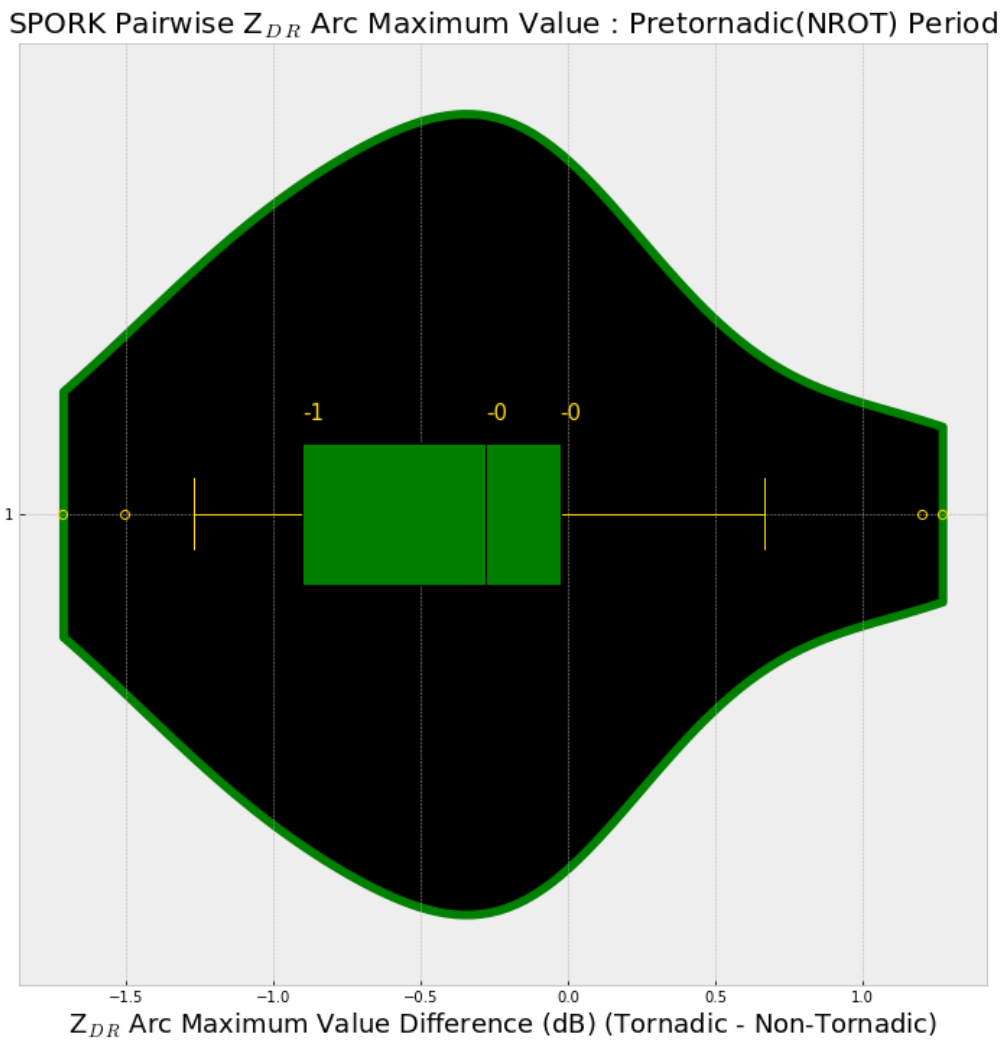

Figure 4.28: As in Figure 4.21., except for median tornadic Z_{DR} arc maximum value minus median non-tornadic Z_{DR} arc maximum value for the pretornadic – pre-maximum NROT analysis period (n = 24; *p* = 0.037).

c. Post-Tornadogenesis/Post-Maximum NROT Comparisons

For the post-tornadogenesis – post-maximum NROT time, only the K_{DP} foot area was statistically different, with tornadic supercells having larger K_{DP} feet (Table 10 and Figure 4.29). All Z_{DR} arc metrics were far from statistically different, however cases able to be used during the post-tornadogenesis – post-maximum NROT times were less than 30 (n=22). Z_{DR} column area was close to statistically different for both the mean and median calculation (Table 10) with tornadic supercells having larger Z_{DR} column areas (Figure 4.30). Hailfall area was far from being statistically different (Figure 4.31). Table 10 presents all statistical values from post-tornadic – post-maximum NROT pairwise comparisons.

Table 10: *P*-values from pairwise comparisons of all polarimetric variables between tornadic and non-tornadic supercells in similar environments for the post-tornadic – post-maximum NROT period. Values in boldface are statistically significant at the 5% significance level.

Variable	Median Comparison	Mean Comparison
Z_{DR} Arc Area	0.372	0.468
Z_{DR} Arc Maximum Value	0.729	0.647
Z_{DR} Arc Mean Value	0.529	0.847
Z_{DR} Arc 10 Maximum Values	0.799	0.797
Z_{DR} Arc Median Value	0.778	0.839
Hailfall Area	0.543	0.517
K_{DP} Foot Area	**0.017**	**0.018**
K_{DP} Foot Maximum Value	0.105	0.091
Reflectivity Area greater than 35 dBZ	0.159	0.192
Reflectivity Maximum	0.140	0.101
Reflectivity Core Average	0.158	0.127
K_{DP}-Z_{DR} Separation Angle	0.819	0.687
K_{DP}-Z_{DR} Separation Distance	0.196	0.244
Z_{DR} Column Area	0.067	0.053
Z_{DR} Column Maximum Depth	0.179	0.105
Z_{DR} Column Mean Depth	0.472	0.456

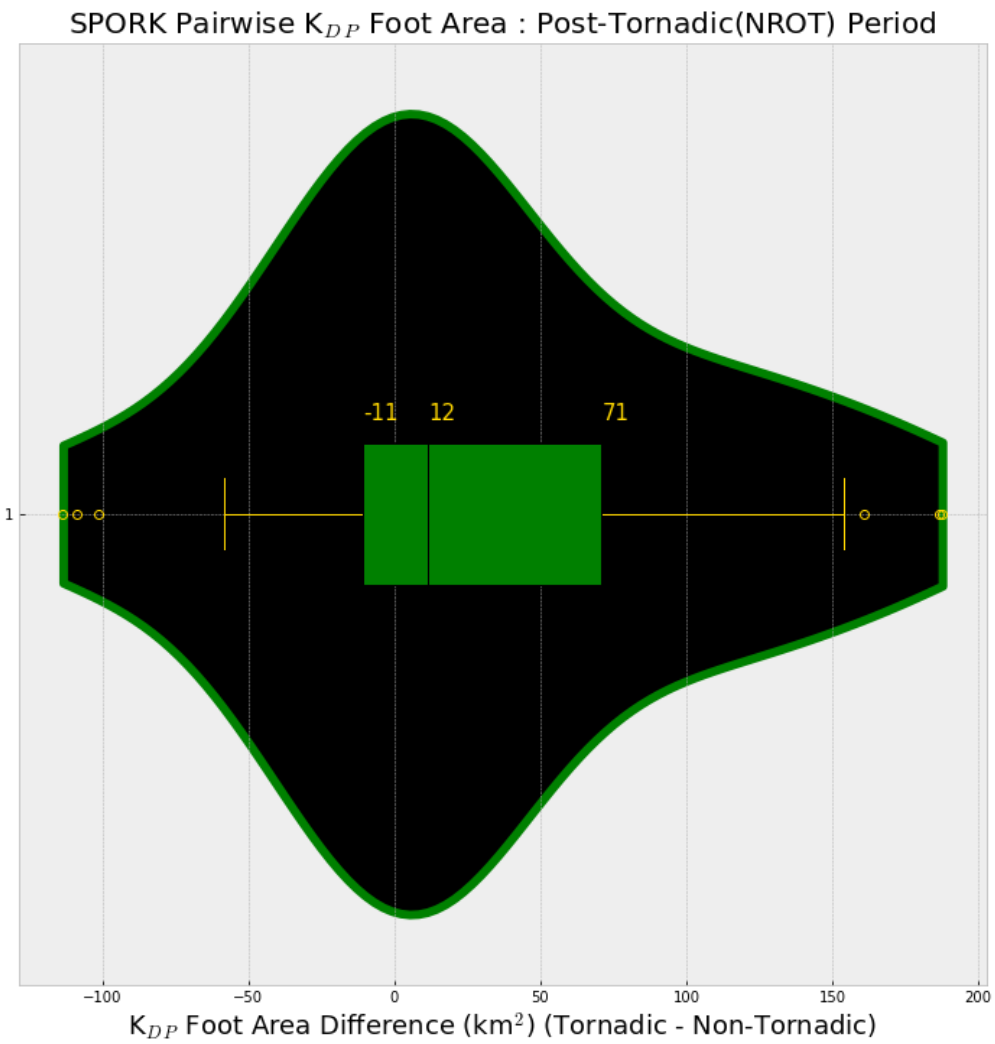

Figure 4.29: As in Figure 4.21., except for median tornadic K_{DP} foot area minus median non-tornadic K_{DP} foot area for the post-tornadogenesis – post-maximum NROT analysis period (n = 46; *p* = 0.017).

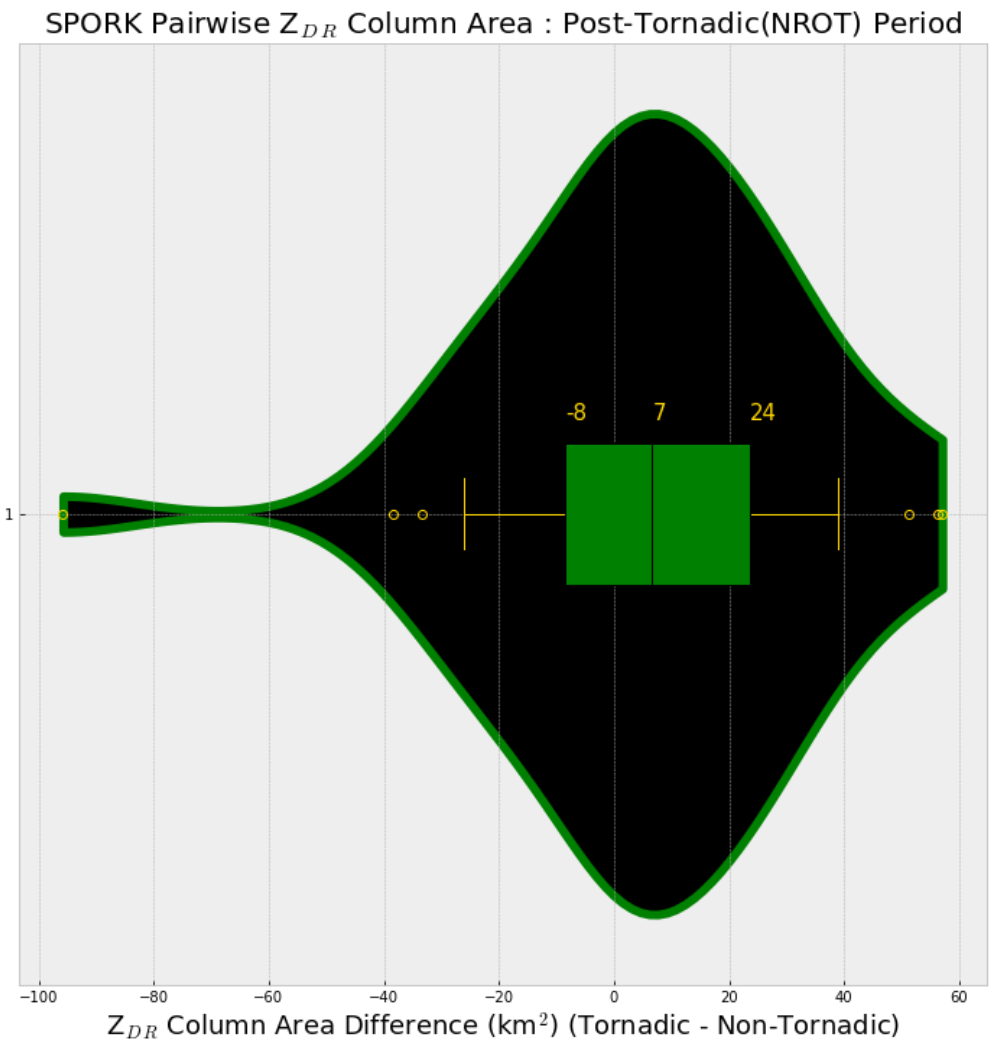

Figure 4.30: As in Figure 4.21., except for median tornadic Z_{DR} column area minus median non-tornadic Z_{DR} column area for the post-tornadogenesis – post-maximum NROT analysis period (n = 46; *p* = 0.067).

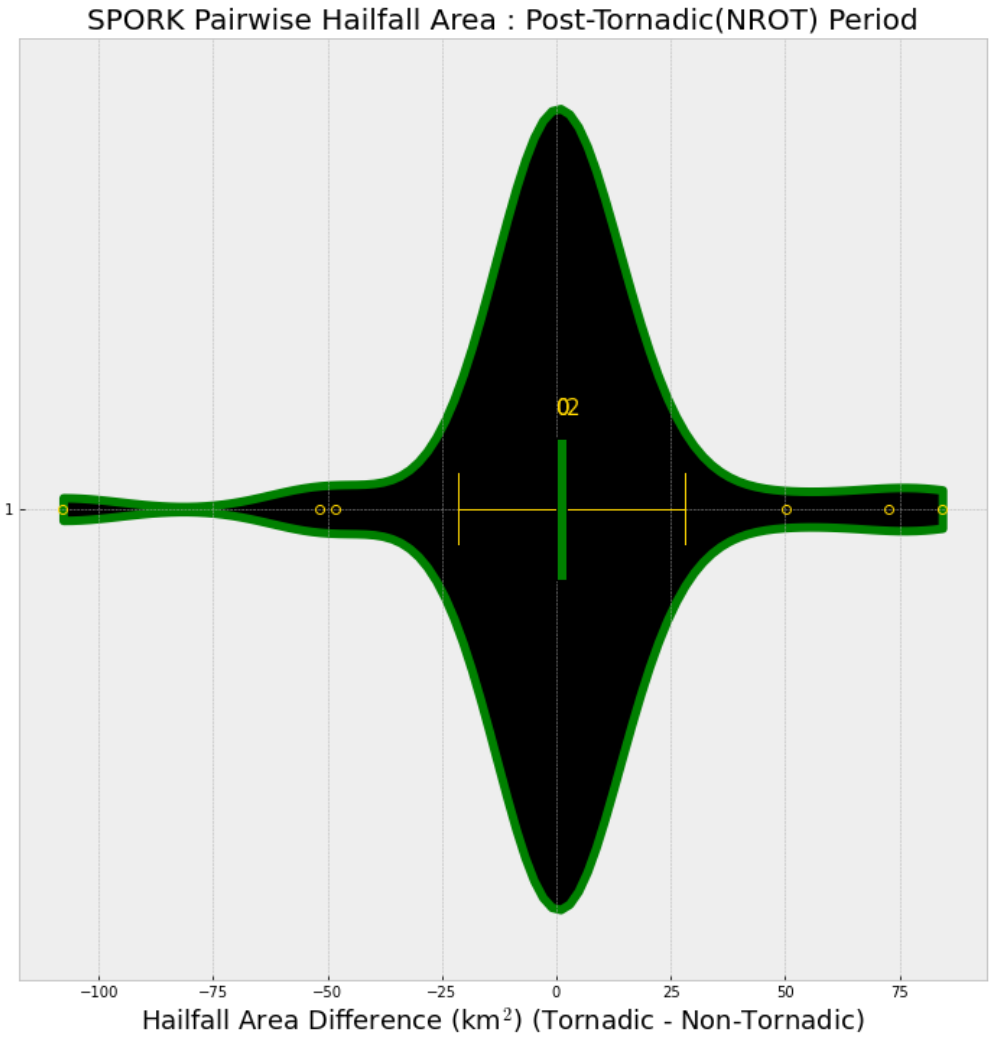

Figure 4.31: As in Figure 4.21., except for median tornadic hailfall area minus median non-tornadic hailfall area for the post-tornadogenesis – post-maximum NROT analysis period (n = 46; p = 0.543).

d. Trends of Polarimetric Signatures and Similarity Correlations

Trend comparisons were only performed for pairwise comparisons (only comparisons within similar environments). Trends were calculated by subtracting the mean pretornadic/pre-maximum NROT signature value from the mean post-tornadic/post-maximum NROT signature value, such that a negative value indicated a decrease in that signature. All signature trends were not statistically different, with the lowest *p*-values being 0.204 and 0.209 for the Z_{DR} arc area and the maximum K_{DP} value, respectively (Table 11). For the K_{DP} maximum values, three storm pairs were removed as there was no K_{DP} foot identified by the algorithm in at least one storm within each of those pairs. For the Z_{DR} arc maximum value and K_{DP}-Z_{DR} separation distance and angle, most storms had to be removed due to lack of identifiable arcs within the pairs for trend comparisons (see Table 11). Therefore, statistical results for these metrics in trend comparisons are likely not robust. Finally, no dual-pol metric differences were found to be correlated with environmental similarity values (Table 12). Therefore, there is no apparent relationship between environmental similarity and any dual-pol metric differences between two proximate supercells in this study.

Table 11: *P*-values for comparisons of all polarimetric signature trends in tornadic – non-tornadic supercell pairs. Note the small sample size for several metrics – asterisks denote variables that likely do not have statistically robust results.

Variable	Trend Comparison *p*-value	Sample Size
Z_{DR} Arc Area	0.205	46
Z_{DR} Arc Maximum Value	0.647	*15
Z_{DR} Arc Mean Value	0.337	*15
Z_{DR} Arc 10 Maximum Values	0.305	*15
Z_{DR} Arc Median Value	0.619	*15
Hailfall Area	0.906	46
K_{DP} Foot Area	0.231	46
K_{DP} Foot Maximum Value	0.209	43
Reflectivity Area greater than 35 dBZ	0.552	46
Reflectivity Maximum	0.579	46
Reflectivity Core Average	0.967	46
K_{DP}-Z_{DR} Separation Angle	0.851	*13
K_{DP}-Z_{DR} Separation Distance	0.546	*15
Z_{DR} Column Area	0.672	46
Z_{DR} Column Maximum Depth	0.399	46
Z_{DR} Column Mean Depth	0.499	46

Table 12: Pearson's correlation values of environmental similarity values and polarimetric signature differences for tornadic – non-tornadic supercell pairs.

Variable	Correlation (*r*)
Z_{DR} Arc Area	0.091
Z_{DR} Arc Maximum Value	0.198
Z_{DR} Arc Mean Value	0.155
Z_{DR} Arc 10 Maximum Values	0.186
Z_{DR} Arc Median Value	0.156
Hailfall Area	-0.309
K_{DP} Foot Area	-0.215
K_{DP} Foot Maximum Value	-0.263
Reflectivity Area greater than 35 dBZ	-0.022
Reflectivity Maximum	-0.087
Reflectivity Core Average	-0.073
K_{DP}-Z_{DR} Separation Distance	0.152
Z_{DR} Column Area	-0.078
Z_{DR} Column Maximum Depth	-0.079
Z_{DR} Column Mean Depth	-0.031

Chapter V: Discussion and Conclusion

Controlling for environment is an important consideration for comparing tornadic and non-tornadic supercells, and this study found that differences in dual-pol signatures do exist between tornadic and non-tornadic supercells when in similar environments. Our primary hypotheses were the following in regard to dual-pol signature differences:

- Tornadic supercells will have larger Z_{DR} columns than non-tornadic supercells in similar environments.
- Tornadic supercells will have larger and more significant Z_{DR} arcs than non-tornadic supercells in similar environments.
- Non-tornadic supercells will have larger hailfall areas than tornadic supercells in similar environments.

The key findings from this study related to each of these hypotheses are as follows:

- Tornadic supercells have larger Z_{DR} column areas than non-tornadic supercells, primarily in the pretornadic times. No differences in Z_{DR} column depth were found between tornadic and non-tornadic supercells.
- Only Z_{DR} arc maximum value was found to be statistically different between tornadic and non-tornadic supercells, with non-tornadic storms having a larger maximum value. This was only true during the pre-maximum NROT times, and results are not as statistically robust for this finding. No other differences between tornadic and non-tornadic Z_{DR} arcs were found.

- Tornadic supercells have larger hailfall area during the pretornadic time than non-tornadic supercells during the pre-maximum NROT time. Hailfall area was not statistically different during any other analysis period.

Despite tornadic supercells having stronger mesocyclones even in similar environments, the results reject our hypothesis that tornadic supercells have larger Z_{DR} arcs. This agrees with the findings of Van Den Broeke (2020) and suggests that Z_{DR} arc characteristics are likely controlled by factors in addition to mesocyclone strength. Trends in the arc characteristics were also not statistically significant. Therefore, Z_{DR} arcs are likely not a useful signature to discriminate between tornadic and non-tornadic supercells operationally. While the maximum Z_{DR} arc value was statistically significant for a median comparison in pretornadic supercells compared to pre-maximum NROT supercells, less than 30 pairs were used for this calculation, therefore, the results are not as statistically robust. Again, further research examining the maximum Z_{DR} arc magnitude in a larger sample size may be worthwhile. Examining Z_{DR} arc area relative to total storm area between tornadic and non-tornadic supercells may also be an area of future research worth pursuing.

A key result from this research that may have operational use is that pretornadic supercells have larger Z_{DR} columns than their non-tornadic counterparts in similar environments. Kuster et al. (2020) found that Z_{DR} columns can be used operationally to improve warning decision processes. Z_{DR} column area difference between pretornadic and pre-maximum NROT supercells shows a nontrivial separation from zero (Figure 4.27). These findings agree with Van Den Broeke (2020) who found that pretornadic supercells had larger Z_{DR} columns. Therefore, operational forecasters should consider monitoring the Z_{DR} column area

when warning supercells in proximity. Van Den Broeke (2020) also found that column depth was larger in pretornadic supercells, which did not appear here. This may be because thermodynamic characteristics of the inflow environment were controlled for in this study, which have been shown to correlate well to Z_{DR} column depth (Van Den Broeke 2016). While it was not investigated here, mesocyclone size between tornadic and non-tornadic supercells in similar environments would be worth examining, as larger Z_{DR} column area may be associated with larger and stronger mesocyclones. Sessa and Trapp (2020) found that pretornadic mesocyclone size correlates well with tornado intensity. Therefore, should Z_{DR} column area be found to correlate to mesocyclone size, this could be a good indicator of tornadic potential within a group of supercells.

Additional findings that were not hypothesized are that tornadic storms have larger K_{DP} feet and separation between the K_{DP} foot and the Z_{DR} arc. The statistically significant difference in K_{DP} foot area between tornadic and non-tornadic supercells is novel, as this signature has not been examined thoroughly to our knowledge in prior research for discriminating between storm outcomes. It is possible that this larger K_{DP} foot in tornadic supercells is also related to the larger Z_{DR} column area. A larger updraft may be more effective at producing more precipitation, which will eventually fall out in a larger area (Romine et al. 2008; Johnson et al. 2016). It may be worthwhile to compare the size of the K_{DP} foot relative to total storm area, as relative sizes may tell a better story about storm-scale dynamics. The larger Z_{DR} column area in pretornadic supercells may be related to the larger separation distance between the K_{DP} foot and the Z_{DR} arc in tornadic supercells. As discussed previously, and as Loeffler and Kumjian (2018) hypothesized, this larger separation may be the result of a strengthening updraft, which

would enhance low-level storm-relative inflow and increase the size sorting and resulting separation. Peters et al. (2020) also found that updraft width within simulated supercells was more dependent on storm-relative flow and deep-layer shear. Given that deep-layer shear was controlled for in this study, storm-relative flow may be the cause for larger Z_{DR} column areas. Further, given that both column area and K_{DP}-Z_{DR} separation distance were larger in tornadic supercells, it is reasonable to hypothesize that these signatures may be connected. Separation angle was not found to be different between supercells as has been found in other studies, however previous studies did not control for environment, and low-level kinematics in particular are thought to be related to separation angles. Research should continue to compare the separation signature between the K_{DP} foot and the Z_{DR} arc, as it is likely that this signature may be useful in discriminating between tornadic and non-tornadic storms.

Perhaps the most surprising result of this research is that tornadic supercells were found to have larger hailfall areas than their non-tornadic counterparts during the period prior to tornadogenesis or maximum rotation. This is contrary to findings by Van Den Broeke (2020) and disagrees with our hypothesis that non-tornadic supercells have larger hailfall areas. However, this result is likely not useful operationally as there was no compelling separation from zero in pairwise plots of tornadic and non-tornadic hailfall areas (Figure 4.26). Additional research with a larger sample size would be valuable to compare to these results and those of Van Den Broeke (2020). Furthermore, it would be valuable to do a more detailed scan-by-scan analysis of hailfall variability. Hailfall area may be larger in tornadic supercells during periods immediately following updraft collapse, when with a larger updraft, more hail would subsequently fall out. Therefore, the variability of hailfall area over time may make it difficult to

compare mean hailfall area between storms. Finally, the lack of statistically significant differences in the trends of all signatures and their metrics suggests that more work is needed in examining changes in signatures with time for proximate supercells before trends can be used with confidence in operations for these situations.

The finding that Z_{DR} column area is larger in pretornadic supercells when in proximity to non-tornadic supercells may be useful operationally and agrees with prior research which indicated the usefulness of the Z_{DR} column to improve severe thunderstorm warnings and anticipate tornado potential. Operational forecasters should consider implementing more methods to use the Z_{DR} column signature in warning processes, particularly for challenging situations when tornadic and non-tornadic supercells coexist in proximity. Future research along this line of work should also consider examining how these dual-pol signatures correlate with low-level mesocyclone strength, particularly in situations when the environment is seemingly similar between two supercells. Removing the environmental differences between supercells and examining differences in mesocyclone strength and dual-pol signatures in these scenarios may be important for determining storm-scale processes that ultimately result in tornadogenesis. Overall, findings from this study encourage future researchers and operational forecasters to continue considering the value in using the Z_{DR} column signature and the separation distance between the K_{DP} foot and the Z_{DR} arc to discriminate between tornadic and non-tornadic supercells, particularly when these coexist in similar environments.

References

Ashley, W. S., 2007: Spatial and temporal analysis of tornado fatalities in the United States: 1880-2005. *Wea. Forecasting*, **22**, 1214–1228, https://doi.org/10.1175/2007WAF2007004.1.

Balakrishnan, N., and D. S. Zrnić, 1990: Use of polarization to characterize precipitation and discriminate large hail. *J. Atmos. Sci.*, **47**, 1525-1540, doi:10.1175/1520-0469(1990)047<1525:UOPTCP>2.0.CO;2.

Beebe, R. G., 1958: Tornado proximity soundings. *Bull. Amer. Meteor. Soc.*, **39**, 195-201, https://doi.org/10.1175/1520-0477-39.4.195.

Benjamin, S. G., and Coauthors, 2016: A North American hourly assimilation and model forecast cycle: The rapid refresh. *Mon. Wea. Rev.*, **144**, 1669–1694, https://doi.org/10.1175/MWR-D-15-0242.1.

Bluestein, H. B., and M. L. Weisman, 2000: The interaction of numerically simulated supercells initiated along lines. *Mon. Wea. Rev.*, **128**, 3128-3149, https://doi.org/10.1175/1520-0493(2000)128%3C3128:TIONSS%3E2.0.CO;2

Brandes, E.A., 1978: Mesocyclone evolution and tornadogenesis: Some observations. *Mon. Wea. Rev.,* **106**, 995-1011, https://doi.org/10.1175/1520-0493(1978)106<0995:MEATSO>2.0.CO;2.

——, 1993: Tornadic thunderstorm characteristics determined with Doppler radar. *The Tornado: Its Structure, Dynamics, Prediction, and Hazards, Geophys. Monogr.*, No. 79, Amer. Geophys. Union, 143–159.

——, A. V. Ryzhkov, and D. S. Zrnić, 2001: An evaluation of radar rainfall estimates from specific differential phase. *J. Atmos. Ocean. Technol.*, **18**, 363–375, https://doi.org/10.1175/1520-0426(2001)018<0363:AEORRE>2.0.CO;2.

Brooks, H. E., and C. A. Doswell, 2001: Normalized damage from major tornadoes in the United States: 1890 – 1999. *Wea. Forecasting*, **16**, 168–176, https://doi.org/10.1175/1520-0434(2001)016%3C0168:NDFMTI%3E2.0.CO;2

Browning, K. A., 1964: Airflow and precipitation trajectories within severe local storms which travel to the right of the winds. *J. Atmos. Sci.*, **21**, 634-639, https://doi.org/10.1175/1520-0469(1964)021<0634:AAPTWS>2.0.CO;2

Bunkers, M. J., B. A. Klimowski, J. W. Zeitler, R. L. Thompson, and M. L. Weisman, 2000: Predicting supercell motion using a new hodograph technique. *Wea. Forecasting*, **15**, 61–79, https://doi.org/10.1175/1520-0434(2000)015%3C0061:PSMUAN%3E2.0.CO;2

——, M. R. Hjelmfelt, and P. L. Smith, 2006: An observational examination of long-lived supercells. Part 1: Characteristics, evolution, and demise. *Wea. Forecasting,* **21**, 673-688, https://doi.org/10.1175/WAF949.1

——, M. B. Wilson, M. S. Van Den Broeke, and D. J. Healey, 2022: Scan-by-scan storm-motion deviations for concurrent tornadic and nontornadic supercells. *Wea. Forecasting* (in review)

Coniglio, M. C., and M. D. Parker, 2020: Insights into supercells and their environments from three decades of targeted radiosonde observations. *Mon. Weather Rev.*, **148**, 4893–4915, https://doi.org/10.1175/MWR-D-20-0105.1.

Conway, J. W., and Zrnić D. S., 1993: A study of embryo production and hail growth using dual-Doppler and multiparameter radars. *Mon. Wea. Rev.,* **121**, 2511-2528, https://doi.org/10.1175/1520-0493(1993)121<2511:ASOEPA>2.0.CO;2

Cooper, D.T. and A. B. Vorst, 2016: Assessing the utility of normalized rotation in detecting tornado development along the Allegheny front. Northeast Regional Operational Workshop XVII, Albany, NY

Crowe, C. C., C. J. Schultz, M. Kumjian, L. D. Carey, and W. A. Petersen, 2012: Use of dual-polarization signatures in diagnosing tornadic potential. *Electron. J. Oper. Meteor*, **13**, 57–78.

Davies-Jones, R., 1984: Streamwise vorticity: The origin of updraft rotation in supercell storms. *J. Atmos. Sci.,* **41**, 2991–3006, doi:10.1175/1520- 0469(1984)0412.0.CO;2.

Dawson, D. T., E. R. Mansell, Y. Jung, L. J. Wicker, M. R. Kumjian, and M. Xue, 2014: Low-level ZDR signatures in supercell forward flanks: The role of size sorting and melting of hail. *J. Atmos. Sci.*, **71**, 276–299, https://doi.org/10.1175/JAS-D-13-0118.1.

Duda, J. D., W. A. Gallus, 2010: Spring and summer Midwestern severe weather reports in supercells compared to other morphologies. *Wea. Forecasting,* **25**, 190-206, doi.org/10.1175/2009WAF2222338.1

Durran, D. R., L. W. Snellman, 1987: The diagnosis of synoptic-scale vertical motion in an operational environment. *Wea. Forecasting*, **2**, 17-31, https://doi.org/10.1175/1520-0434(1987)002%3C0017:TDOSSV%3E2.0.CO;2

Davies-Jones, R., P., 1982: Observational and theoretical aspects of tornadogenesis. *Intense Atmos. Vorticies*, Conference paper, 175-189, doi:10.1007/978-3-642-81866-0_14

——, Brooks, H. E., 1993: Mesocyclogenesis from a theoretical perspective. *The Tornado: Its Structure, Dynamics, Prediction, and Hazards, Volume 79*. https://doi.org/10.1029/GM079p0105

Esterheld, J. M., and D. J. Giuliano, 2008: Discriminating between tornadic and non-tornadic supercells: A new hodograph technique. *Elec. J. Severe Storms Meteor.*, **3**, 1–50.

Fawbush, E. J., and Miller, R. C., 1954: The types of airmasses in which North American tornadoes form. *Bull. Amer. Meteor. Soc.*, **35**, 154-165, https://doi.org/10.1175/1520-0477-35.4.154.

French, M. M., D. W. Burgess, E. R. Mansell, and L. J. Wicker, 2015: Bulk hook echo raindrop sizes retrieved using mobile, polarimetric Doppler radar observations. *J. Appl. Meteorol. Climatol.*, **54**, 423–450, https://doi.org/10.1175/JAMC-D-14-0171.1.

Gibson, M., 2017: FAQ: NROT and GR-MDA Products. *GRlevelx User Forums.*

Gilmore, M. S., J. M. Straka, and E. N. Rasmussen, 2004: Precipitation and evolution sensitivity in simulated deep convective storms: Comparisons between liquid-only and simple ice and liquid phase microphysics. *Mon. Wea. Rev*., **132**, 1897–1916, doi:10.1175/1520-0493(2004)132,1897:PAESIS.2.0.CO;2

Hastings, R. M., and Y. P. Richardson, 2010: Storm mergers. Part 1: Preliminary numerical investigations of merger events. Preprints, *25th Conf. on Severe Local Storms*, Denver, CO,

Amer. Meteor. Soc., 7A.5. [Available online at https://ams.confex.com/ams/pdfpapers/176048.pdf.]

Herzegh, P. H., and A. R. Jameson, 1992: Observing precipitation through dual-polarization radar measurements. *Bull. Amer. Meteor. Soc.*, **73**, 1365-1376, https://doi.org/10.1175/1520-0477(1992)073<1365:OPTDPR>2.0.CO;2.

Homeyer, C. R., T. N. Sandmæl, C. K. Potvin, and A. M. Murphy, 2020: Distinguishing characteristics of tornadic and nontornadic supercell storms from composite mean analyses of radar observations. *Mon. Weather Rev.*, **148**, 5015–5040, https://doi.org/10.1175/MWR-D-20-0136.1.

Houser, J. L., Bluestein H. B., and Snyder J. C., 2015: Rapid-scan, polarimetric, Doppler radar observations of tornadogenesis and tornado dissipation in a tornadic supercell: The "El Reno, Oklahoma" storm of 24 May 2011. *Mon. Wea. Rev.*, **143**, 2685–2710, doi:10.1175/MWR-D-14-00253.1.

Houston, A. L., Niyogi D., 2007: The sensitivity of convective initiation to the lapse rate of the active cloud-bearing layer. *Mon. Wea. Rev.*, **135**, 3013-3032, https://doi.org/10.1175/MWR3449.1

Illingworth, A. J., J. W. F. Goddard and S. M. Cherry, 1987: Polarization studies of precipitation development in convective storms. *Quart. J. Roy. Meteor. Soc.,* **113**, 469-489, https://doi.org/10.1002/qj.49711347604

Jameson, A. R., 1994: Measuring rainwater content by radar using propagation differential phase shift. *J. Atmos. Oceanic Technol.,* **11**, 299-310, https://doi.org/10.1175/1520-0426(1994)011<0299:MRCBRU>2.0.CO;2.

Johnson, M., Y. Jung, D. T. Dawson, and M. Xue, 2016: Comparison of simulated polarimetric signatures in idealized supercell storms using two-moment bulk microphysics schemes in WRF. *Mon. Wea. Rev.*, **144**, 971–996, https://doi.org/10.1175/MWR-D-15-0233.1.

Kerr, B. W., and G. L. Darkow, 1996: Storm-relative winds and helicity in the tornadic thunderstorm environment. *Wea. Forecasting*, **11**, 489–505, https://doi.org/10.1175/1520-0434(1996)011<0489:SRWAHI>2.0.CO;2.

Klees, A. M., Y. P. Richardson, P. M. Markowski, C. Weiss, J. M. Wurman, and K. K. Kosiba, 2016: Comparison of the tornadic and nontornadic supercells intercepted by VORTEX2 on 10 June 2010. *Mon. Wea. Rev.*, **144**, 3201–3231, https://doi.org/10.1175/MWR-D-15-0345.1.

Kumjian, M. R., and A. V. Ryzhkov, 2007: Polarimetric characteristics of tornadic and nontornadic supercell thunderstorms. Preprints, 33rd Conf. on Radar Meteorology, Cairns, Queensland, Australia, Amer. Meteor. Soc., P10.1. [Available online at http://ams.confex.com/ams/pdfpapers/122882.pdf.]

——, and A. V. Ryzhkov, 2008: Polarimetric signatures in supercell thunderstorms. *J. Appl. Meteor. Climatol.*, **47**, 1940–1961, https://doi.org/10.1175/2007JAMC1874.1.

——, A. V. Ryzhkov, V. M. Melnikov, and T. J. Schuur, 2010: Rapid-scan super-resolution observations of a cyclic supercell with a dual-polarization WSR-88D. *Mon. Wea. Rev.*, **138**, 3762–3786, https://doi.org/10.1175/2010MWR3322.1.

——, A. P. Khain, N. Benmoshe, E. Ilotoviz, A. V. Ryzhkov, and V. T. J. Phillips, 2014: The anatomy and physics of Z_{DR} columns: Investigating a polarimetric radar signature with a spectral bin microphysical model. *J. Appl. Meteorol. Climatol.*, **53**, 1820–1843, https://doi.org/10.1175/JAMC-D-13-0354.1.

Kuster, C. M., T. J. Schuur, T. T. Lindley, and J. C. Snyder, 2020: Using Z_{DR} columns in forecaster conceptual models and warning decision-making. *Wea. Forecasting*, **35**, 2507–2522, https://doi.org/10.1175/WAF-D-20-0083.1.

Lemon, L. R., 1977: New severe thunderstorm radar identification techniques and warning criteria: A preliminary report. NOAA Tech. Memo. NWS NSSFC-1, 60 pp.

——, and C. A. Doswell, 1979: Severe thunderstorm evolution and mesocyclone structure as related to tornadogenesis. *Mon. Wea. Rev.,* **107**, 1184–1197, doi:10.1175/1520-0493(1979)1072.0.CO;2.

Loeffler, S. D., and M. R. Kumjian, 2018: Quantifying the separation of enhanced Z_{DR} and K_{DP} regions in nonsupercell tornadic storms. *Wea. Forecasting*, **33**, 1143–1157, https://doi.org/10.1175/WAF-D-18-0011.1.

——, M. R. Kumjian, M. Jurewicz, and M. M. French, 2020: Differentiating between tornadic and nontornadic supercells using polarimetric radar signatures of hydrometeor size sorting. *Geophys. Res. Lett.*, **47**, 1–9, https://doi.org/10.1029/2020GL088242.

Naylor, J., and M. S. Gilmore, 2014: Vorticity evolution leading to tornadogenesis and tornadogenesis failure in simulated supercells. *J. Atmos. Sci.*, **71**, 1201–1217, https://doi.org/10.1175/JAS-D-13-0219.1.

Nowotarski, C. J., and A. A. Jensen, 2013: Classifying proximity soundings with self-organizing maps toward improving supercell and tornado forecasting. *Wea. Forecasting*, **28**, 783–801, https://doi.org/10.1175/WAF-D-12-00125.1.

——, P. M. Markowski, Y. P. Richardson, and G. H. Bryan, 2015: Supercell low-level mesocyclones in simulations with a sheared convective boundary layer. *Mon. Wea. Rev.*, **143**, 272–297, https://doi.org/10.1175/MWR-D-14-00151.1.

——, and E. A. Jones, 2018: Multivariate self-organizing map approach to classifying supercell tornado environments using near-storm, low-level wind and thermodynamic profiles. *Wea. Forecasting*, **33**, 661–670, https://doi.org/10.1175/WAF-D-17-0189.1.

——, J. M. Peters, J. P. Mulholland, 2020: Evaluating the effective inflow layer of simulated supercell updrafts. *Mon. Wea. Rev.,* **148**, 3507-3532, https://doi.org/10.1175/MWR-D-20-0013.1

Parker, M. D., 2014: Composite VORTEX2 supercell environments from near-storm soundings. *Mon. Wea. Rev.*, **142**, 508–529, https://doi.org/10.1175/MWR-D-13-00167.1.

Peters, J. M., C. J. Nowotarski, J. P. Mulholland, and R. L. Thompson, 2020: The influences of effective inflow layer streamwise vorticity and storm-relative flow on supercell updraft properties. *J. Atmos. Sci.*, **77**, 3033–3057, https://doi.org/10.1175/JAS-D-19-0355.1.

Potvin, C. K., K. L. Elmore, S. J. Weiss, 2010: Assessing the impacts of proximity sounding criteria on the climatology of significant tornado environments. *Wea. Forecasting*, **25**, 921-930, https://doi.org/10.1175/2010WAF2222368.1

Romine, G. S., D. W. Burgess, and R. B. Wilhelmson, 2008: A dual-polarization-radar-based assessment of the 8 May 2003 Oklahoma City area tornadic supercell. *Mon. Wea. Rev.*, **136**, 2849–2870, https://doi.org/10.1175/2008MWR2330.1.

Rotunno, R., 1981: On the evolution of thunderstorm rotation. *Mon. Wea. Rev.,* **109**, 577-586, https://doi.org/10.1175/1520-0493(1981)109<0577:OTEOTR>2.0.CO;2

Rousseau-Rizzi, R., D. J. Kirshbaum, and M. K. Yau, 2017: Initiation of deep convection over an idealized mesoscale convergence line. *J. Atmos. Sci.*, **74**, 835-853, https://doi.org/10.1175/JAS-D-16-0221.1

Ryzhkov, A. V., T. J. Schuur, D. W. Burgess, and D. S. Zrnić, 2005: Polarimetric tornado detection. *J. Appl. Meteorol.*, **44**, 557–570, https://doi.org/10.1175/JAM2235.1.

Seliga, T. A., and V. N. Bringi, 1976: Potential use of radar differential reflectivity measurements at orthogonal polarizations for measuring precipitation. *J. Appl. Meteor. Climatol.,* **15**, 69–76, doi:10.1175/1520- 0450(1976)0152.0.CO;2.

Sessa, M. F., and R. J. Trapp, 2020: Observed relationship between tornado intensity and pretornadic mesocyclone characteristics. *Wea. Forecasting*, **35**, 1243–1261, https://doi.org/10.1175/WAF-D-19-0099.1.

Stumpf, G. J., A. Witt, E. D. Mitchell, P. L. Spencer, J. T. Johnson, M. D. Eilts, K. W. Thomas, and D. W. Burgess, 1998: The National Severe Storms Laboratory mesocyclone detection algorithm for the WSR-88D. *Wea. Forecasting*, **13**, 304–326. https://doi.org/10.1175/1520-0434(1998)013<0304:TNSSLM>2.0.CO;2

Tanamachi, R. L., P. L. Heinselman, and L. J. Wicker, 2015: Impacts of a storm merger on the 24 May 2011 El Reno, Oklahoma, tornadic supercell. *Wea. Forecasting*, **30**, 501–524, https://doi.org/10.1175/WAF-D-14-00164.1.

Thompson, R. L., R. Edwards, J. A. Hart, K. L. Elmore, and P. Markowski, 2003: Close proximity soundings within supercell environments obtained from the rapid update cycle. *Wea. Forecasting*, **18**, 1243–1261, https://doi.org/10.1175/1520-0434(2003)018<1243:CPSWSE>2.0.CO;2.

——, C. M. Mead, and R. Edwards, 2007: Effective storm-relative helicity and bulk shear in supercell thunderstorm environments. *Wea. Forecasting*, **22**, 102–115, https://doi.org/10.1175/WAF969.1.

——, B. T. Smith, J. S. Grams, A. R. Dean, and C. Broyles, 2012: Convective modes for significant severe thunderstorms in the contiguous United States. Part II: Supercell and QLCS tornado environments. *Wea. Forecasting*, **27**, 1136–1154, https://doi.org/10.1175/WAF-D-11-00116.1.

Trapp, R. J., 1999: Observations of nontornadic low-level mesocyclones and attendant tornadogenesis failure during VORTEX. *Mon. Wea. Rev.*, **127**, 1693–1710, https://doi.org/10.1175/1520-0493(1999)127<1693:oonllm>2.0.co;2.

——, G. J. Stumpf, and K. L. Manross, 2005: A reassessment of the percentage of tornadic mesocyclones. *Wea. Forecasting*, **20**, 680–687, https://doi.org/10.1175/WAF864.1.

Wade, A. R., M. C. Coniglio, and C. L. Ziegler, 2018: Comparison of near- and far-field supercell inflow environments using radiosonde observations. *Mon. Wea. Rev.*, **146**, 2403-2415, https://doi.org/10.1175/MWR-D-17-0276.1

Weygandt, S. S., and Coauthors, 2015: Rapid Refresh: Version 2 upgrade at NCEP and work toward version 3 and the North American Rapid Refresh Ensemble (NARRE). *Fifth Conf. on Transition from Research to Operations*, Phoenix, AZ, Amer. Meteor. Soc., 4.1, https://ams.confex.com/ams/95Annual/webprogram/ Paper267898.html.

Wilson, M. B., and M. S. Van Den Broeke, 2021: An automated python algorithm to quantify Z_{DR} arc and K_{DP}–Z_{DR} separation signatures in supercells. *J. Atmos. Oceanic Technol.*, **38**, 371–386, https://doi.org/10.1175/JTECH-D-20-0056.1.

Van Den Broeke, M. S., 2015: Polarimetric tornadic debris signature variability and debris fallout signatures. *J. Appl. Meteor. Climatol.*, **54**, 2389–2405, https://doi.org/10.1175/JAMC-D-15-0077.1.

——, 2016: Polarimetric variability of classic supercell storms as a function of environment. *J. Appl. Meteor. Climatol*., **55**, 1907–1925, doi:10.1175/JAMC-D-15-0346.1.

——, 2017: Polarimetric radar metrics related to tornado life cycles and intensity in supercell storms. *Mon. Wea. Rev.,* **145**, 3671–3686, doi:10.1175/MWR-D-16- 0453.1.

——, and S. T. Jauernic, 2014: Spatial and temporal characteristics of polarimetric tornadic debris signatures. *J. Appl. Meteor. Climatol.,* **53**, 2217–2232, doi:10.1175/JAMC-D-14-0094.1.

——, J. M. Straka, and E. N. Rasmussen, 2008: Polarimetric radar observations at low levels during tornado life cycles in a small sample of classic Southern Plains supercells. *J. Appl. Meteor. Climatol*., **47**, 1232–1247, doi:10.1175/2007JAMC1714.1.

——, 2020: A preliminary polarimetric radar comparison of pretornadic and nontornadic supercell storms. *Mon. Wea. Rev.,* **148**, 1567-1584, doi:10.1175/MWR-D-19-0296.1.

——, 2021: Polarimetric radar characteristics of tornadogenesis failure in supercell thunderstorms. *Atmos.*, **12**, 581, https://doi.org/10.3390/atmos12050581.

Weaver, J. F., and J. F. W. Purdom, 1995: An interesting mesoscale storm-environment interaction observed just prior to changes in severe storm behavior. *Wea. Forecasting,* **10**, 449-453, https://doi.org/10.1175/1520-0434(1995)010<0449:AIMSEI>2.0.CO;2.

Weisman, M. L. and J. B. Klemp, 1982: The dependence of numerically simulated convective storms on vertical wind shear and buoyancy. *Mon. Wea. Rev.,* **110**, 504– 520, doi:10.1175/1520-0493(1982)1102.0.CO;2.

Zrnić, D. S. and A. V. Ryzhkov, 1999: Polarimetry for weather surveillance radars. *Bull. Amer. Meteor. Soc.,* **80**, 389–406, doi:10.1175/1520- 0477(1999)0802.0.CO;2.